Dublin City University

School of Mechanical and Manufacturing Engineering

A Thesis Presented For The Degree Of Doctor Of Philosophy

Development of a Microfluidic Platform and Detection System for Platelet Function Analysis

by

Nigel J. Kent B.Eng

Supervisors: Dr. Brian Corcoran

Prof. Brian MacCraith

Dublin, 2009

Declaration

I hereby certify that this material, which I now submit for assessment on the programme of study leading to the award of Doctor of Philosophy is entirely my own work and has not been taken from the work of others save and to the extent that such work has been cited and acknowledged within the text of my work.

Signed: _____ (Candidate) ID No. _____

Date: _____

"The first principle is that you must not fool yourself - and you are the easiest person to fool."

Richard P. Feynman

Acknowledgements

This body of work would not have been possible without a number of significant inputs, across a range of disciplines. Firstly, and most importantly, I would like to thank my 'team' of research supervisors. While some people are lucky enough to study under a single accomplished supervisor, I was extremely fortunate to study under, effectively though unofficially, three.

Brian Corcoran, your ability to immediately deconstruct problems and identify the fundamental issues with such clarity, was of immeasurable benefit over the last few years.

Brian MacCraith, your constant drive and refusal to rest on the many laurels you have, was a constant source of inspiration throughout this work. It is a quality to which I can only aspire and hope it is somewhat reflected in this work.

Finally to Tony Ricco, your breath of knowledge across seemingly unrelated topics was invaluable. Further, your willingness to assist, at all hours of day and night, and your ability to explain abstract concepts in just the right way has left its mark throughout this body of work.

In terms of all things platelet related, my thanks go to the Royal College of Surgeons in Ireland. Particularly to Gerardene Meade, your patience in explaining the most fundamental aspects of platelet biology, and willingness to put others before yourself have progressed this body of work more than

you can know. My thanks also go to Dermot Kenny for taking a chance and letting an engineering influence permeate through his lab. To say your enthusiasm for this work was infectious, is an understatement. Thanks also go to Sinead O Brien, always on hand to carry out experiments, just to satisfy my curiosity, even if some were crude and primitive!

Further acknowledgements also go to the students and staff of the Biomedical Diagnostics Institute and National Centre for Sensor Research, based in Dublin City University, for providing a challenging and extremely rewarding working atmosphere. Particular thanks to the lads in S103 (past and present), scones just don't taste the same anymore!

Particular thanks also goes to Celine Heffernan for bending countless rules in her willingness accommodate me with non-scientific delays to the progression of this work. Also, a big word of thanks goes to Barry O'Connell for his patience with all things electronics. It can't have been easy watching me blow up all those components.

Thanks must also go to my family and friends for the frequent reminders that I am, in fact, a nerd. I should say this fact had never escaped me, but your reminders at least showed you cared enough to also know. For family and friends who have read this far, I was joking you don't have to read this.

Thanks also to the funding agent for this work:

This work was supported by Science Foundation Ireland under Grant No. 05/CE3/B754.

Abstract

This work details the development a point-of-care diagnostic sensor system for early warning of diseases or disorders that involve changes in the activation state of platelets. The sensing system tracks the changes in platelet coverage on a well characterised Von Willebrand Factor coated surface using customised image analysis to objectively quantify fluid-shear-mediated platelet-surface interactions for statistically meaningful numbers of platelets from a single blood sample. A novel mass-manufacturable microfluidic device provides well-defined shear at the surface and hydrodynamically focuses the sample stream into contact with the surface, providing assay results from < 200 μL of undiluted whole blood. The custom detection system integrates low-cost optical components with fluidic and thermal control components for stand-alone fluorescence-based platelet assay in whole blood.

The developed sensor system was validated using surface coverage analysis from 'normal' blood samples compared to samples treated with ReoPro (abciximab or c7E3 Fab): ReoPro treatment inhibits the α IIbβ3 receptor on the platelet surface, thus interfering with stable adhesion to VWF, rendering platelets "less sticky." A similar assay could prove diagnostic for platelet dysfunction in interactions with alternative vascular matrices and facilitate study or diagnosis of thrombosis. This approach will also enable the study and diagnosis of the effects of platelet drug treatment under controlled fluid shear conditions.

Contents

Chapter 1

Introduction

Cardiovascular disease (CVD) resulted in almost one third of global deaths in 2003 and by 2010 will be the leading cause of death in developing countries [1]. Cardiovascular events, such as heart attack or stroke, are caused by thrombosis, i.e. the formation of clots which occur as a result of blood platelet activation. The events initiating thrombosis after vessel injury or plaque rupture are now relatively well understood [2]. Although thrombosis is prevented in part by aspirin and anti-platelet agents, heart attacks and stroke still occur frequently. This suggests that platelet behaviour in individuals differs, as does individual response to platelet therapy. In particular, it is difficult to predict those individuals likely to suffer from cardiovascular disease or cardiovascular events.

Unfortunately, platelets are only suited to meaningful functional analysis for approximately four to six hours after being taken from the body. The process of preparing platelets for ex vivo experimentation shortens this time span. In view of this limitation, typically, only a small number of tests can be performed using prepared platelets. In turn, such studies only provide a small amount of relevant information on platelet function. As a result it is still unclear what constitutes normal platelet function.

The ability to characterise platelet function under haemodynamically relevant conditions would be of benefit, as it would yield valuable prognostic, diagnostic and therapeutic information. In particular, the ability to assess platelet function rapidly in the clinic or at the bedside, and more particularly, without any biochemical preparation or alteration of the platelets following their removal from the body, would allow for a more accurate prediction of cardiovascular risk. It would also enable tailoring of anti-platelet therapy to the needs of an individual patient in order to minimise the risks of thrombosis and bleeding.

1.1 Platelets

Platelets or thrombocytes are small discoid (2-4 μm by $\backsim$ 0.5 μm) cell fragments that circulate in the blood stream and are involved in the cellular mechanisms of haemostasis leading to the formation of blood clots [3]. They are the second most numerous corpuscle in the blood with a concentration between 150 - 400 x 10^9/L and can circulate in the bloodstream for approximately 10 days [4]. Due to their shape and size, particle fluid dynamics dictates that platelets will travel close to the endothelial layer of a vessel wall [3]. This endothelial layer is a thin layer of cells which line the circulatory system and provide an interface between circulating blood and the rest of the vessel wall. Under normal conditions, the endothelium provides a non thrombotic surface, promoting blood flow. However, if the endothelium becomes altered or the vessel wall damaged, a combination of extracellular proteins become exposed, regulating a complex functional response in platelets, which results in the rapid formation of a platelet plug that occludes the site of injury to prevent blood loss. The response depends on the extent of the damage, the matrix proteins exposed and the flow conditions of the blood [7]. From a fluid mechanics perspective, among

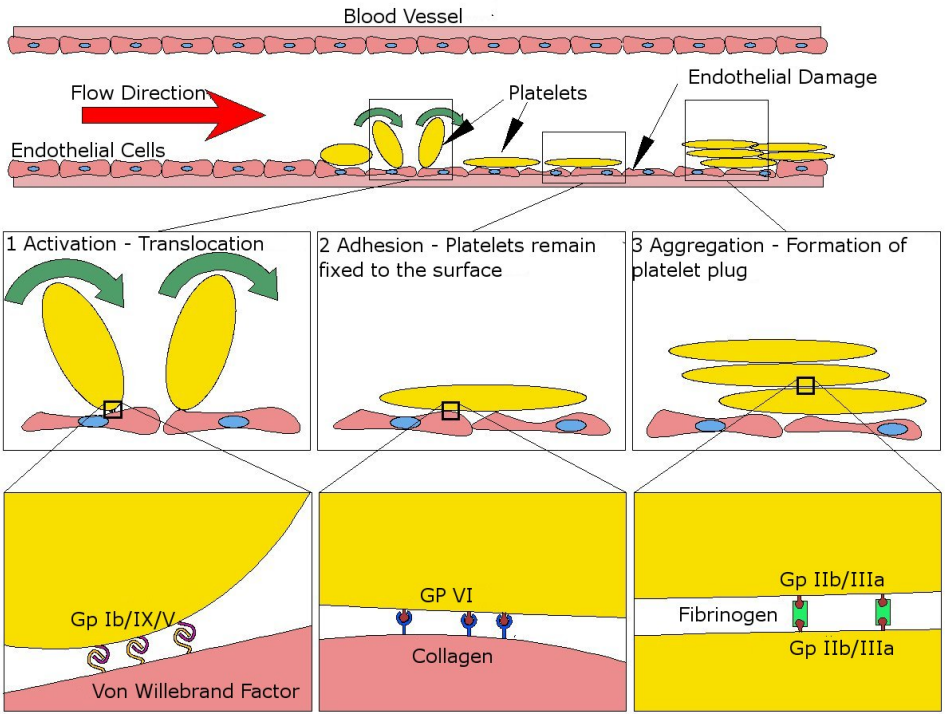

Figure 1.1: Basic platelet interactions

the more critical of these flow parameters has been shown to be the shear force generated at the vessel wall [8, 9]. This has significant implications, particularly in the case of atherosclerotic stenosis [10] where the increase in blood flow velocity through the narrowing of the artery causes an increase in shear forces generated promoting thrombus formation which can lead to myocardial infarction or stroke. As a result, the mechanisms that support platelet activation and aggregation under conditions of high shear force are currently of particular interest in thrombosis research.

The entire mechanism of platelet activation and aggregation is complex with many interdependent biochemical processing occurring simultaneously. However, the three main processes are summarised in Figure 1.1.

1. Activation. On detection of vascular damage, platelets are initially bound to the surface via interactions between Von Willebrand Factor

(VWF), released by the damaged endothelium, and Glyco protein Ib/IX/V (Gp Ib/IX/V) on the platelet surface. This interaction slows the platelets and causes a characteristic translocating or rolling of the platelets along the damaged surface. This VWF - Gp Ib/IX/V interaction has been shown to be highly shear force dependent [8].

2. Adhesion. As the platelets slow under shear-force, the interaction between the exposed collagen at the site of injury and Gp VI on the activated platelet surface cause the platelets to firmly adhere to the damaged vasculature.

3. Aggregation. This adhesion results in intracellular signalling and release of pro-coagulants, thereby promoting further platelet recruitment to the damaged area resulting in the formation of a platelet-platelet aggregates mediated by fibrinogen binding to Gp IIb/IIIa.

If there is a defect in any of these interactions or there are other abnormalities resulting in a low platelet number, haemostasis can be affected and increased bleeding may result. In contrast, if the platelet count is abnormally high this can lead to unnecessary thrombus formation increasing risk of CVD and other platelet function related disorders such as cancer [11]. As a result, the need for platelet function analysis systems is currently of critical importance. Traditionally, platelet function tests have been used to specifically identify potential causes of abnormal bleeding [12]. However, recent advances in medical diagnostics and trends towards point of care devices have led to the development of a small number of devices being developed to investigate alternative aspects of platelet function.

1.1.1 Platelet Function Analysis Systems

Current State of the Art

Although there is a significant volume of laboratory based literature available on platelet function analysis, there still remains relatively few systems for platelet function analysis commercially available. Recent publications [7, 12, 13] have independently discussed a selection of commercially available platforms. The following section summarises some of the better characterised platelet function tests while a more comprehensive list can be found in Appendix A.

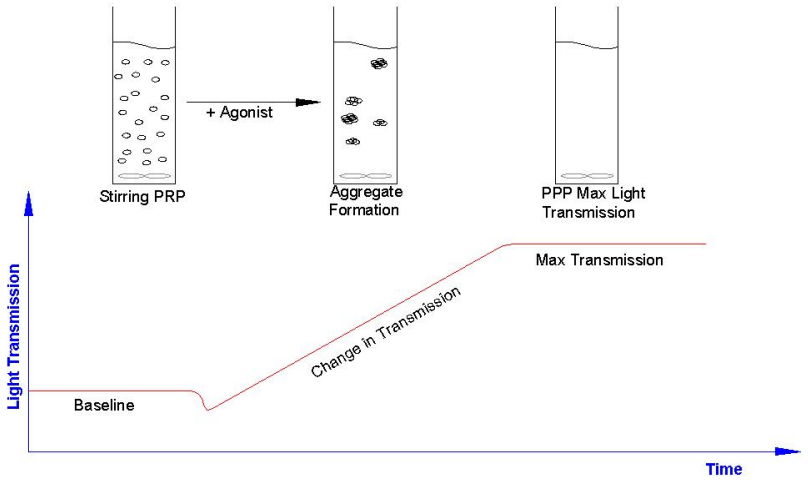

Figure 1.2: Light Transmission Aggregometry

The current gold standard test for platelet function is Light Transmission Aggregometry (LTA). Figure 1.2 illustrates the general principle of LTA. A platelet-rich plasma sample is stirred in a cuvette and light transmission through the platelet medium is measured. A potential platelet agonist is added and, as the platelets aggregate, the light transmission through the platelet carrying medium is increased until a plateau is reached indicating maximum platelet aggregation. By adding a series of agonists over a range

of concentrations it is possible to obtain a large amount of data in relation to different aspects of platelet function.

Unfortunately, the standard aggregometer test is limited in that the procedure takes a considerable amount of time to perform and significant sample volumes and preparation are required. Also, LTA systems are generally expensive and, as a result, use of these systems is typically confined to specialised laboratories. Furthermore, aggregometry is not a measure solely or simply of platelet activation status. The aggregation process depends on a complex biochemical and physical sequence, of which platelets are one key part.

The PFA (platelet function analyzer)-100 ^{TM} device measures time to clotting (known in this case as closure time) after exposure of whole blood to collagen and epinephrine (CEPI) or collagen and ADP (CADP). Anticoagulated whole blood is drawn under vaccuum through a stainless capillary. The high shear forces generated initiate platelet activation. The blood then passes through a small aperture in a membrane coated in either CEPI or CADP (see Figure 1.3). The high shear forces promote initial adhesion of the platelets to this membrane and subsequent biochemical interactions cause the platelets to aggregate and block or 'close' the small aperture restricting blood flow. While the transduction method is relatively simple, there are many factors which affect closure time such as platelet count, hematocrit levels and baseline measurement of von Willebrand factor in plasma. As a result, a single output of time to closure from such a device may not be an accurate representation of purely platelet function. Further, comparison of the results provided by a PFA-100 ^{TM} device with those of the gold standard platelet function test indicates differences [7] and thus the PFA-100 ^{TM} device has limited suitablility.

The Accumetrics Verify Now ^{TM} device can be used at the bedside and uses whole blood to assess platelet function. This device represents a signif-

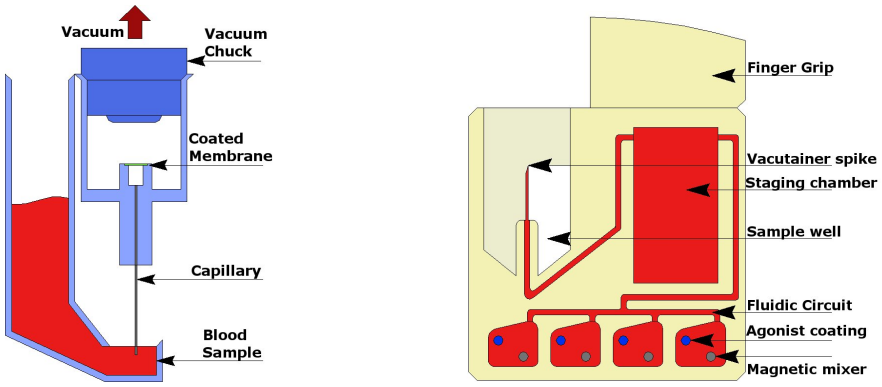

Figure 1.3: PFA100^{TM} (shown left) and Verify Now^{TM} (shown right)Schematic

icant advance towards a Point of Care type diagnostic device. The device is based on light aggregometry but provides an advantage over the gold standard in that the measurements can be performed in whole blood. The disposable Verify Now^{TM} cartridge consists of an inlet for connection to a standard vacutainer used for blood draws. The blood is then divided into four chambers. Inside the chambers are a steel ball to promote mixing and polystyrene beads coated with platelets agonists (See Figure 1.3). When the blood is introduced into the chambers, the platelets begin to aggregate and light transmission through the chambers is measured as previously described. However, as previously stated, aggregometry is not solely a measure of platelet function as many processes occur simultaenously, also as for the PFA-100 ^{TM} device, this device also only provides a limited amount of information regarding platelet reactivity. Further, the Verify Now^{TM} cartridges are inflexible and are currently only available for platelet function analysis in response to Aspirin, Clopidogrel and response to changes in Gp IIb/IIIa.

Diamed - Impact-R is a device for testing platelet function under close to physiological conditions. This device tests shear-force mediated platelet adhesion and aggregation in anti-coagulated whole blood under arterial flow

conditions. The Impact-R can be used to study platelet function, screening of primary haemostasis abnormalities and provides a quick method for monitoring platelet response to various anti-platelet drugs. For standard operation, 130 μL of whole blood is placed in a well and a defined shear rate of 1800s^{-1} is applied via a cone plate appendage as part of the device (See Figure 1.4).

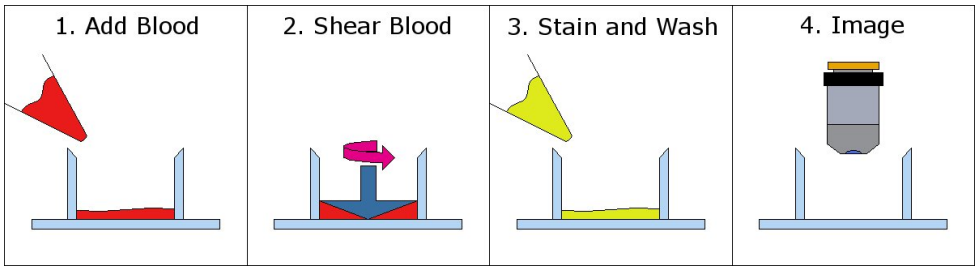

Figure 1.4: Diamed - Impact-R Schematic

This shear is applied for 120 secs and the plate is then washed and the remaining platelets stained and imaged under a microscope housed within the Impact-R device. Since this is only a relatively new apparatus there is little widespread experience of its use. However, while the test conditions of the Impact-R are hemodynamically relevant, the device ultimately measures a single time point of a highly dynamic process. This results in a significant amount of potentially valuable data being undetected by the device.

Research-based tests for platelet function vary depending on the particular aspect of platelet function under investigation. For experiments involving shear-mediated response in platelets the standard metrics used are cone plate viscometry or parallel plate flow devices (See section 1.2.1). While many research groups use custom-designed chambers, parallel plate devices are commercially available from Glycotech [14]. The chambers currently provided, require assembly to form the complete chamber and also require the use of a vacuum pump to form a seal of the chamber components: a top

plate (or flow deck), silicon rubber gaskets (the dimensions of which, form the flow path area) and glass coverslips. For clinical haemodynamic studies, the assembly of the flow chambers and sample provision is technically laborious and requires training. In addition, the volume of blood sample required for haemodynamic studies is considerable. Furthermore, these flow chambers normally require use with relatively expensive fluorescent microscopy suites requiring environmental stability control. This extraneous hardware typically confines the use of these parallel plate flow chambers to specialised laboratories.

An additional characteristic of these systems, however, is the ability to generate a significant amount of data from a single experiment. The data are typically in the form of fluorescent images taken at user defined intervals over a flow run. At appropriate magnifications these data sets can contain both platelet-specific data and information pertaining to the entire platelet population of the donor. To date however the analysis of these data sets has proved challenging; for example, in the case of platelet motions generic rules for particle tracking does not apply and the Gp Ib/IX/V - VWF interaction is largely independent of sample volume and so the assumptions made by particle image velocimetry do not apply. Also many of the commercial image processing packages are geared toward the analysis of adhered cells or constituents of the sub-cellular matrix. Although there is some literature relating to image based platelet function analysis [6] this typically involves significant sample manipulation such as platelet dilutions or laborious manual image analysis on only a fraction of the captured data.

To highlight some of the current problems in relation to platelet function testing, a recent official communication by the scientific and standardisation committee of the International Society on Thrombosis and Haemostasis [15], published a series of points highlighting the current issues with use and development of the current flow tests used to evaluate bleeding risk. Among

the points were:

1. Use of controlled (quantity of) collagen as adhesive substrate
2. Use of different shear rates
3. Use of non-anticoagulated blood, preferably at physiological cation concentrations
4. Use of single-pass, small capacity flow devices
5. Time-dependent measurement of thrombus build-up

While the list was specifically generated with a view towards VonWillebrands disease, many of the points are of a generic nature and are applicable to many platelet function assays. In short, the communication highlights the need for controlled platelet agonist substrates, tunable shear rates, use of small volumes of non - anticoagualted blood for time dependent measurements. With a view to the development of Point of Care systems, inherent in these suggestions is the requirement for low cost, robust, integrated readout and analysis systems.

1.2 MEMS development

The last number of years have seen a marked increase in the field of microelectromechanical systems (MEMS) and microfabrication technologies. The earliest embodiments of these devices are now in every day use in many facets of the world around us. Instruments as apparently diverse as inkjet printers and airbag deployment sensors have all been enabled by developments in the rapidly expanding area of microsystems technology *.Many of

*The area of microelectromechanical systems (MEMS) is also known as microsystems technology (MST) and can also be, although predominantly in Japan, termed micromachines.

the enabling technologies for this increase in MEMS development can be largely attributed to the semiconductor industry where the requirement for improved speed and efficiency of devices became significantly important, particularly for integrated circuits. While MEMS devices have built on the already existing semiconductor technologies the field has rapidly expanded and many new MEMS specific techniques have been developed. This in turn has facilitated microsystems technologies being applied across a number of diverse fields, in particular to the area of life sciences.

In parallel with the development of next generation MEMS has been the advances made in the area of microfluidics. Microfluidics is a broad term encapsulating the control, behaviour and understanding of volumes of fluids in the pico-microlitre range. On this scale, the macroscopic behaviour of physics does not necessarily hold true as other effects typically begin to influence the system. Surface to volume ratios of fluids in MEMS devices tend to be dramatically different from those in the macro world and causes surface effects, such as electrostatics, to dominate over inertial effects. Viscous forces also typically dominate over inertial forces, resulting in low Reynolds numbers which is characteristic of most microfluidic MEMS devices. Among the main practical implications of these low Reynolds number systems is that fluid behaviour remains in the laminar regime. This results in mixing on the micro scale being a primarily diffusive process. As with many apparent peculiarities on the microscale this effect can be exploited to develop new technologies or compensated for where the effect is detrimental to the function of the overall system [16].

Of particular interest in recent years has been the evolution and application of biological microelectromechanical systems (Bio-MEMS). In conjunction with basic MEMS components such as microchannels, microvalves, micropumps and micromixers, Bio-MEMS offers the ability to integrate many laboratory functions on a single low cost device. These 'Lab-on-a-Chip'

(LoaC) devices offer significant potential in biomedical and clinical analysis [5], in particular the ability to perform point-of-care measurements. The term Lab-on-a-Chip can be used to encompass devices designed to miniaturise analytical or bioanalytical techniques and integrate them into a microfabricated format. BioMEMS, with a focus specifically on biological applications can be considered a subset of Lab-on-a-Chip. Along with potential device specific advantages, LoaC devices are typically advantageous because they have:

- low fluid volumes consumption, because of the low internal chip volumes
- higher analysis and control speed of the chip and better efficiency due to short mixing times (short diffusion distances), fast heating (short distances, high wall surface to fluid volume ratios, small heat capacities).
- compactness of the systems, due to large integration of functionality and small volumes.
- potential parallelisation due to compactness, which allows high throughput analysis.
- lower fabrication costs, allowing cost-effective disposable chips, fabricated in mass production.
- safer platform for chemical, radioactive or biological studies because of low volumes.

1.2.1 BioMEMS for Cell Based Analysis

Current State of the Art

MEMS technology has an inherent potential for providing the next generation of cell culture and cell analysis tools where large numbers of single cells or small cell populations can be probed inexpensively, at high throughput, and in a cellular microenvironment of increased physiological relevance with respect to present cell culture methods [17].

There are a significant number of various MEMS based flow devices for an ever increasing number of applications [18–24]. The two detailed below are among the main types of devices used when considering cell oriented MEMS devices under flow conditions.

Parallel Plate

A significant body of work has already been carried out in the area of shear effects on biological species under flow conditions. [9, 25–28] The predominant chamber design of choice has been the parallel plate flow chamber (Figure 1.5). Following on from these parallel plate flow chamber trials, efforts have been made to gain a deeper understanding of the impact of the various design parameters. As a result, a large body of work has been developed, investigating the implications of adjusting variables such as aspect ratio, entrance length and inlet design on overall performance of the device. [29–31]

One of the advantages of the parallel plate flow chamber design is the relative ease in which these parameter changes can be modelled from a fluid behaviour point of view. The nature of the parallel plate flow chamber is the low aspect ratio channel, where the width of the channel (w) is far in excess of the height (h) (see Figure 1.5). The fact that the channel width is so much larger than the channel height results in a significant simplification

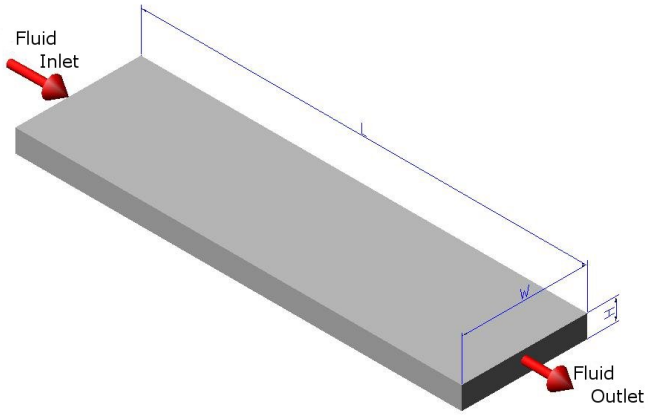

Figure 1.5: Parallel plate flow chamber schematic

of the governing equations and makes any calculations for shear relatively simple. This will be dealt with further in Chapter 2.

Hydrodynamic Focusing

Another common device strategy for the manipulation of cells is termed hydrodynamic focusing. It exploits the fact that, due primarily to dimensional constraints, flow in micro-devices is predominantly in the laminar regime resulting in transfer of species based mainly on diffusion. This allows fluid streams to be manipulated in non intuitive ways. [32–35] Standard hydrodynamic focusing is a technique whereby a central sample stream is shaped and focused by a number of buffer streams with any mixing that may occur being predominantly a function of the diffusivity of the media (Figure1.6).

In Figure 1.6 flow streams Q_1 and Q_3 serve to restrict the flow of sample Q_2. This restriction is such that sample stream Q_2 is reduced to approximately the width of a single cell. The results in the cells of interest flowing in single file through the sample stream. This allows individual cells be interrogated (usually by optical means, in this case laser excitation coupled with microscope detection) and statistically relevant information be ob-

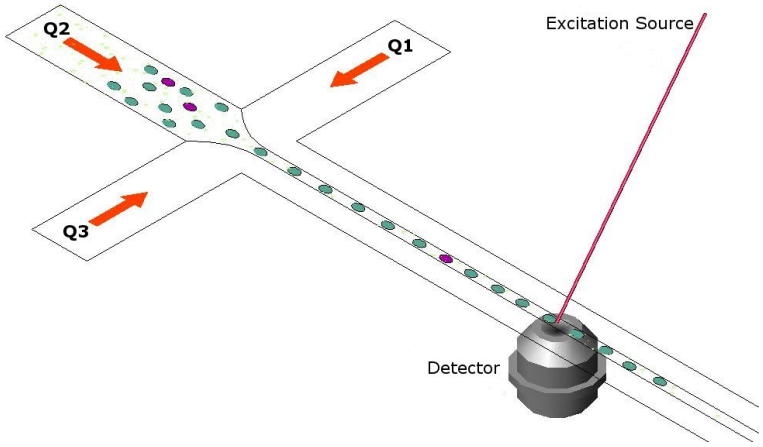

Figure 1.6: Principle of Hydrodynamic focussing

tained from a relatively small sample volume. By tuning relative flowrates, one can control the width of the sample stream. Typically one sets $Q_1 = Q_3$ however these can also be manipulated independently to allow for stream switching [36].

One of the most common uses for this technique is in flow cytometry. Flow cytometry is a technique for measuring microscopic particles flowing single file through a fluid medium. This technique can then interrogate each particle separately. The technique is useful for counting cell or particle populations or identifying sub-populations of particles. Hydrodynamic focusing is a method whereby this single file flow of particles can be relatively easily achieved and characterised. In the last few years there have been a marked increase in the number of these micro scale cytometers developed and tested. [37, 38]

1.3 Fabrication

A critical component in the development of Lab-on-a-Chip devices is the ability to rapidly and reproducibly fabricate the structures required to manipulate fluids on the microscale level. While initial MEMS devices were predominantly silicon based [39], advances in the field of microsystems created the possibility of developing technologies for fabrication in other materials where silicon was unsuitable for a particular application. Among the main disadvantages with using silicon for MEMS is its lack of optical transparency.

The ability to microfabricate in an optically transparent medium creates a plethora of opportunities for new applications of MEMS devices. Not least of these is the area of BioMEMS where optically transparent substrates are typically of significant importance for biological and chemical analysis, as it facilitates the use of optical detection strategies and microscopy measurements. As a result, initial BioMEMS devices were fabricated in glass as many of the existing semiconductor techniques could be modified and applied to glass substrates. While this was advantageous from the perspective of chemical and biological compatibility, mass production of this technology on glass proved costly. Since a typical bio-sensor is often a single use, disposable device, due to platform contamination by the biological or chemical sample, there is a need for a method of producing multiple devices with a short lead time and ultimately at low cost.

In the search for alternative materials, polymers have become the popular alternative for Bio-MEMS or Lab-on-a-Chip devices [40]. Polymers offer several major advantages that are not immediately available in silicon or glass. These include a wide range of material characteristics, biochemical compatibility, ease of processing and prototyping, and lower costs. Broadly speaking, from a manufacturing perspective, polymer micro ma-

chining strategies can be divided into two main sub groups; direct or replication techniques.

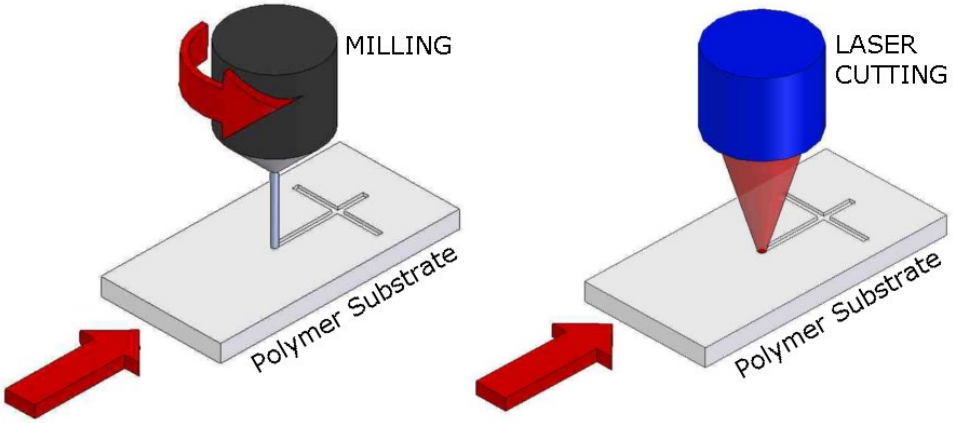

Figure 1.7: Direct machining techniques

Direct machining, as the name suggests, involves directly patterning a surface, typically by material removal, to define a network of fluidic channels of controlled depth and widths for a particular application. Typical polymer direct machining techniques involve laser writing [41] or micro milling [42]. These techniques are extremely flexible and offer rapid turnaround and as such are particularly suited to prototyping of MEMS devices.

Replication techniques, on the other hand, involve an additional, typically expensive, master fabrication step from all which all subsequent devices are fabricated from. Replication strategies include injection moulding [43], embossing [42] or die cutting techniques. Master fabrication strategies may include using traditional machining techniques such as milling, turning or spark erosion however silicon machining or photo lithographic techniques may also be employed. The master fabrication step can vary depending on the replication strategy used.

Typically however, this master fabrication step involves additional time and cost for a single device. As such, replication techniques are typically not

suitable for prototyping. However, since the cycle time per device for replication techniques is typically significantly shorter than direct techniques replication techniques are more suited to pilot to mass production. The

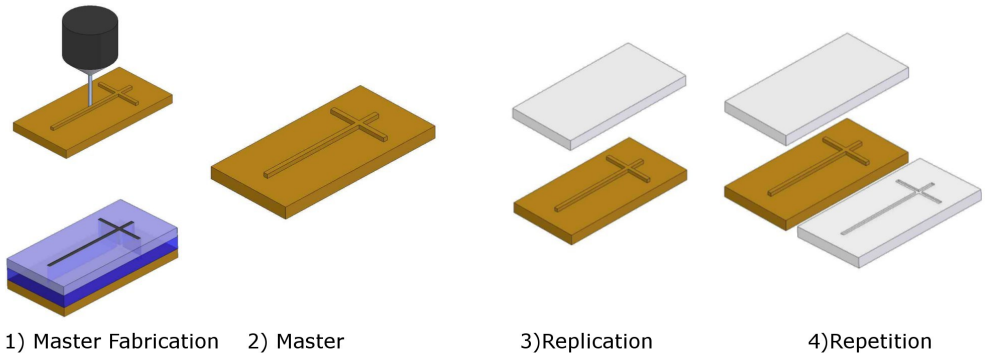

Figure 1.8: Replication manufacturing schematic

techniques mentioned above are all well suited to planar fluidic devices. However, use of laminate technologies has the propensity to rapidly develop 3D fluidic devices while also being compatible with mass production techniques. Laminate technology involves the use of a thin polymer films of various thicknesses with adhesive material on one or both sides. This adhesive nature of the layer can be activated through pressure or in some cases temperature. This pressure sensitive adhesive (psa) can then be patterned and stacked in layers to created a 3D structure. Laminates also have the advantages of being able to easily develop a hybrid chip where glass (used for its biocompatibility) can be easily sealed to polymer used for its ease of manufacture.

1.3.1 Microsystems Fabrication Technologies

Current State of the Art

The development of microsystems for BioMEMS applications is an area of intense research, especially when combined with the development of microfluidic systems. Polymer processing techniques have been widely exploited to this end and among the most commonly employed materials in a laboratory setting is Polydimethlysiloxane (PDMS). Use of this elastomeric polymer was pioneered by Whitesides [44] and has since been used for a variety of applications from standard planar fluidic devices [45] to three dimensional devices [46]. The elastomeric nature of the material also facilitates the development of microfluidics valves [47]. Lee et al [48] have used PDMS for the development of micro lens arrays and pumps have been described by Mathies and Dallas et al [49, 50].

Although PDMS fluidic networks have been used in commercial devices, this remains the exception as thermoset polymers tend to be better suited to mass production techniques. This is reflected in the literature; as the development in Lab on a Chip devices moves from demonstration to utility [17], there has been an increase in the number of publications describing devices developed in thermoset polymers.

Hot embossing has been widely reported in a range of materials such as polystyrene (PS), polyethylenetetraphthalate glycol(PETG), polymethylmethacrylate (PMMA), polyvinylchloride (PVC), polystyrene, and polycarbonate [51–55]. Instruments for automated hot embossing were developed and sold commercially by Jenoptik Mikrotechnik GmbH in Germany.

Laser ablation was introduced in the literature as a method for fabricating polymer microfluidic channels in 1997 by Roberts et al [56] and has since been extensively used by Kutter et al [57, 58]. Ablation has been reported in a range of materials such as PMMA, PETG, PVC, polycarbonate,

polystyrene, and polyimide [51].

Injection moulding for microchannels was first described by Aclara Biosciences and literature describing replication in PMMA [59], and polycarbonate [60, 61] has been published. Many commercial vendors of injection moulded platforms, such as Åmic or Gyros, utilise Compact Disc (CD) injection moulding equipment as the feature sizes required for standard CD replication are typically smaller than those required for microsystems replication. Other groups [62] have utilised this CD format to exploit the centrifugal forces generated on rotation to aid fluid delivery to the device.

Laminate techniques have been widely described by Micronics Inc and A-line technologies [63–65] and have also been incorporated in NASAs GeneSat program for the study of E.coli response in zero gravity [66].

1.4 Summary

Cardiovascular disease is a leading killer in developing countries. As a result platelet function research is currently a very active field of research. However, many current commercial platelet function systems are limited and many laboratory based systems are expensive, laborious and require a high level of technical proficiency to operate. Current developments in the field of micro electromechanical systems (MEMS), in particular BioMEMS, has the potential to revolutionise platelet function analysis. The typical BioMEMS characteristics of low sample volume consumption coupled with high throughput analysis all at low cost opens up exciting prospects for future platelet function devices. Fabrication of these devices however can be challenging especially with the requirement of an economically viable method for mass production. This has resulted in a significant body of work being established in the area of polymer microfabrication, with existing conventional manufacturing techniques modified and new techniques

developed in order to enable low cost fabrication of polymer MEMS devices.

1.5 Thesis Structure

Chapter 2 deals with the governing equations of fluidics with particular emphasis on micro-scale effects. The chapter details these equations as applied to rectangular microchannels and also introduces Computational Fluid Dynamics as an important tool in the characterisation of micro fluidic devices.

Chapter 3 discusses the available fabrication techniques and details the merits of the chosen technique. An initial proof of concept device is detailed from a design and manufacturing perspective.

Chapter 4 describes the experimental procedure for data extraction from the fabricated device. In addition, the concept for an automated image analysis is introduced the algorithm is developed and results are obtained from the proof of concept device.

Chapter 5 introduces a revised device exploiting MEMS specific phenomenon in order to improve throughput of the device. Furthermore, the development of a miniaturised detection system incorporating thermal control, epifluorescense microscopy and fluid delivery is detailed.

Chapter 6 Outlines experimental data from the revised system and discusses any difference in results. Conclusions are drawn based on experimental as to the merits of both experimental systems.

Chapter 7 draws conclusions from the work reported here and highlights possible future applications.

1.6 Thesis Objectives

The objective of this project is to develop a point of care diagnostic tool for early warning indication of platelet-related disorders. To this end, the following are the specific objectives:

1. To design a robust platform to characterise platelet-surface interactions in whole blood under vascular shear rates in response to VWF.

2. To develop an algorithm to objectively quantify platelet-surface interactions in whole blood under physiologically relevant shear rates.

3. To utilise developments in the area of BioMEMS to significantly reduce the sample volume required for an experimental run.

4. To develop an integrated low cost miniaturised detection system, incorporating all fundamental aspects of existing laboratory detection systems.

Bibliography

[1] Cardiovascular disease: prevention and control. *http://www.who.int/dietphysicalactivity/publications/facts/cvd/en/*, page Last accessed 7th April 2008.

[2] G. Davi and C. Patrono. Platelet Activation and Atherothrombosis. *New England Journal of Medicine*, 357(24):2482, 2007.

[3] R. R. Seeley, T. D. Stephens, and P. Tate. *Essentials of Anatomy and Physiology*. McGraw-Hill, 2002.

[4] J.N. George. Platelets. *The Lancet*, 355(9214):1531–1539, 2000.

[5] E. Verpoorte. Microfluidic chips for clinical and forensic analysis. *Electrophoresis*, 23(5), 2002.

[6] N.A. Mody, O. Lomakin, T.A. Doggett, T.G. Diacovo, and M.R. King. Mechanics of Transient Platelet Adhesion to von Willebrand Factor under Flow. *Biophysical Journal*, 88(2):1432–1443, 2005.

[7] Alan D. Michelson. *Platelets Second Ed.* Elsevier Academic Press, 2007.

[8] M. H. Kroll, J. D. Hellums, L. V. McIntire, A. I. Schafer, and J. L. Moake. Platelets and shear stress. *Blood*, 88(5):1525–1541, Sep 1 1996.

[9] A. S. Kantak, B. K. Gale, Y. Lvov, and S. A. Jones. Platelet Function Analyzer: Shear Activation of Platelets in Microchannels. *Biomedical Microdevices*, 5(3):207–215, 2003.

[10] R. Ross. Atherosclerosis is an inflammatory disease. *American Heart Journal*, 138(5 part 2):S419, 1999.

[11] O.J.T. McCarty, S.A. Mousa, P.F. Bray, and K. Konstantopoulos. Immobilized platelets support human colon carcinoma cell tethering, rolling, and firm adhesion under dynamic flow conditions. *Blood*, 96(5):1789, 2000.

[12] P. Harrison. Platelet function analysis. *Blood reviews*, 19(2):111–123, Mar 2005.

[13] A.D. Michelson. Platelet Function Testing in Cardiovascular Diseases, 2004.

[14] Brown, David and Larson, Richard. Improvements to parallel plate flow chambers to reduce reagent and cellular requirements. *BMC Immunology*, 2(1):9, 2001.

[15] JJ Zwagina, KS Sakariassen, MR King, TG Diacovo, EF Grabowski, G. Nash, M. Hoylaerts, and JWM Heemskerk. Can blood flow assays help to identify clinically relevant differences in von Willebrand factor functionality in von Willebrand disease types 1-3? 1. *Journal of Thrombosis and Haemostasis*, 5(12):2547–2549, 2007.

[16] T.H. Schulte, R.L. Bardell, and B.H. Weigl. Microfluidic technologies in clinical diagnostics. *Clinica Chimica Acta*, 321(1-2):1–10, 2002.

[17] DA Beebe. Folch,The Science and Applications of Cell Biology in Microsystems,. *Lab on a Chip*, 5:10–11, 2005.

[18] S. D. Minteer. *Microfluidic techniques*. Humana Press, 2006.

[19] NT Nguyen and ST Wereley. *Fundamentals and Applications of Microfluidics*. Artech House, 2002.

[20] P.J. Hung, P.J. Lee, P. Sabounchi, R. Lin, and L.P. Lee. Continuous perfusion microfluidic cell culture array for high-throughput cell-based assays. *Biotechnology and Bioengineering*, 89(1):1–8, 2005.

[21] S.W. Rhee, A.M. Taylor, C.H. Tu, D.H. Cribbs, C.W. Cotman, and N.L. Jeon. Patterned cell culture inside microfluidic devices. *Lab on a Chip*, 5(1):102–107, 2005.

[22] A. Tourovskaia, X. Figueroa-Masot, and A. Folch. Differentiation-on-a-chip: A microfluidic platform for long-term cell culture studies. *Lab on a Chip*, 5(1):14–19, 2005.

[23] W.C. Chang, L.P. Lee, and D. Liepmann. Biomimetic technique for adhesion-based collection and separation of cells in a microfluidic channel. *Lab on a Chip*, 5(1):64–73, 2005.

[24] A. Revzin, K. Sekine, A. Sin, R.G. Tompkins, and M. Toner. Development of a microfabricated cytometry platform for characterization and sorting of individual leukocytes. *Lab on a Chip*, 5(1):30–37, 2005.

[25] A. Bonnefoy, Q. Liu, C. Legrand, and M. M. Frojmovic. Efficiency of platelet adhesion to fibrinogen depends on both cell activation and flow. *Biophysical journal*, 78(6):2834–2843, Jun 2000.

[26] Y. Ikeda, M. Handa, K. Kawano, T. Kamata, M. Murata, Y. Araki, H. Anbo, Y. Kawai, K. Watanabe, and I. Itagaki. The role of von Willebrand factor and fibrinogen in platelet aggregation under varying shear stress. *The Journal of clinical investigation*, 87(4):1234–1240, Apr 1991.

[27] H. Lu, L. Y. Koo, W. M. Wang, D. A. Lauffenburger, L. G. Griffith, and K. F. Jensen. Microfluidic shear devices for quantitative analysis of cell adhesion. *Analytical Chemistry*, 76(18):5257–5264, Sep 15 2004.

[28] N. A. Mody, O. Lomakin, T. A. Doggett, T. G. Diacovo, and M. R. King. Mechanics of transient platelet adhesion to von Willebrand factor under flow. *Biophysical journal*, 88(2):1432–1443, Feb 2005.

[29] M. Bahrami, MM Yovanovich, and JR Culham. PRESSURE DROP OF FULLY-DEVELOPED, LAMINAR FLOW IN MICROCHANNELS OF ARBITRARY CROSS-SECTION. *Proceedings of 3rd international conference on microchannels and minichannels, Toronto, Canada*, 2005.

[30] DP Bakker, A. van der Plaats, GJ Verkerke, HJ Busscher, and HC van der Mei. Comparison of Velocity Profiles for Different Flow Chamber Designs Used in Studies of Microbial Adhesion to Surfaces. *Applied and Environmental Microbiology*, 69(10):6280–6287, 2003.

[31] I. Papautsky, B. K. Gale, S. Mohanty, T. A. Ameel, and A. B. Frazier. Effects of rectangular microchannel aspect ratio on laminar friction constant. *Proceedings of SPIE-The International Society for Optical Engineering, Proceedings of the 1999 Microfluidic Devices and Systems II, Santa Clara*, 3877:147–158, 1999.

[32] James B. Knight, Ashvin Vishwanath, James P. Brody, and Robert H. Austin. Hydrodynamic Focusing on a Silicon Chip: Mixing Nanoliters in Microseconds. *Physical Review Letters*, 80(17):3863, 04/27/ 1998.

[33] Gwo-Bin Lee, Chen-I Hung, Bin-Jo Ke, Guan-Ruey Huang, Bao-Herng Hwei, and Hui-Fang Lai. Hydrodynamic Focusing for a Micromachined Flow Cytometer. *Journal of Fluids Engineering*, 123(3):672–679, 2001.

[34] R. Miyake, H. Ohki, I. Yamazaki, and R. Yabe. A development of micro sheath flow chamber. *Micro Electro Mechanical Systems, 1991, MEMS'91, Proceedings.'An Investigation of Micro Structures, Sensors, Actuators, Machines and Robots'.IEEE*, pages 265–270, 1991.

[35] Z. Wu and N. T. Nguyen. Hydrodynamic focusing in microchannels under consideration of diffusive dispersion: theories and experiments. *Sensors and Actuators B*, 107(2):965–974, 2005.

[36] Gwo-Bin Lee, Bao-Herng Hwei, and Guan-Ruey Huang. Micromachined pre-focused MN flow switches for continuous multi-sample injection. *Journal of Micromechanics and Microengineering*, 11(6):654–661, 2001.

[37] S. Chung, S. J. Park, J. K. Kim, C. Chung, D. C. Han, and J. K. ER . Chang. Plastic microchip flow cytometer based on 2- and 3-dimensional hydrodynamic flow focusing. *Microsystem Technologies*, 9(8):525–533, 10// 2003.

[38] Anne Y. Fu, Charles Spence, Axel Scherer, Frances H. Arnold, and Stephen R. Quake. A microfabricated fluorescence-activated cell sorter. *Nat Biotech*, 17(11):1109–1111, 11//print 1999. M3: 10.1038/15095; 10.1038/15095.

[39] S.A. Wang, W. Soper. *Bio-MEMS Technologies and Applications*. CRC Press, 2007.

[40] H. Becker and C. Gartner. Polymer microfabrication methods for microfluidic analytical applications. *Electrophoresis*, 21(1):12–26, 2000.

[41] H. Klank, J.P. Kutter, and O. Geschke. CO 2-laser micromachining and back-end processing for rapid production of PMMA-based microfluidic systems. *Lab on a Chip*, 2(4):242–246, 2002.

[42] É. Tyrrell, C. Gibson, B.D. MacCraith, D. Gray, P. Byrne, N. Kent, C. Burke, and B. Paull. Development of a micro-fluidic manifold for copper monitoring utilising chemiluminescence detection. *Lab on a Chip*, 4(4):384–390, 2004.

[43] R. Blue, N. Kent, L. Polerecky, H. McEvoy, D. Gray, and BD MacCraith. Platform for enhanced detection efficiency in luminescence-based sensors. *Electronics Letters*, 41(12):682–684, 2005.

[44] Y. Xia and G.M. Whitesides. Soft lithography. *Angew. Chem. Int. Ed*, 37(5):550–575, 1998.

[45] M.L. Chabinyc, D.T. Chiu, J.C. McDonald, A.D. Stroock, J.F. Christian, A.M. Karger, and G.M. Whitesides. An integrated fluorescence detection system in poly (dimethylsiloxane) for microfluidic applications. *Analytical Chemistry*, 73:4491–4498, 2001.

[46] J.R. Anderson, D.T. Chiu, R.J. Jackman, O. Cherniavskaya, J.C. McDonald, H. Wu, S.H. Whitesides, and G.M. Whitesides. Fabrication of topologically complex three-dimensional microfluidic systems in PDMS by rapid prototyping. *Analytical Chemistry*, 72:3158–3164, 2000.

[47] M.A. Unger, H.P. Chou, T. Thorsen, A. Scherer, and S.R. Quake. Monolithic Microfabricated Valves and Pumps by Multilayer Soft Lithography. *Science*, 288(5463):113–116, 2000.

[48] N. Chronis, G. Liu, K.H. Jeong, and L. Lee. Tunable liquid-filled microlens array integrated with microfluidic network. *Optics Express*, 11(19):2370–2378, 2003.

[49] W.H. Grover, A.M. Skelley, C.N. Liu, E.T. Lagally, and R.A. Mathies. Monolithic membrane valves and diaphragm pumps for practical large-

scale integration into glass microfluidic devices. *Sensors & Actuators: B. Chemical*, 89(3):315–323, 2003.

[50] JM Berg, R. Anderson, M. Anaya, B. Lahlouh, M. Holtz, and T. Dallas. A two-stage discrete peristaltic micropump. *Sensors & Actuators: A. Physical*, 104(1):6–10, 2003.

[51] T.J. Johnson, E.A. Waddell, G.W. Kramer, and L.E. Locascio. Chemical mapping of hot-embossed and UV-laser-ablated microchannels in poly (methyl methacrylate) using carboxylate specific fluorescent probes. *Applied Surface Science*, 181(1-2):149–159, 2001.

[52] H. Becker, W. Dietz, P. Dannberg, and G. Jena. MICROFLUIDIC MANIFOLDS BY POLYMER HOT EMBOSSING FOR jt-TAS APPLICATIONS. *Micro Total Analysis Systems' 98: Proceedings of the [Mu] TAS'98 Workshop, Held in Banff, Canada, 13-16 October 1998*, 1998.

[53] H. Becker and U. Heim. Hot embossing as a method for the fabrication of polymer high aspect ratio structures. *Sensors & Actuators: A. Physical*, 83(1-3):130–135, 2000.

[54] K. Ueno, F. Kitagawa, H.B. Kim, T. Tokunaga, S. Matsuo, H. Misawa, and N. Kitamura. Fabrication and Characteristic Responses of Integrated Microelectrodes in Polymer Channel Chip. *Chemistry Letters*, 29(8):858–859, 2000.

[55] S.A. Soper, S.M. Ford, S. Qi, R.L. McCarley, K. Kelly, and M.C. Murphy. Polymeric microelectromechanical systems. *Analytical chemistry(Washington, DC)*, 72(19):642–651, 2000.

[56] M.A. Roberts, J.S. Rossier, P. Bercier, and H. Girault. UV Laser Machined Polymer Substrates for the Development of Microdiagnostic Systems. *Science*, 261:895–897, 1993.

[57] D. Snakenborg, H. Klank, and J.P. Kutter. Microstructure Fabrication with a CO_2 Laser System. *Journal of Micromechanics and Microengineering*, 14(2):182–189, 2004.

[58] M. Bowden, O. Geschke, J.P. Kutter, and D. Diamond. CO 2 laser microfabrication of an integrated polymer microfluidic manifold for the determination of phosphorus. *Lab on a Chip*, 3(4):221–223, 2003.

[59] R.M. McCormick, R.J. Nelson, M.G. Alonso-Amigo, D.J. Benvegnu, and H.H. Hooper. Microchannel electrophoretic separations of DNA in injection-molded plastic substrates. *Anal. Chem*, 69(14):2626–2630, 1997.

[60] GJ Kellogg, TE Arnold, BL Carvalho, DC Duffy, and NF Sheppard Jr. Centrifugal microfluidics: Applications. *Micro Total Analysis Systems 2000: Proceedings of the TAS 2000 Symposium*, pages 239–242, 2000.

[61] N. Thomas, A. Ocklind, I. Blikstad, S. Griffiths, M. Kenrick, H. Derand, G. Ekstrand, C. Ellström, A. Larsson, and P. Andersson. Integrated cell based assays in microfabricated disposable CD devices. *Micro Total Analysis Systems 2000: Proceedings of the TAS 2000 Symposium*, pages 249–252, 2000.

[62] T. Brenner, T. Glatzel, R. Zengerle, and J. Ducrée. Frequency-dependent transversal flow control in centrifugal microfluidics. *Lab on a Chip*, 5(2):146–150, 2005.

[63] B.H. Weigl, J. Kriebel, K.J. Mayes, T. Bui, and P. Yager. Whole Blood Diagnostics in Standard Gravity and Microgravity by Use of

Microfluidic Structures (T-Sensors). *Microchimica Acta*, 131(1):75–83, 1999.

[64] B.H. Weigl, R. Bardell, T. Schulte, F. Battrell, and J. Hayenga. Design and Rapid Prototyping of Thin-Film Laminate-Based Microfluidic Devices. *Biomedical Microdevices*, 3(4):267–274, 2001.

[65] B.H. Weigl, R.L. Bardell, and C.R. Cabrera. Lab-on-a-chip for drug development. *Advanced Drug Delivery Reviews*, 55(3):349–377, 2003.

[66] Fluidics Subsystem for GeneSat Experimental Payload. *http://genesat.arc.nasa.gov/fluidics.html*, page Last accessed 7th April 2008.

Chapter 2

Theoretical Background and Design Considerations

2.1 Introduction

From a fluid mechanics perspective matter consists of only two states, fluid or solid. Although the difference between the two states may seem perfectly obvious, a rigorous definition of a fluid can prove difficult to formulate. While definitions such as 'a substance tending to flow or conform to the outline of its container' [1] gives us a sense of what a fluid is it does not provide an appropriate technical description that can be applied in any meaningful way. The technical difference between a fluid and a solid has been defined by their response to shear (tangential) stress. *A solid can resist shear stress by a static deformation. A fluid cannot* [2]. This definition facilitates the application of principles of classical continuum mechanics to determine if matter is fluid or solid. In order to further describe the motion of a fluid in response to these forces, Claude-Louis Navier and George Gabriel Stokes developed a set of equations by applying Newtons second law of motion to a body of fluid (See Appendix B). These equations are

now known as the Navier-Stokes equations and are particularly useful in describing a large number of fluid-based phenomena such as ocean currents, stars in a galaxy and blood flow in capillaries. Since these equations are a set of second order non-linear equations they can be computationally intensive to solve and in many cases only approximate solutions can be obtained. Many solution strategies have been enabled with the advent of the personal computer and free and commercial software packages have been developed. These packages have become collectively known as Computational Fluid Dynamics (CFD) software and will be discussed further in section 2.5. In the case of MEMS however, assumptions about the behaviour of the fluid can be made so as to significantly simplify the governing equations. Fluid flow in microsystems is predominantly laminar due primarily to the small length scales of typical devices. This has the effect of removing the rotational components of the Navier-Stokes equations and dictates that viscous effects dominate over inertial effects thereby removing gravitational aspects from many devices. In some special cases the Navier-Stokes equations can be solved exactly and, with some further assumptions, these exact solutions can be applied to describe fluid flow in micro-devices. In relation to blood flow through micro devices, while whole blood is non-Newtonian in nature, for the purposes of this work blood can be considered to behave as a Newtonian fluid [3]. This can be justified when the shear thinning response of whole blood is considered as shown in Figure 2.1.

As the shear rate increases a reorganisation of the red blood cells causes a reduction in measured viscosity. This reorganisation has fully completed before a shear rate of 100^{-1}, after which viscosity of blood remains constant. In the case of investigations into shear response in platelets, shear rates are typically in the range of 1200 s^{-1} to 1800 s^{-1} [7] meaning for the purposes of this work blood can be considered Newtonian fluid.

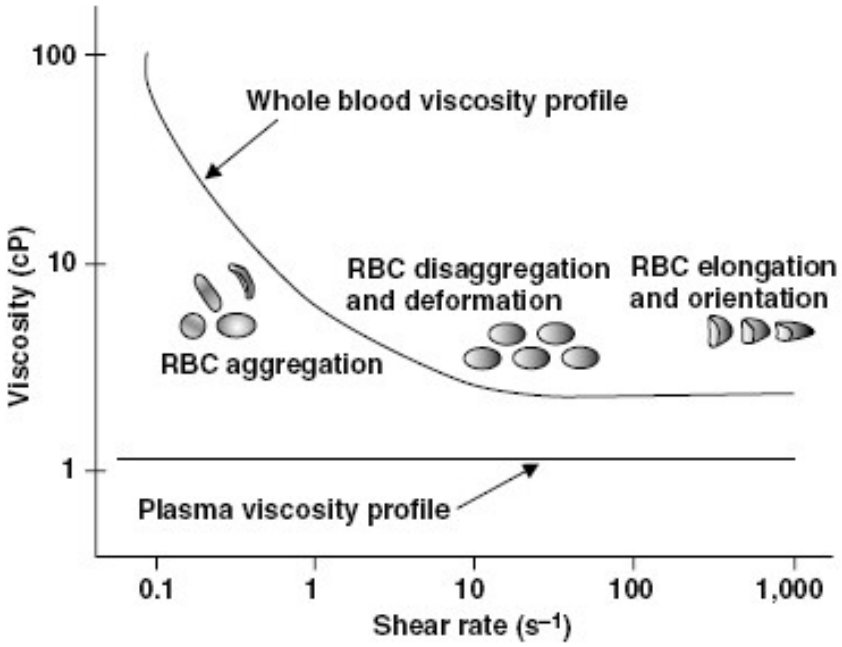

Figure 2.1: Viscosity changes in whole blood in response to Shear

2.2 Steady Flow Between Parallel Plates

Depending on the technique used, fabrication of MEMS devices, can produce channels with various shapes of cross sectional areas. Silicon etching, for example, results in a trapezoidal cross sectional profile while laser cutting results in a characteristic 'U' or 'V' shape cross sectional profile. In many cases however (e.g. milling, photolithography, laminate stacking), the typical channel cross sectional area is rectangular in shape. Further, in the case of shear force-related studies of platelet function, in response to platelet activation agents under flow conditions, low aspect ratio rectangular channel profiles are widely used [4, 5]. This section describes the governing equations of fluid mechanics in such parallel plate channels and discusses the advantages of a low aspect ratio channel when studying shear

force related platelet responses.

Consider a fluid of viscosity μ, flowing between two fixed, infinitely wide parallel plates of length L, separated by a distance a as shown in Figure 2.2. Assuming a constant pressure drop along the length L the Navier-Stokes can be simplified to yield eqn 2.1.

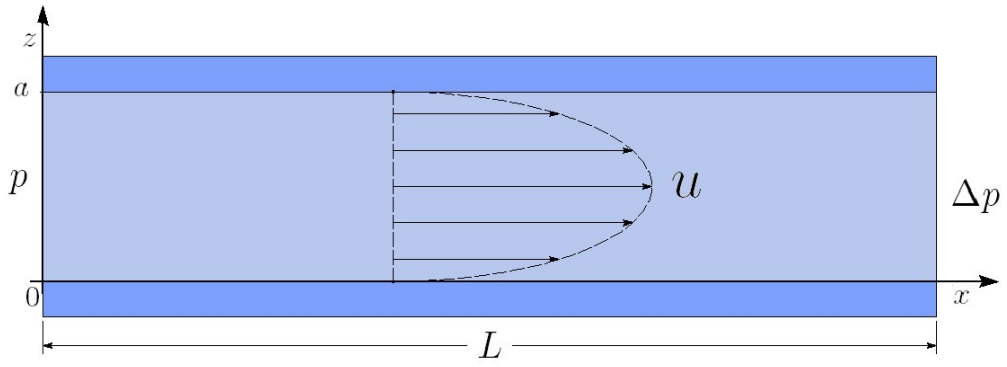

Figure 2.2: Rectangular flowchamber notation

$$\frac{\partial^2 u}{\partial z^2} = \frac{1}{\mu}\frac{dp}{dx} \tag{2.1}$$

Applying the following boundary conditions stating the velocity is zero at both walls

$$u = 0 \quad @ \quad z = 0$$

$$u = 0 \quad @ \quad z = a$$

a solution for the velocity can be obtained in terms of channel geometry, pressure drop and fluid viscosity.

$$u = \frac{1}{2\mu}\frac{dp}{dx}(z-a)z \tag{2.2}$$

and the flow rate Q through a section of width w can be approximated by

$$Q = \int_0^b dy \int_0^a \frac{1}{2\mu}\frac{dp}{dx}(z-a)z\, dz = \frac{a^3 b}{12\mu}\frac{dp}{dx} \tag{2.3}$$

Since equation 2.2 is based on the assumption of infinitely wide parallel plates, equation 2.3 is a highly aspect-ratio-dependent approximation of volume flow rate and breaks down as the aspect ratio approaches 1. In the case of an aspect ratio of one third, $a = b/3$, the error is as much as 23% but falls to 7% for an aspect ratio of one tenth, $a = b/10$.

In spite of these discrepancies equation 2.3 is typically used to describe the shear forces through parallel plate flow devices as typical aspect ratios are on the order of one twentieth to one fiftieth. The main reason however, for utilising such low aspect ratio chambers is evident if the equation describing two dimensional flow through a rectangular duct is plotted over a range of aspect ratios as shown in Figure 2.3. As the aspect ratio increases, the impact of the vertical wall on the flow profile decreases and the flow can be assumed to become one dimensional across almost all the chamber width, as described in equation 2.2. Coupled with a simplification of the governing equations this type of chamber has practical implications in terms of microscopy analysis. When imaging data from such a device, the end user would not be required to position the platform, relative to the microscope objective, with a large degree of accuracy in order to ensure a consistent shear force over a number of experiments.

In order to calculate the wall shear force, τ_w, we use the shear force equation

$$\tau_w = \mu \left| \frac{du}{dz} \right|_{z=0,z=a} = \frac{a}{2} \frac{dp}{dx} \tag{2.4}$$

For practical analysis, equations 2.3 and 2.4 can be combined to give

$$\tau_w = \frac{6\mu Q}{a^2 b} \tag{2.5}$$

which allows the calculation of wall shear force in terms of chamber dimensions, fluid viscosity and volume flow rate.

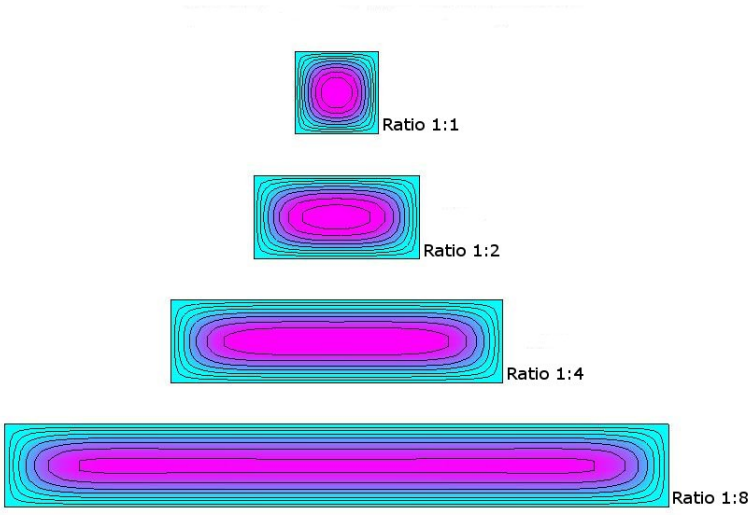

Figure 2.3: Velocity profiles through rectangular ducts of varying aspect ratio.

2.3 Two phase flow

Two-phase flow is of significant importance in MEMS, where it is often desirable to combine two liquids for further treatment, to perform chemical analysis or to manipulate a sample fluid stream. In the case of microfluidics, the characteristic of low Reynolds number systems means that mixing is primarily a diffusive process allowing for unconventional manipulation of fluid streams.

Consider the fixed infinitely wide parallel plates as previously described in Section 2.2. In this case, however, consider the steady state flow of two liquids between the plates under a constant pressure drop. The interface between the two liquids is at a height h as shown in Figure 2.4.

The velocity profile can be described from two differentiable fields [6] where

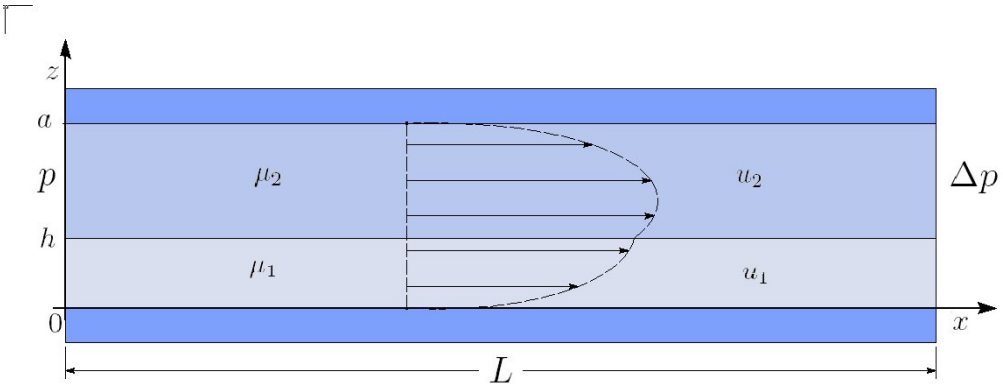

Figure 2.4: Rectangular flow chamber notation

$$u = \begin{cases} u_1 & for \quad 0 < z < h \\ u_2 & for \quad h < z < a \end{cases} \tag{2.6}$$

In this case, the boundary conditions invoked are those of no wall slip as in the case of the single fluid but also the additional conditions of continuous velocity and shear stress at the interface $z = h$.

$$\begin{aligned} u_1 &= 0 && @\, z = 0 \\ u_2 &= 0 && @\, z = a \\ u_1 &= u_2 && @\, z = h \\ \mu_1 \frac{\partial u_1}{\partial z} &= \mu_2 \frac{\partial u_2}{\partial z} && @\, z = h \end{aligned} \tag{2.7}$$

Applying these boundary conditions facilitates the solution

$$\begin{aligned} u_1 &= \frac{1}{2\mu_1} \frac{dp}{dx}(h_1 - z)z \\ u_2 &= \frac{1}{2\mu_2} \frac{dp}{dx}(a - z)(z - h_2) \end{aligned} \tag{2.8}$$

where h_1 and h_2 are obtained from the last two boundary conditions and are given by

$$\begin{aligned} h_1 &= a + h_2 \\ h_2 &= \frac{(\frac{\mu_1}{\mu_2} - 1)(1 - \frac{h}{a})}{\frac{\mu_1}{\mu_2}(1 - \frac{h}{a}) + \frac{h}{a}}.h \end{aligned} \tag{2.9}$$

In a similar manner to the single phase system, the volume flow rate Q across a width b can be approximated by

$$Q_{TOT} = Q_1 + Q_2 = \int_0^b dy \int_0^h \frac{1}{2\mu_1}\frac{dp}{dx}(h_1 - z)zdz + \int_0^b dy \int_h^a \frac{1}{2\mu_2}\frac{dp}{dx}(a - z)(z - h_2)dz \tag{2.10}$$

$$= \frac{b}{12}\frac{dp}{dx}\left[\frac{1}{\mu_1}\Big(2h^3 - 3h_1h^2\Big) - \frac{1}{\mu_2}\Big(2h^3 - (a + h_2)3h^2 + (6a^2 + h_2a)h + a^3\Big)\right] \tag{2.11}$$

Equation 2.3 describes the volume flow rate through the chamber in terms of the height of the fluid interface, the pressure drop along the length, the chamber geometry and the fluid viscosities.

In this case, the shear stress at the walls must be calculated from the piecewise differentials making up the velocity profile and are given by

$$\begin{aligned} \tau_{w(z=0)} &= \mu_1 \left|\frac{du_1}{dz}\right|_{z=0} = \frac{h_1}{2}\frac{dp}{dx} \\ \tau_{w(z=a)} &= \mu_2 \left|\frac{du_2}{dz}\right|_{z=a} = \frac{a + h_2}{2}\frac{dp}{dx} \end{aligned} \tag{2.12}$$

2.4 Forces on Platelets

While platelet-wall interactions have been shown to be highly dependent on fluidic shear stress [7, 8] the mechanics of this dependence is not well

understood. Further, once the platelet has contacted the activating surface the forces involved in maintaining contact, causing translocation or adhesion are largely fluid force independent. There has been some work carried out in an effort to develop a greater understanding of the roles these forces play in relation to thrombosis. Much of the literature, however, is based on simplifications, based on non-physiologically relevant systems or on statistically few platelets [9–11]. These simplifications result from the difficulties in developing a greater understanding of what is an extremely complex and dynamic system.

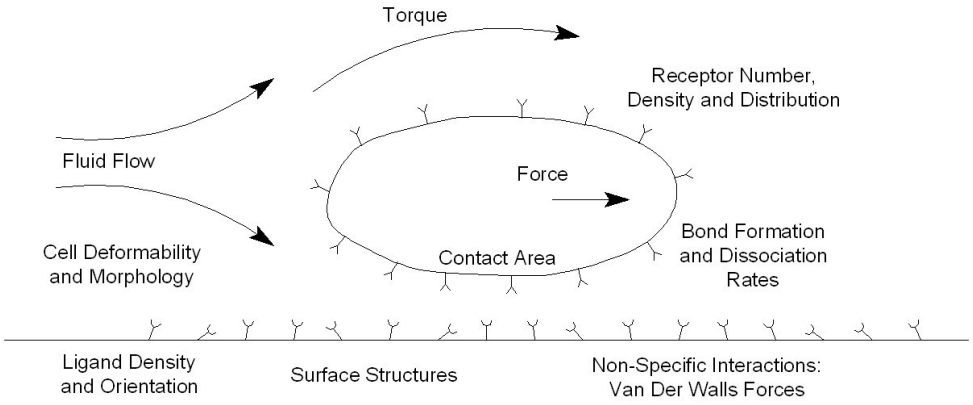

Figure 2.5: Rectangular flowchamber notation

Consider a single platelet, single receptor system as shown in Figure 2.5. The platelet motion can be characterised by a combination of physical and biochemical interactions. The predominant physical force results from fluid flow while, the imparted shear stress and torque affect the local and global motion of the platelet near the surface. The platelet morphology and deformability dictates how these externally applied forces are transmitted

through or around the platelet. The biochemical interactions are primarily receptor-ligand mediated. The factors affecting the biochemical forces are the surface density and orientation of the ligand along the surface as well as the surface density, number of receptors and receptor distribution over the platelet surface. A key component of these ligand receptor interactions are the binding rates and binding affinity. The binding affinity dictates the strength of attraction of the receptor to the ligand surface while the binding rates determines the speed of bond formation and dissociation. It should be noted that these physical and biochemical forces are not mutually exclusive and the net motion of the platelet as indicated in Figure 2.5 is a result of both the physical and biochemical forces.

Even from the relatively simple single platelet single receptor situation the complexity of developing a robust model depends on a number of well defined paramteters. Coupling this with what is required to make a model more physiologically relevant significantly adds to this complexity. When considerations such as multi-platelet, multi-receptor systems are taken into account the model changes dramatically as physical platelet-platelet interactions must be taken into account, along with inter and intra cellular signalling across multiple receptors. Taking these extra biochemical interactions into account, using current computational techniques to develop a robust model of these interactions, would prove extremely difficult, computationally extensive and cost prohibitive to develop since simulation times would require a significantly longer time to prediction than current diagnostics require for time to result.

2.5 Computational Fluid Dynamics

While the development of a robust model for overall platelet function analysis is unfeasible using current technologies, certain aspects of a platelet func-

tion analysis may be modelled to give meaningful data for the design of next generation devices. This is particularly true in the case of fluid modelling. An understanding of how a fluid interacts with its surroundings can be of significant benefit in the design of new technologies and techniques to study platelet function, in particular, in the design of devices oriented towards shear stress related response to an agonist under flow. While the governing equations of fluid dynamics can be complex many software packages have been developed to implement the algorithms, and numerical methods, required to solve fluid flow problems. Collectively these packages come under the umbrella of Computational Fluid Dynamics (CFD) software.

CFD allows insight into flow patterns that may be difficult, expensive or impossible to study using traditional, experimental techniques. It typically, does not replace the measurements completely, more the amount of experimentation. Further, the overall cost of development can be significantly reduced, this is particularly true in the development of a new design.

While CFD can be a very useful tool it is important to remember that the results of a CFD simulation are always a predicted measure based on user defined assumptions of a system. Any discrepancy between the modelled and experimental results may be due to

- the input data may relying inaccurate assumptions
- the mathematical model of the problem at hand being incomplete
- the accuracy of the results becoming limited by the available computing power

2.5.1 Application of CFD

Irrespective of the software vendor the application of CFD methods can be characterised under three main headings.

Pre-processing

The preprocessing stage of model development is typically the most labour intensive and time consuming aspect of model development. In the preprocessing stage the phyisical bounds of the model are defined, usually, in the case of specialised software, by means of a graphical user interface. The physical properties of the model are defined in terms of variables required to solve the appropriate governing equations, for example a defined fluid viscosity would be a prerequisite for the appropriate solution of the Navier Stokes equations. Along with model physical bounds and properties, boundary conditions of the model are also specified at the preprocessing stage.

The boundary conditions describe fluid behaviour and properties at defined areas of the model. This leads to a general solution of the partial differential equations for the specific model being developed. Knowing the solution of the governing equations at certain specific points of the model facilitates the ability to solve, or partially solve, the equations for the overall model. See Section 2.3.

Another critical aspect of the preprocessing stage is the discretisation or mesh generation strategy. This strategy determines how the modelled area containing the continuous fluid is treated as distinct packets of space by the processor to facilitate the solution through the entire model. The most commons strategies are

- **Finite Volume Analysis** This strategy is most commonly used for fluid mechanics problems and the involves calculating the fluid property of interest at the centroid of each individual control volume defined by the mesh size and interpolating across each control volume to build up a solution.

- **Finite Element Analysis** This strategy calculates the fluid property

of interest along the grid or mesh lines for each control volume and builds up a representative image of fluid behaviour in this fashion.

- **Finite Difference Analysis** This strategy calculates the fluid property at each node or intersection point of the mesh and based on calculated values at the surrounding nodes interpolates the value at the node of interest. Calculating a value for each node a representative model of the entire system can be generated.

Simulation

During this stage of model development the computer processor solves the equations based on the input from the preprocessing stage over based on either a steady state or transient response. This stage of model development is highly CPU intensive but requires little, if any, in the way of user input.

Post-processing

The post processing stage involves the analysis of the simulated solutions. Typical software interfaces allow the visualisation of calculated parameters such velocity profiles and pressure distribution while also allowing the user to specify user defined quantities of interest.

2.5.2 Conclusion

The complicated nature of the governing equations of fluid mechanics was outlined and detailed (See Appendix B). In the case of MEMS-based devices it was seen that these equations could be simplified greatly to obtain exact solutions for specific cases of geometries. These equations could then be directly applied to practical cases of fluid flow through MEMS devices. In addition the inherent complications of fully modelling a typical biological

systems were described in terms of difficulties in both physical and biochemical modelling. However, it was shown that while modelling an entire system proves difficult there is value to be gained by modelling certain aspects of a device and the principles of computational fluid dynamics were outlined along with its limitations and standard application procedure.

Bibliography

[1] M.W. Inc. *Merriam-Webster's collegiate dictionary*. Merriam-Webster, 2003.

[2] F.M. White. *Fluid Mechanics*. McGraw-Hill, 2003.

[3] Alan D. Michelson. *Platelets Second Ed*. Elsevier Academic Press, 2007.

[4] DP Bakker, A. van der Plaats, GJ Verkerke, HJ Busscher, and HC van der Mei. Comparison of Velocity Profiles for Different Flow Chamber Designs Used in Studies of Microbial Adhesion to Surfaces. *Applied and Environmental Microbiology*, 69(10):6280–6287, 2003.

[5] Brown, David and Larson, Richard. Improvements to parallel plate flow chambers to reduce reagent and cellular requirements. *BMC Immunology*, 2(1):9, 2001.

[6] H. Bruus. *Theoretical microfluidics*. Oxford University Press, USA, 2008.

[7] M. H. Kroll, J. D. Hellums, L. V. McIntire, A. I. Schafer, and J. L. Moake. Platelets and shear stress. *Blood*, 88(5):1525–1541, Sep 1 1996.

[8] A. S. Kantak, B. K. Gale, Y. Lvov, and S. A. Jones. Platelet Function Analyzer: Shear Activation of Platelets in Microchannels. *Biomedical Microdevices*, 5(3):207–215, 2003.

[9] DA Hammer and SM Apte. Simulation of cell rolling and adhesion on surfaces in shear flow: general results and analysis of selectin-mediated neutrophil adhesion. *Biophysical Journal*, 63(1):35–57, 1992.

[10] N.A. Mody, O. Lomakin, T.A. Doggett, T.G. Diacovo, and M.R. King. Mechanics of Transient Platelet Adhesion to von Willebrand Factor under Flow. *Biophysical Journal*, 88(2):1432–1443, 2005.

[11] P. Tandon and SL Diamond. Hydrodynamic effects and receptor interactions of platelets and their aggregates in linear shear flow. *Biophysical Journal*, 73(5):2819–2835, 1997.

Chapter 3

Fabrication Strategies and Design

3.1 Introduction

Much of the current BioMEMS literature describes fabrication strategies that, do not, in the main, lend themselves to mass production. The predominant material of choice for these prototype platforms is Polydimethylsiloxane (PDMS). While fabrication of microdevices using PDMS have been commercialised these devices are typically encased in a more robust thermoset polymer. Thermoset polymer microdevices are typically more suitable for end use by untrained operators than PDMS devices and their physical robustness can offer additional advantages such as reproducible platform to platform location on readout or detection systems. Among the main advantages of PDMS however, is its flexibility in rapid prototyping new designs. This makes PDMS an excellent research tool facilitating the ability to produce complex designs in relatively low numbers. However, while there are rapid prototyping techniques available for thermoset polymers there still remains a gap between techniques suitable for rapid prototyping

and those suitable for pilot scale or mass production. This chapter looks at the main techniques for microfabrication of thermoset polymer and proposes a possible solution to the problem of transferring a device from prototype to mass production. This solution is then implemented into a parallel plate flow chamber design as previously described. (Chapter 1 Section 1.2.1). Furthermore, this design in then characterised using a computational fluid model and coated with an known platelet activating agent (agonist) in preparation for studies into platelet response.

3.2 Fabrication

3.2.1 Injection moulding

Injection molding as a technique for fabricating microchannels was first described in literature by researchers at Aclara Biosciences [1]. A typical injection moulding process involves the controlled heating of a plastification chamber containing polymer pellets. See Figure 3.1

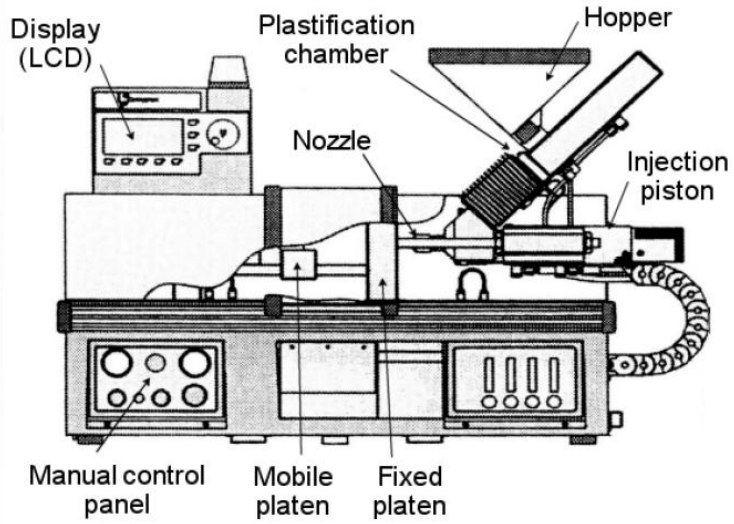

Figure 3.1: Injection Moulder Schematic [3]

The chamber temperature is increased to a sufficiently high temperature so as to melt the polymer pellets fed to the chamber via the hopper. This 'melt' is then forced by the injection piston through the fixed platen via the heated nozzle into a mould cavity and forced to flow over a master mould. The mould typically consists of two metal plates, at least one of which has been machined in order to form a defined cavity for replication of parts. One half of the mould defining cavity is attached to the fixed platen while the other is placed on a hydraulically actuated platen to facilitate mould release.

On cooling of the melt, the polymer re-solidifies and takes the shape of the negative of the master mould. The mobile platen retracts and the replicated polymer part is ejected by means of hydraulically actuated hardened steel pins contained within the mould cavity of the mobile platen. Once the part has been released the mobile platen is re-mated with the fixed platen to reform the mould cavity and the process is repeated. By adjusting the process times and temperature, injection molded parts can be fabricated with excellent precision. Injection molding has been used to reproducibly fabricate plastic microfluidic channels in a range of polymers such as PMMA [1], and polycarbonate [2, 4].

3.2.2 Embossing

Embossing or imprinting techniques for plastic microchannel fabrication were first described in the late 1990s by several groups [5–8]. Some of the initial methods described the use of wires for imprinting features in polymer substrates [7]. Recently however, a silicon or metal micromachined stamp is more commonly used as the imprinting tool for the fabrication of polymer microfluidic devices.

To imprint or emboss microchannels, a silicon or metal stamp is placed

on top of a hard polymer sheet. The stamp and polymer are then placed in a hydraulic press and pressure is applied. Embossing is typically performed at temperatures close to the softening temperature of the polymer and at user defined forces of between 10-200 kN. Alternatively, polymer devices can be imprinted at room temperature with elevated pressures. When devices are hot embossed, the resulting plastic microchannel dimensions are the exact mirror of the silicon stamp. When devices are imprinted at room temperature however, the microchannel dimensions are much more dependent on several parameters including imprinting pressure, imprinting time and properties of the polymer itself [9].

Figure 3.2: Hot Embossing model HEX 02 from Jenoptik

Many common plastics have been successfully imprinted or hot embossed with excellent device-to-device reproducibility. These include polystyrene (PS), polyethylenetetraphthalate glycol(PETG), polymethyl-methacrylate (PMMA), polyvinylchloride (PVC), polystyrene, and polycarbonate [10–14]. Although many research groups have developed in-house embossing instruments. Commercial systems for automated hot embossing were devel-

oped and sold commercially by Jenoptik Mikrotechnik GmbH in Germany. See Figure 3.2

3.2.3 Laser processing

Laser ablation was introduced in the literature, in the early nineties, as a method for fabricating polymer microfluidic channels by Roberts et al. [15].

In the photoablation process, a polymer is exposed to a pulsed Ultra Violet (UV) laser source, and the absorption of that light energy causes the molecular bonds of the polymer backbone to break resulting in the removal of a layer of polymer from the surface [16]. Excimer lasers with emissions of 193 nm (ArF) or 248 nm (KrF) are both effective in polymer ablation but to varying degrees depending on the absorption spectra of the polymer. Polymers that have significant absorption at the emission wavelength of the laser are the most effectively ablated. In contrast to the UV laser, a CO_2-laser emits infrared radiation at a wavelength of 10.6 μm. This means that the CO_2-laser beam always ablates the underlying material photothermally [17]. This leads to a broader range of machinable polymers for CO_2-laser systems but also a large variation in feature quality obtainable from such systems.

Ablation processes can be mask based or direct write systems (See Figure 3.3). In the case of mask based systems, the mask is made from a material that does not have significant absorption at the laser wavelength, e.g. some metals. For a direct write system, the polymer substrate material is placed on a moveable, typically programmable, stage, and the substrate is moved under the focused laser beam to create the desired structure. The laser beam may be further defined by passing it through an aperture of appropriate dimension and shape prior to focusing. The direct-write micromachining process is advantageous in that a mask does not have to be created to

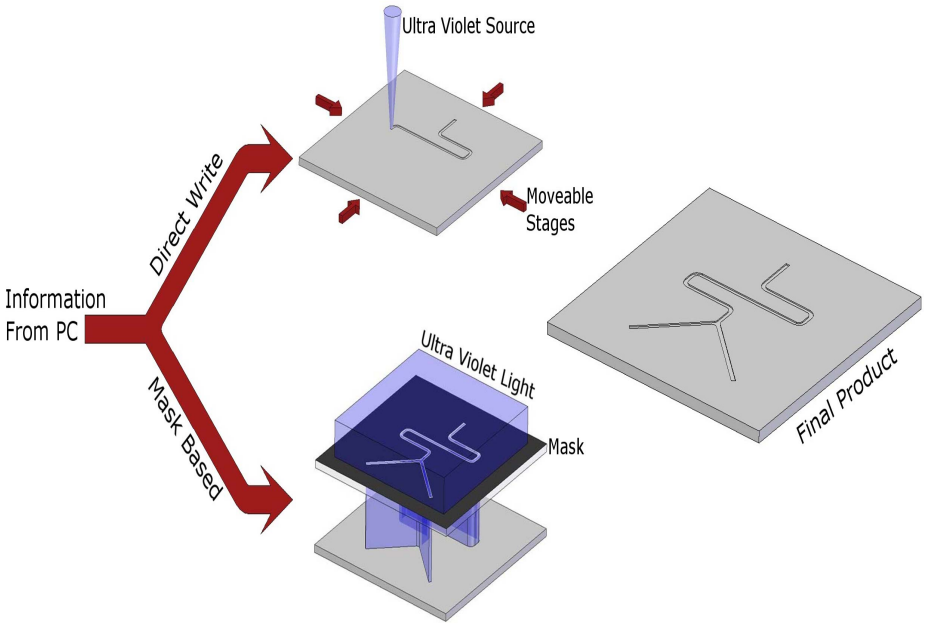

Figure 3.3: Direct and Mask based Laser Ablation processes

change the design of the microchannel network; therefore, channel design can be changed rapidly during the prototyping process. The disadvantage to this approach is that parts are made in a sequential manner thereby limiting the ability to mass produce devices for commercial applications.

3.2.4 CNC Micro milling

Computer Numerically Controlled (CNC) milling is a direct machining process based on physical material removal from a substrate facilitated by a rotary cutter spinning about an axis. The cutter is brought into contact with the material to be machined via computer controlled stepper motors and in contrast to the standard drilling process the milling cutter can be moved laterally relative to the workpiece, also via computer controlled stepper motors. This lateral motion along whats known as the cutter tool path results in a profile of the milling tool being cut from the workpiece mate-

rial. Using multiple defined tool paths, typically generated by means of a computer aided design package, the milling process has the capability to machine complex structures in a broad range of materials.

The ability to fabricate in a broad range of materials makes the micromilling process a very attractive option for both rapid prototyping and mass production capabilities. During the prototyping phase a range of devices can be designed and tested by machining directly into a chosen polymer. Once the design has been finalised the negative of this design can then be machined into an alternative material suitable for further use as a replication tool in any one of the processes mentioned in Sections 3.2.1 and 3.2.2.

3.2.5 Laminates

Although not strictly a fabrication technique, the use of laminates, in a unique way, facilitates the fabrication of MEMS devices and are suited to rapid prototyping and mass production methodologies coupled with some additional advantages making them a very attractive option for the development of platforms to investigate platelet function in response to shear stress.

Many of these laminate films are manufactured with extremely tight thickness tolerances and are available with an increasing number of options; porous, conductive, foil backed, dissolvable and drug eluting films are all currently available as either commercial or research grade and can be supplied over a range of thicknesses from 10 - 200 μm. Standard laminates are commercially available with heat or pressure activated adhesive on one or both sides making them extremely useful for sealing micro devices. Among the more technical issues with the development of thermoset microfluidic platforms is the ability to seal the fluidic channels in order

to form a closed flow chamber. While many groups have provided laboratory specific solutions for specific grades of polymers [18, 19] this does not provide a generic solution to what can be a significant technical challenge. Furthermore, many existing techniques require elevated temperature to ensure sufficient bonding between the parts and this can lead to channel ingress and deformation along the flow cavity [20]. Use of single or double sided pressure sensitive adhesive (psa) laminate layers facilitates a rapid solution to sealing microdevices on a range of polymers, and other MEMS materials, where the wall material properties are not of critical concern.

While sealing existing microfluidics devices is of obvious benefit these laminate films, in particular psa, can be further utilised if the film itself is patterned. This results in the laminate layer defining the flow chamber and the height tolerance defined by the thickness of the laminate. The width tolerances are defined by the patterning process but are generally not as tight as the height tolerances due to both the patterning process and the effects of the adhesive ingressing into the channel. The level of ingress into the channel is laminate specific and a function of the adhesive material itself, the adhesive layer thickness, the sealing temperature and the pressure applied.

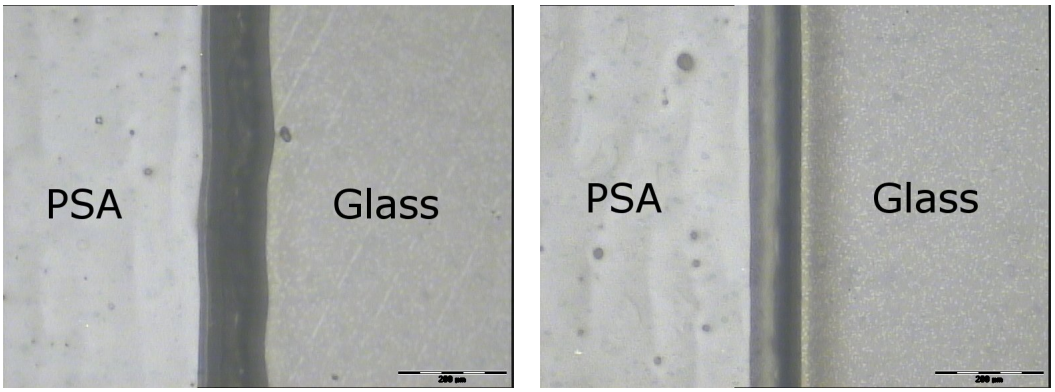

$(a) Laser\ Cut$ $(b) Die\ Cut$

Figure 3.4: PSA Cut Quality

Although width tolerances of 10μm have been reported [21] this tolerance is highly production technique specific. Patterning laminates using a CO_2 laser is very useful when developing initial prototypes due to its flexibility however the photothermal ablation process causes relatively large thermal distortion and can cause considerable, although relatively reproducible, edge ooze effects. See Figure 3.4 *(a)*. For mass production however a rotary tool and die configuration results in excellent edge quality, minimal edge ooze and an extremely rapid method of patterning laminate films. See Figure 3.4 *(b)*. These patterning or conversion techniques are commercially well established developed initially for the labelling industry, where large scale reproducible patterning of adhesive labels is common practice.

3.2.6 Summary

	Feature Sizes	Materials	Prototyping	Mass Production	Multi Layer
Inj. Moulding	sub μm	Polymers/ Composites	No	Yes	Difficult
Hot Embossing	sub μm	Polymer	Yes	No	No
Milling	10s μm	Polymers/ Metals	Yes	No	Difficult
Laser	sub μm	Polymers	Yes	Yes	No
Laminates	10s μm	Polymers/ Metals	Yes	Yes	Yes

Table 3.1: Table comparing fabrication techniques.

Table 3.1 summarises the aforementioned fabrication techniques with a view to choosing an appropriate technique for a given application. The table is by no means a comprehensive overview of available techniques but

should serve as a guide in the decision making process. Each technique may have device specific advantages or disadvantages promoting or inhibiting the technique as suitable or unsuitable for a given application.

3.3 Platform Design

One of the primary objectives of this work was to develop a robust platform to objectively characterise shear-force dependent platelet-surface interactions in whole blood. To this end, the chamber type was chosen to be of parallel plate type design due to, its simplification of the governing equations and practicality of use. Further, a fabrication technique was required that was both flexible in terms of testing alternative designs and also facilitated a smooth transition from a prototype development phase to the pilot scale production required for more rigorous testing of numerous blood samples. It was for this reason primarily, that the use of laminates was the chosen fabrication methodology. Use of laminates however, are not without other advantages in the development of a parallel plate platform. These include:

- The very tight thickness tolerance of commercial laminates is extremely useful when the laminate layer itself is patterned to define the flow channel. Since the flow channel was chosen to be parallel plate in nature the channel height has a significant impact on the shear stress generated (see Chapter 2 Section 2.2). Using the laminate to define the flow area significantly reduces the possibility of platform to platform height variations, particularly in the prototyping/batch production stage of development.

- Adhesive based laminates facilitate sealing of microfluidic devices and this is of importance when defining channel cross sectional area. It

is the flexibility of sealing provided by adhesive laminates that is extremely advantageous. While various sealing techniques are available in the literature these can be labour intensive and typically limited to sealing two or more substrates of the same polymer and of similar thickness. Use of laminates eliminates these issues and facilitates relatively simple bonding of different materials over a range of material thicknesses.

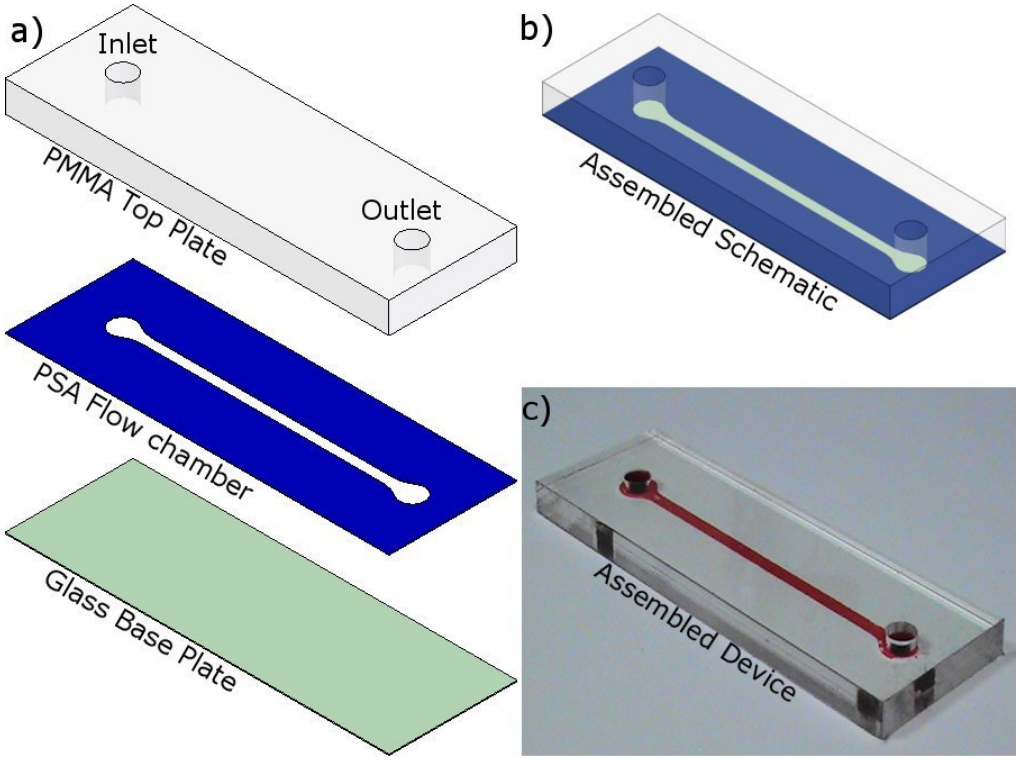

Figure 3.5: Single inlet single outlet platelet function device

In terms of platform design, the initial platform consists of a three layer design as shown in Figure 3.5. The top plate was chosen to be Polymethylmethacrylate (PMMA). PMMA is among the more common materials used in polymer MEMS production, due to its high optical transmission and relative ease of machining making it useful for injection moulding or alternative

replication techniques. For top plate manufacture, 6mm thick PMMA stock was milled to dimensions of 75mm long and 25mm wide corresponding to a standard microscope slide. This piece was then drilled and tapped to facilitate the required inlet and outlet connection ports as shown in Figure 3.5 a.

The middle layer material, defining the flow path, was chosen to be a commercially available double sided laminate from Adhesives Research. ArCARE™8890 is a 12.5 μm polyester film coated on both sides with an acrylic medical grade adhesive resulting in an overall thickness of 50 μm. For ease of transportation and handling the film is protected on both sides with a 50 μm thick polyester release liner as shown in Figure 3.6.

The flow path layer was manufactured using a Coherent GEM-100^{TM} liquid cooled CO_2 laser embedded in a Micromaster Turnkey dual head laser system. The flow path design is drawn in AutoCAD and imported to the machine in R14.dxf format. The laser software then translates the drawing to machine readable code translating the computer drawing to a functional part of the overall design. As with the top-plate the outer dimensions of the laminate or gasket layer corresponds to microscope slide dimensions. This facilitates the ease of use of the platform in existing commercial detection systems for validation purposes. The length of the flow channel is 50 mm. This length ensures ease of access to the inlet and outlet ports of the platform when the platform is positioned within the existing detection system. The flow chamber height is determined by the laminate height i.e. 50 μm while the width was laser patterned to a width of 2mm. The width of 2mm was chosen so as to ensure relative ease of alignment of the platform over the detection area of the readout system. This 2mm channel width results in a flow channel aspect ratio of 0.025 (1:40) and a cross sectional area of 100 x 10^{-9} m^2 compared to the cross sectional area of 1.27 x 10^{-6} m^2 for the existing commercial parallel platform. In practical terms, this results

in a reduction of the volume flowrate required to generate a physiologically relevant shear stress of 6N/m^2 from 2.41 mL/min to 0.075 mL/min. This reduction corresponds to approximately a 97% reduction in required volume flowrate.

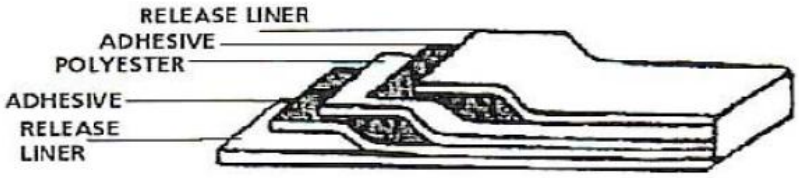

Figure 3.6: ArCARE™8890

As the flow path is a critical aspect of the design, this fabricated layer was characterised (see Figure 3.7) using white-light interferometry techniques using a WYKO NT100 from Veeco. The height of the PSA measures 48.5 μm (material thickness specification: 50 μm), while the overall width of the flow path, 2.10 mm, is within 5% of the 2.0 mm design target. The sidewall roughness associated with the manufacturing process and adhesive ingress into the channel, was viewed empirically using brightfield microscopy and the maximum ingress was seen to be 35 μm for a series of 10 measurements made along the channel sidewall (5 measurements per sidewall). This ingress can be deemed insignificant to the operation of the device due to the geometry and very low aspect ratio (1:40) of the flow path. The measured dimensions for flow path height and width, compared to the design dimensions, imply a difference of wall shear force of just over 1% relative to design.

The base layer of the platform is a commercially available glass microscope coverslip, chosen for three reasons:

- The majority of standard protein deposition techniques are already well established on glass surfaces. Further, many protein layer char-

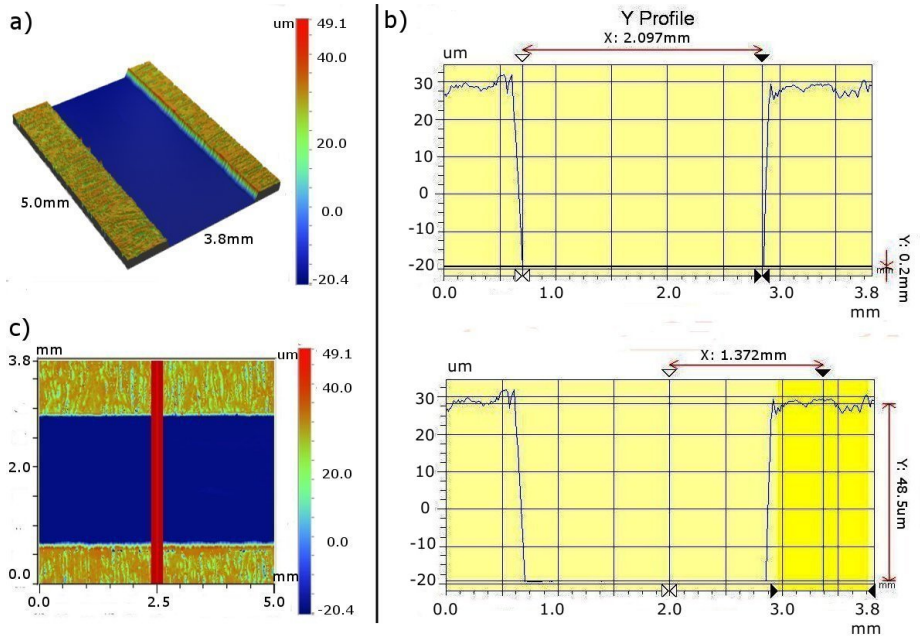

Figure 3.7: Dimensional characterization of fabricated microfluidic parallel-plate device using white-light interferometry

acterisation techniques have also been developed based on glass surfaces.

- The thickness and refractive index of the slides are compatible with existing oil immersion lens for optical detection of platelet surface interactions.

- High quality glass coverslips are a widely available commodity with tightly controlled dimensional, optical, and surface-finish tolerances, in addition to having predictable and reliable surface chemistry.

To assemble the device, the glass cover slip was placed in a custom machined alignment jig, the release liner removed from the psa layer, and aligned over the glass cover slip. The remaining release liner was then removed from the psa layer, and the PMMA plate aligned over the top of the exposed psa layer. The entire fixture was then removed and pressed

together through two rollers to form a sealed device (see Figure 3.5 (c)). In order for the sealed device to be employed as a platelet function analysis platform both glass coverslip and machined top plate are passed through a cleaning protocol involving a wash step with absolute ethanol which is then allowed to evaporate prior to chamber assembly and rinsing by perfusion with aqueous buffer (PBS) post assembly. Further, a computational fluid dynamic (CFD) model was developed to validate shear stress predictions. Also the internal surfaces were coated with Von Willebrand Factor, a protein prevalent in initial adhesion of platelets on the site of vascular injury.

3.3.1 CFD Analysis

While the equations governing laminar flow of a single phase medium, through a rectilinear channel are relatively simple, the development of a CFD model allows a rapid way to visualise the effect of changing boundary conditions, fluid properties or flow conditions. To this end a CFD model of the platform as described in Section 3.3 was developed. While the device itself is relatively straight forward, there are some modifications which can be made to make the model more efficient. This efficiency can be translated into either a reduction in post processing time for the model or as increased resolution of results depending on the type of analysis required. The simplification for this particular model is based around symmetry of the governing equations for flow through a rectilinear channel.

As seen in Figure 3.8 the velocity profiles can be considered symmetrical about the horizontal and vertical planes through the centre of the channel. This symmetry results in a significant simplification of the model as only a single quadrant of the device requires modelling in order to give meaningful data for the overall device. This resulted in a significantly shorter post processing time and allows for more rapid analysis of the device behaviour.

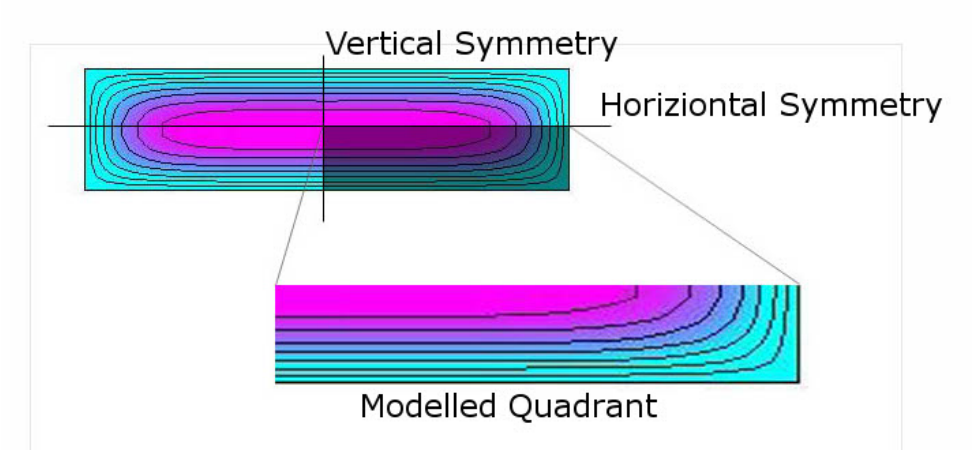

Figure 3.8: Modelled Simplification of Flow Device

A 3-D model of the lower right quadrant of the platform, as shown in Figure 3.8 was generated using CFD-GEOM. CFD-GEOM is the pre processing component of CFD ACE+, a commercially available multi physics package available from ESI Software. This modelling package was used to model fluid flow throughout this body of work unless otherwise stated. Applying the symmetrical simplifications the model cross sectional area was 1mm wide and 25 μm high. The channel length was arbitrarily chosen to be 20mm in length as the velocity profile is independent of distance along the channel based on the an assumption of steady state flow through the device. Since the model was relatively simple, a homogeneously distributed, structured mesh was generated containing a total 34,029 cells.

For the simulation phase blood was modelled as a continuum fluid with a density (ρ) of $997kg/m^3$ and a dynamic viscosity (μ) of $0.004Pa.s$. The symmetrical boundary conditions, as described, were imposed on the geometry and the mass flow rate through the device was determined to be $3.115x10^{-7}kg/s$ This value was found using equations describing volume flow rate detailed in Chapter 2 and also taking into account the symmetrical boundary conditions and based on a wall shear stress of $6N/m^2$ rep-

resentative of a typical vascular shear stress. The default solver for CFD ACE+ utilises the finite volume method as described in Chapter 2 Section 2.5.1 and running the model under these conditions resulted in a model convergence after 57 iterations with a run time of 64 secs.

Results

The graphical results from the analysis can be seen in Figures 3.9 and 3.10. Both figures show a perspective view of the modelled channel quadrant with a section cut through the channel as indicated, and flow direction indicated by a velocity vector field (blue arrows). Each section cut is colour coded; based on Velocity in the case of Figure 3.9 and Shear Rate in the case of Figure 3.10. The inset graph on each figure shows a plot of the specified property as a function of the channel height taken along the mid point of the channel. It should be noted that the inset graphs are representative of a single quadrant of the flow channel, as indicated in Figure 3.8, and as such the graphs shown in Figure 3.9 and Figure 3.10 are representative of the velocity and shear rate, respectively, within a single quadrant of the flow chamber.

Figure 3.9 shows the classic parabolic velocity flow profile, as expected, and returns a calculated maximum velocity of $0.01898 m/s$.

Figure 3.10 shows the generated shear rate in the channel based on a blood viscosity of $0.004 Pa.s$ The modelled wall shear rate is shown to be $1498 s^{-1}$ which is in close agreement with the calculated value of $1500 s^{-1}$ using equations developed in Chapter 2

Other points to note from both figures is the effect of the low aspect ratio channel. In particular, in the case of Figure 3.10 it can be seen the maximum shear rate, indicated in red along the 'Section Cut', occurs at the wall of the channel and is almost constant across the entire width of the

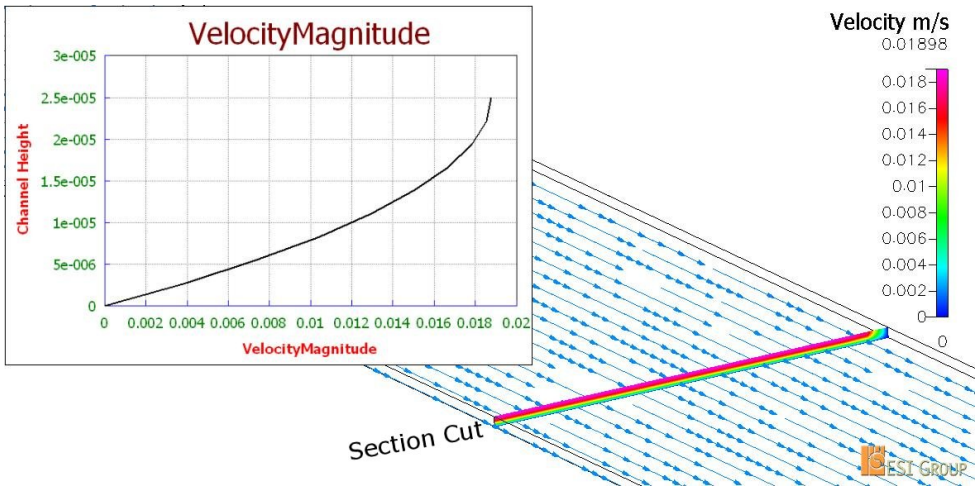

Figure 3.9: CFD Velocity Profiles

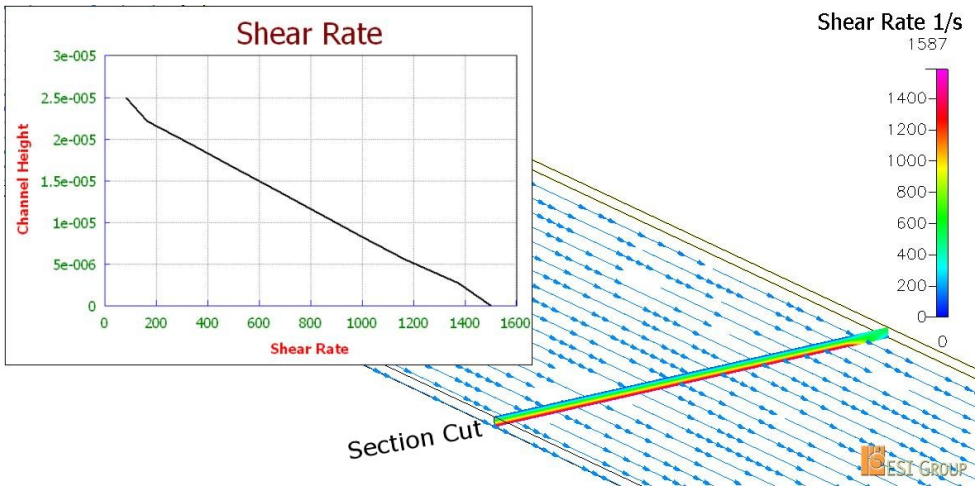

Figure 3.10: CFD Shear Rate Results

channel. As previously described, this has practical implications when it comes to using the platform for shear stress mediated response of platelet function as it largely eliminates the requirement for accurate alignment of the device over the imaging optics of a detection system.

3.3.2 Chemistry Deposition

In order to develop a platform for successful characterisation of platelet function in response to various agonists, coupled with the a well defined and characterised platform is the requirement for a well defined and characterised activating surface. While there are a number of strategies for immobilising biological species onto surfaces among the simplest is termed physisorption. Physisorption at its simplest is allowing a solution containing a known concentration of the biological species of interest sit on the substrate, onto which immobilisation is to occur, for a period of thirty minutes to two hours. The attraction is caused by inter-molecular, van der Waals forces between the species and the substrate of interest. While this immobilisation strategy is among the simplest to implement it can be susceptible to errors in reproducibility due to the relatively weak van der Waals attractive forces.

In order to investigate the surface coverage and density of Von Willebrand Factor (VWF) through physisorption two characterisation techniques were employed. The simpler of these techniques involves fluorescent staining of immobilised VWF over a range of concentrations. Four glass cover slips were coated with different concentrations of VWF ranging from $1ug/ml$ to $100ug/ml$ for two hours. The slides were then washed with Phosphate Buffer Solution (PBS). The slides were then coated with a Fluorescein isothiocyanate (FITC) labelled antibody against von Willebrand Factor for 15 minutes and subsequently washed using PBS. These slides were then imaged under a Zeiss LSM-510 Meta laser scanning confocal microscope and results are shown in Figure 3.11

While not quantitative, the data shows a clear increase in fluorescent signal with increasing concentrations of Von Willebrand Factor. This suggests that physisorbtion is a suitable method for immobilising VWF on a glass

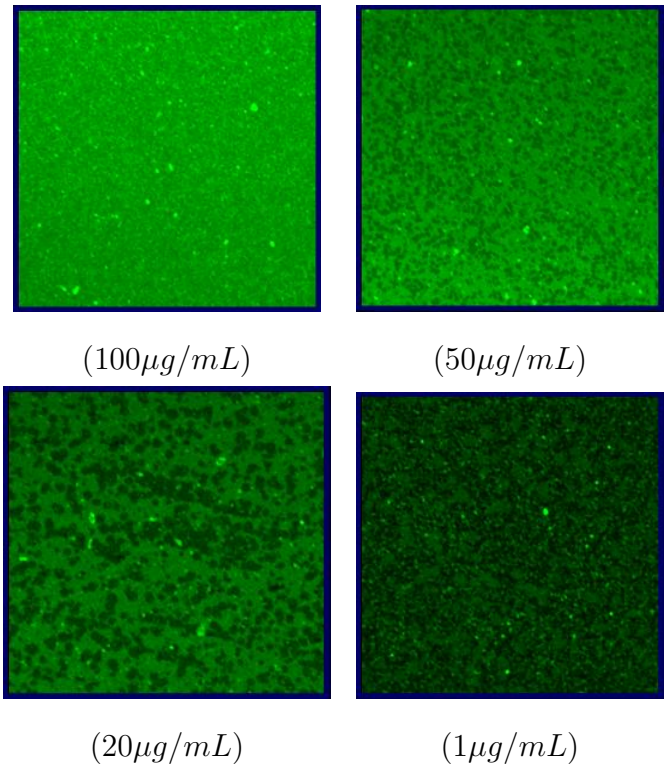

Figure 3.11: Various concentrations of immobilised VWF

surface. In order to acquire more quantitative data however, a technique known as ellipsometry was employed. Ellipsometry is an optical technique that, in its most basic configuration, exploits changes in phase and polarisation of reflected or transmitted light from or through a substrate. Sample properties such as refractive index or film thickness causes a phase shift and changes the polarisation state of the incident light. The ability to measure and characterise these changes allows the user to determine specific information, such as film thickness, from the film of interest.

In the case of characterising Von Willebrand Factor coatings of various concentrations of VWF in solution were deposited on a silicon wafer in a similar manner as the previously described on glass. Since reflection ellipsometry was being employed, silicon was deemed to be a more suitable surface for characterisation as internal reflections from glass substrates

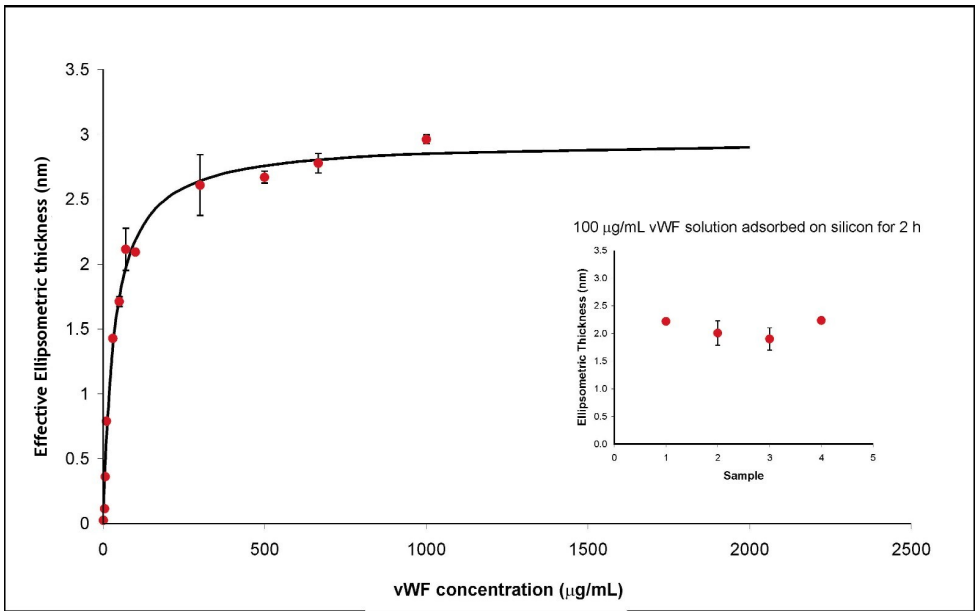

Figure 3.12: Ellipsometry data of von Willebrand Factor on Silicon

could potentially influence results. Since silicon and glass have similar material properties the van der Waals attractive forces were considered to be of a similar magnitude resulting in comparable film thickness on both glass and silicon for a given concentration of Von Willebrand Factor. The VWF solutions were deposited on silicon, left to sit for two hours, and excess VWF subsequently washed off using a combination of PBS and deionised water. Each sample was then interrogated in five individual locations, in an effort to determine coating homogeneity, using a UVISEL Spectroscopic Ellipsometer from Horiba Jobin Yvon and the results can be seen in Figure 3.12.

It should be noted that ellipsometric film thickness measurements are *effective* thickness measurements, measured over an interrogation spot size. In the case of relatively low protein concentrations, e.g. 20μg/mL as shown in Figure 3.11, ellipsometric measurements are a representation of both occupied and unoccupied protein locations and should not be confused with

homogeneous protein coverage over the entire surface.

Nonetheless the results show an increase in effective protein coating thickness with increasing concentration as expected. The saturation point occurs at a concentration point of approximately $500\mu g/mL$ and coating thickness of approximately $3nm$. The inset graph shows the reproducibility of the deposition technique for a single concentration of $100\mu g/mL$ over four individual samples. As in the previous experiment each of these samples were individually interrogated five times at different locations in an effort to characterise coating homogeneity. Overall, from both sets of experiments, the results clearly show phisisorbtion to be a reproducible and characterisable method for controlled deposition of Von Willebrand Factor on glass surfaces.

3.4 Conclusion

This chapter has detailed the main prototyping and replication techniques for thermoset polymers used in the area of BioMEMS fabrication. While some techniques are particularly suitable for rapid prototyping bridging the gap between this initial phase and pilot to mass production can be difficult as the master tools required for many replication techniques are often cost prohibitive. Manufacturing using thin film laminates was offered as a relatively new alternative to the problem of bridging this apparent gap as the patterning techniques for these films lend them selves well to prototyping technologies ,in terms of laser cutting, and mass production techniques, in terms of rotary tool and die configurations routinely used in the labelling industry. The availability of various configurations of these laminates was also highlighted in terms of offering other potential advantages for BioMEMs device development such as the adhesive nature of the many laminates facilitating the ability to rapidly seal devices and easily create multi-material,

multi-layer hybrid devices.

Using the already described laminate technologies, the design and build of a platelet function analysis device for shear mediated response in the presence of an agonist was detailed. The device exploits the tight thickness tolerances of the laminate adhesive, the ability to rapidly create hybrid polymer-glass devices and the low aspect ratio of the device builds on the flow theory as developed in Chapter 2.

A computational fluid model of the device was generated using a commercial fluid simulation software package known as CFD ACE+. This facilitated the ability to study the predicted effects of changing boundary conditions and fluid properties of the device with particular emphasis on how these changes impacted on the shear stress profile generated within the device. In order to finalise the prototype for initial testing a strategy of immobilising an activating protein on a surface was described. This strategy, among the simpler of the available techniques relies on the molecular attractions between the glass wall of the device and the protein in question, in this case Von Willebrand Factor. This strategy was then validated using fluorescence labelling of the Von Willebrand Factor imaged under a confocal microscope and further characterised in terms of protein concentration versus coating thickness, coating homogeneity over a single coated glass slide and coating reproducibilty from glass slide to glass slide. In short, the designed device for investigations into shear mediated platelet response to Von Willebrand Factor was built, characterised and made available for initial testing.

Bibliography

[1] R.M. McCormick, R.J. Nelson, M.G. Alonso-Amigo, D.J. Benvegnu, and H.H. Hooper. Microchannel electrophoretic separations of DNA in injection-molded plastic substrates. *Anal. Chem*, 69(14):2626–2630, 1997.

[2] A. van den Berg, W. Olthuis, and P. Bergveld. *Micro Total Analysis Systems 2000: Proceedings of the [Mu] Tas 2000 Symposium, Held in Enschede, the Netherlands, 14-18 May 2000*. Kluwer Academic Publishers, 2000.

[3] Babyplast 6/10 Instruction Manual *Chronoplast S.L. Barcelona*.

[4] G.J. Kellogg, T.E. Arnoldt, B.L. Carvalho, D.C. Dulfy, and N.F. Sheppard Jr. Centrifugal Microfluidics: Applications. *Micro Total Analysis Systems 2000: Proceedings of the [Mu] Tas 2000 Symposium, Held in Enschede, the Netherlands, 14-18 May 2000*, 2000.

[5] L. Lin, C.J. Chiu, W. Bache, and M. Heckele. Microfabrication using silicon mold inserts and hot embossing. *Micro Machine and Human Science, 1996., Proceedings of the Seventh International Symposium*, pages 67–71, 1996.

[6] H. Becker, W. Dietz, P. Dannberg, and G. Jena. MICROFLUIDIC MANIFOLDS BY POLYMER HOT EMBOSSING FOR μTAS APPLICATIONS. *Micro Total Analysis Systems' 98: Proceedings of the [Mu] TAS'98 Workshop, Held in Banff, Canada, 13-16 October 1998*, 1998.

[7] L. Martynova, L.E. Locascio, M. Gaitan, G.W. Kramer, R.G. Christensen, and W.A. MacCrehan. Fabrication of Plastic Microfluid Channels by Imprinting Methods. *Burns*, 144:147.

[8] L. Locasci&, M. Gaitan, J. Hong, and M. Eldefrawi. PLASTIC MICROFLUID DEVICES FOR CLINICAL MEASUREMENTS. *Micro Total Analysis Systems' 98: Proceedings of the [Mu] TAS'98 Workshop, Held in Banff, Canada, 13-16 October 1998*, 1998.

[9] J. Xu, L. Locascio, M. Gaitan, and C.S. Lee. Room-Temperature Imprinting Method for Plastic Microchannel Fabrication. *Science*, 261:895, 1993.

[10] T.J. Johnson, E.A. Waddell, G.W. Kramer, and L.E. Locascio. Chemical mapping of hot-embossed and UV-laser-ablated microchannels in poly (methyl methacrylate) using carboxylate specific fluorescent probes. *Applied Surface Science*, 181(1-2):149–159, 2001.

[11] H. Becker and U. Heim. Hot embossing as a method for the fabrication of polymer high aspect ratio structures. *Sensors & Actuators: A. Physical*, 83(1-3):130–135, 2000.

[12] K. Ueno, F. Kitagawa, H.B. Kim, T. Tokunaga, S. Matsuo, H. Misawa, and N. Kitamura. Fabrication and Characteristic Responses of Integrated Microelectrodes in Polymer Channel Chip. *Chemistry Letters*, 29(8):858–859, 2000.

[13] K. UCHIYAMA, W. XU, M. YAMAMOTO, T. SHIMOSAKA, and T. HOBO. Development of Imprinted Polymer Microchannel Capillary Chip for Capillary Electrochromatography. *Analytical Sciences*, 15(9):825–826, 1999.

[14] SA Soper, SM Ford, S. Qi, RL McCarley, K. Kelly, and MC Murphy. Polymeric microelectromechanical systems. *Anal Chem*, 72(19):642A–651A, 2000.

[15] M.A. Roberts, J.S. Rossier, P. Bercier, and H. Girault. UV Laser Machined Polymer Substrates for the Development of Microdiagnostic Systems. *Science*, 261:895–897, 1993.

[16] S. Lazare and R. Srinivasan. Surface properties of poly (ethylene terephthalate) films modified by far-ultraviolet radiation at 193nm (laser) and 185nm (low intensity). *The Journal of Physical Chemistry*, 90(10):2124–2131, 1986.

[17] M. Bowden, O. Geschke, J.P. Kutter, and D. Diamond. CO2 laser microfabrication of an integrated microfluidic manifold for application in environmental monitoring. *Lab-on-a-Chip*, 3(4):221–223, 2003.

[18] L. Brown, T. Koerner, J.H. Horton, and R.D. Oleschuk. Fabrication and characterization of poly (methylmethacrylate) microfluidic devices bonded using surface modifications and solvents. *Lab on a Chip*, 6(1):66–73, 2006.

[19] J. Li, D. Chen, and G. Chen. Low-Temperature Thermal Bonding of PMMA Microfluidic Chips. *Analytical Letters*, 38(7):1127–1136, 2005.

[20] É. Tyrrell, C. Gibson, B.D. MacCraith, D. Gray, P. Byrne, N. Kent, C. Burke, and B. Paull. Development of a micro-fluidic manifold for

copper monitoring utilising chemiluminescence detection. *Lab on a Chip*, 4(4):384–390, 2004.

[21] B.H. Weigl, R. Bardell, T. Schulte, F. Battrell, and J. Hayenga. Design and Rapid Prototyping of Thin-Film Laminate-Based Microfluidic Devices. *Biomedical Microdevices*, 3(4):267–274, 2001.

Chapter 4

Results and Analysis

4.1 Introduction

Following design, fabrication and characterisation of the parallel plate platform, the next stage in the development of the device, was to apply real world samples in order to validate the efficacy of the new design. To this end, a dual approach was taken. For the newly designed parallel plate device to be considered successful, it must first be seen to function in a comparable manner to existing commercial devices i.e. cell surface interactions must take place. Further, however, in order to be deemed a successful working prototype, the device must demonstrate the ability to function as a diagnostic indicator in its own right.To this end two sets of experiments were devised.

To validate the device itself, minimally treated, whole blood was passed through both the commercial parallel plate flow device and the newly designed device and the resulting interactions were imaged using fluorescent microscopy.

To investigate the diagnostic potential of the device, minimally treated whole human blood was compared to whole blood to which an integrin-

blocking c7E3-Fab fragment, known as Abciximab, was added. This c7E3-Fab fragment inhibits the receptor αIIbβ3 on the platelet surface. This inhibition has a dual effect preventing both, stable adhesion to VWF, as well as inhibiting fibrinogen-mediated platelet-platelet binding. Abciximab, distributed under the trade name ReoPro, is commonly used in individuals undergoing angioplasty with or without stent placement. Use of ReoPro in this setting is associated with a reduction in procedural-related ischemic complications [1]. Side effects however, can include gastrointestinal hemorrhage [2] or in rare cases thrombocytopenia [3]. While ReoPro can be seen to take effect in under ten minutes, its effects on platelet function are evident after 48 hours and low level Gp αIIbβ3 inhibition can be present for up to 15 days. In short, utilising ReoPro to characterise the efficacy of the new chip, provides an ideal test platform for the device. ReoPro sales exceeded the 380 million dollar mark in 2007, and a device offering rapid results on the efficacy of the drug in an individual would be of obvious benefit.

Among the more attractive options with using ReoPro as a test case for the device was the ability to carry out multi-parameter testing. Since ReoPro inhibits both stable adhesion of platelets on VWF and also fibrinogen-mediated platelet-platelet binding, this allowed for a dual analysis approach focussing on each interaction independently. In order to measure variations in these interactions, customised image analysis software was developed. The software was developed specifically to evaluate:

- Changes in surface coverage over time, characterising the inhibition of αIIbβ3 on stable platelet adhesion to VWF.
- Platelet cluster analysis after a predefined length of time, characterising the inhibition of fibrinogen-mediated platelet-platelet aggregation.

Specifics of the software analysis strategy are further detailed in Section 4.3.1.

4.2 Experimental Procedure

The experimental configuration used to test the parallel plate device is shown in Figure 4.1. The experimental setup consists of a Zeiss Axiovert-200 epi-fluorescence microscope (Carl Zeiss Light Microscopy, Germany) used for imaging platelet surface interactions under flowing conditions, a Harvard PhD 2000 (Harvard Apparatus) syringe pump for sample delivery to the parallel plate flow device, a temperature-controlled chamber to maintain the device at 37^o C (controller from Prior Electronics), and a liquid-cooled Quantix-57 CCD camera (Photometrics Ltd, Tuscon, AZ, USA) that records platelet adhesion events and saves them to a PC for subsequent analysis.

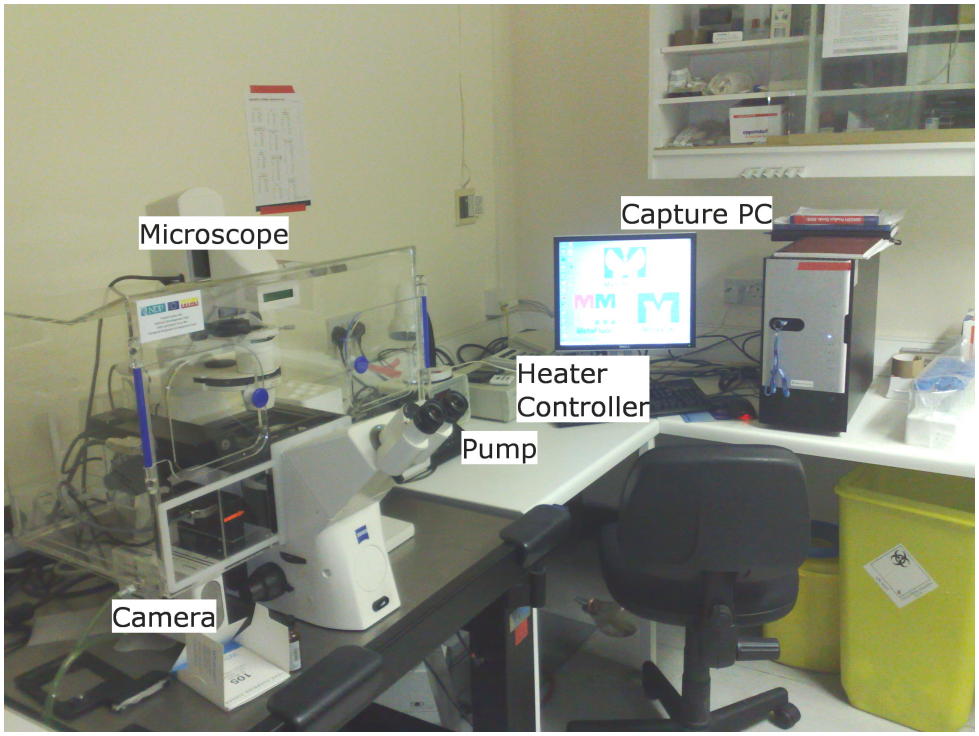

Figure 4.1: Experimental Setup

Prior to experimental runs, the channels of assembled platelet function devices were coated with Von Willebrand Factor at a concentrations of

100μg/mL in Phosphate Buffer Solution (PBS). The flow chamber was incubated for two hours at room temperature and subsequently blocked using a 1% Bovine Serum Albumin (BSA) solution for one hour. The chamber was then washed by perfusion using PBS. The intermediate step of blocking with BSA ensures platelet activation is caused only the VWF bound to the surface and any potentially exposed glass does not contribute to the observed experimental results.

In parallel to platform preparation, whole human blood was drawn from the antecubital vein of healthy donors who were not known to have taken any medication within the previous 10 days, using a 19 gauge needle. The first 5 mL of blood collected was routinely discarded to prevent any possible activation of platelets, and blood was drawn into a clean polypropylene syringe containing trisodium citrate as anticoagulant (final concentration of 0.32%, 1:9 ratio of citrate to blood). In the case of ReoPro-treated whole blood, ReoPro (20 μg/mL in whole blood; Eli Lilly & Co., Indianapolis, USA) was added to the whole blood sample 20 min prior to experimental analysis. For fluorescence imaging of platelets, both whole blood samples were labelled with 3,3'-dihexyloxacarbocyanine iodide ($DiOC_6(3)$) (1 μM; Invitrogen, USA), a fluorescent dye commonly used for platelet function studies. The labelling was carried out by by addition and gentle mixing by inversion followed by incubation for 10 min prior to experimental analysis at 37^oC.

Once the parallel plate device and whole blood have been prepared as described, the device is placed over the microscope objective and the inlet port is plumbed to a reservoir of whole blood, using 1/16' inner diameter Silastic^{TM} tubing via 1/16' threaded polypropylene connectors attached to the devices inlet and outlet ports. The outlet port of the device is plumbed to the pump via a syringe. Both the reservoir of whole blood and the chip remain inside the temperature controlled chamber at all times during the

experimental run.

Whole blood samples were assayed at a wall shear force (stress) of 6 N/m^2, which, assuming a constant blood viscosity of 0.004 Pa.s (4 cP), occurs at a volumetric flow rate through the device of 75 μL/min. This corresponds to an arterial wall shear rate of 1,500s^{-1}. In all cases, whole blood samples were assayed within two hours of the initial blood draw, as described. For each experiment, 3000 images (256 pixels x 256 pixels) were recorded at a capture rate of 24 frames/s, corresponding to an overall run time of 125 seconds; in that time, a total blood volume of 156 μL was consumed. In comparison to the existing commercial system, wherein 5 mL would have been consumed under the same shear force conditions, this represents a reduction of just under 97% in sample volume consumption.

In total, ten experiments were carried out, requiring ten parallel plate devices to be fabricated as assembled. FIve of the ten experiments carried out used whole blood treated with ReoPro, and five remained minimally treated as described ($DiOC_6(3)$ and trisodium citrate as anticoagulant). The captured images from each experimental flow run, performed as described, were then passed to a PC for investigations into the effect of ReoPro on whole blood.

4.3 Analysis

4.3.1 Image Analysis

The image analysis strategy consisted of a number of sequential steps primarily involving translating the captured image files into meaningful platelet function data followed by the application of suitable data analysis techniques depending on the metric under consideration. The first of these sequential steps involved the development of a software algorithm to auto-

matically determine platelets or platelet aggregates in a given image. Since the detection method for platelets was based on fluorescence, the software strategy utilised in platelet detection in a given image (frame) involved identifying areas of high fluorescent intensity relative to background from the given frame. In order to automate this process and increase throughput, a software package known as LabVIEW (National Instruments TX USA) was utilised. LabVIEW is a graphical programming suite capable of employing standard programming and data analysis techniques while also incorporating an extensive range of image processing capabilities making it a suitable programming environment for the application in question.The systematic approach implemented in LabVIEW can be seen summarised in Figure 4.2.

In practice, the user supplies the file name of an image, or an initial image from a sequence of images to be analysed. In the case of a sequence of images, each image file name is saved in numerically ascending order corresponding to the time point of capture. The custom software subsequently analyses each image in ascending order from this user-defined image sequence, up until a user-defined number of images is reached or until the end of the given sequence. Using this raw image (e.g Figure 4.2(a)) the software automatically selects areas of high intensity representing platelet adhesion events.

In order to determine what is to be considered an area of high intensity and what is to be considered background data, an automated threshold algorithm is implemented in LabVIEW. Any pixel value falling below this calculated threshold value is deemed by the software to be background data and given the numeric value 0 while any pixel value above the threshold is given the numeric value 1 signifying particle detection at that pixel. This automated thresholding algorithm comes predefined within the LabVIEW suite of image processing capabilities. The calculated threshold limit (k) is determined to be that pixel value k where the expression 4.1 is minimised.

This threshold algorithm is implemented for each individual image ensuring an optimum threshold value (k) is calculated for each image, thus accounting for effects such as changing background due to increased areas of platelet aggregation.

$$k = \sum_{i=0}^{i=k} h(i)|(i-\mu_1)| + \sum_{i=k+1}^{i=N-1} h(i)|(i-\mu_2)| \tag{4.1}$$

where

- μ_1 is the mean of all pixel values between 0 and k
- μ_2 is the mean of all pixel values between $k+1$ and $N-1$
- i is the gray level value
- $h(i)$ represents the number of pixels in the image at at each grey level value
- N is the total number of gray levels in the image (256 in the case of 8-bit images)

Once the threshold algorithm has been applied to the image, the resulting output is in the form of a binarised image, Figure 4.2(b), thereby allowing the software to unambiguously detect the presence or otherwise of a particle on a pixel by pixel basis. On obtaining the binarised image the next step in the data analysis involves converting this binarised image to a particle image or, in other words, converting the pixel by pixel data to particle data. Housed within LabVIEW is a particle analysis suite of tools that can store groups of contiguous non-zero particle clusters and record information related to particular attributes such as shape, size and location. In this case, particle clusters of less than 35 pixels were determined empirically to be contributing to extraneous noise and as such were disregarded by the software.

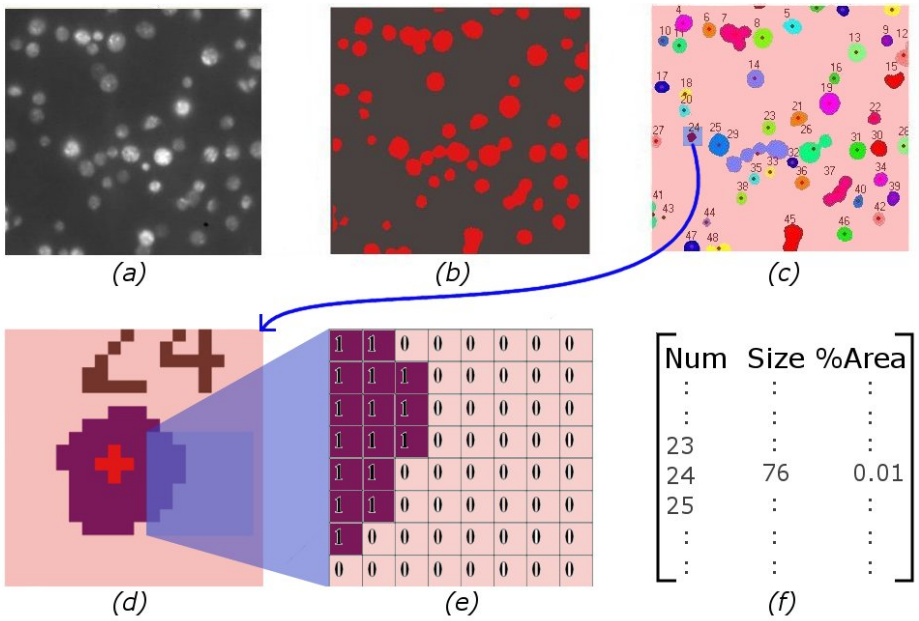

Figure 4.2: Result of image analysis algorithm

Each platelet or group of platelets is highlighted using a false colour and also numbered against a constant colour background (See Figure 4.2(c)). While there are some discrepancies between the raw and processed image, the processed image does, in the main, correlate extremely well with the raw image in terms of detecting locations and sizes of high fluorescent intensity particles i.e. adhered platelets. For each of these detected particles, for example particle number 24 in Figure 4.2(d), both the area of the particle itself and its percentage contribution to the overall image area was calculated and recorded based on individual pixel contribution (Figure 4.2(e)). The values for particle number, overall cluster size and contribution to overall image area was output to a spread sheet file for further analysis, Figure 4.2(f). This entire sequence of steps was repeated for each image for a selected flow run and data recored for subsequent analysis.

4.3.2 Data Analysis

Since ReoPro inhibits the αIIbβ3 receptor on the platelet surface, it was expected that this should affect both the amount of surface coverage via its interaction with Von Willebrand Factor and also the amount of platelet-platelet aggregation via fibrinogen-mediated platelet-platelet binding to active αIIbβ3 on the platelet surface. To this end a dual approach was taken to analysing the data as obtained from LabVIEW.

The first of these approaches involves summing the individual percentage contribution to the overall image area of each detected particle in any given image to gain an overall particle percentage coverage for that image. This is then repeated for each image in a flow run and a plot of detected changes in surface coverage can be generated for a single flow run.

The second approach takes the area of each detected particle (measured in pixels) and outputs those values so that particle areas can be compared with a view to determining aggregate sizes.

While there are a number of repetitive steps involved in the analysis, the software has been designed such that the end user need simply specify the initial image for a given flow run. The processes described have been automated and run independently of user input once the first image from a given sequence has been selected. This makes the software extremely user friendly and requires limited technical ability to operate. For analysis of a given flow run of 3000 images, the runtime of the analysis software, on a 2Ghz Core 2 processor, with 2 Gb RAM is under 60 seconds.

4.4 Results

4.4.1 Surface Coverage

As anticipated, the resulting plots of detected changes in surface coverage over time show clear differences between the untreated and ReoPro treated whole blood samples. Figure 4.3 shows the plotted surface coverage for each of the five untreated blood samples. The images on the right show representative images of an untreated flow run at the beginning, middle and final stage of an experiment. As can be seen from the images and as indicated from the graph, the surface coverage of platelets increases over time due to platelet-platelet and platelet-surface interactions.

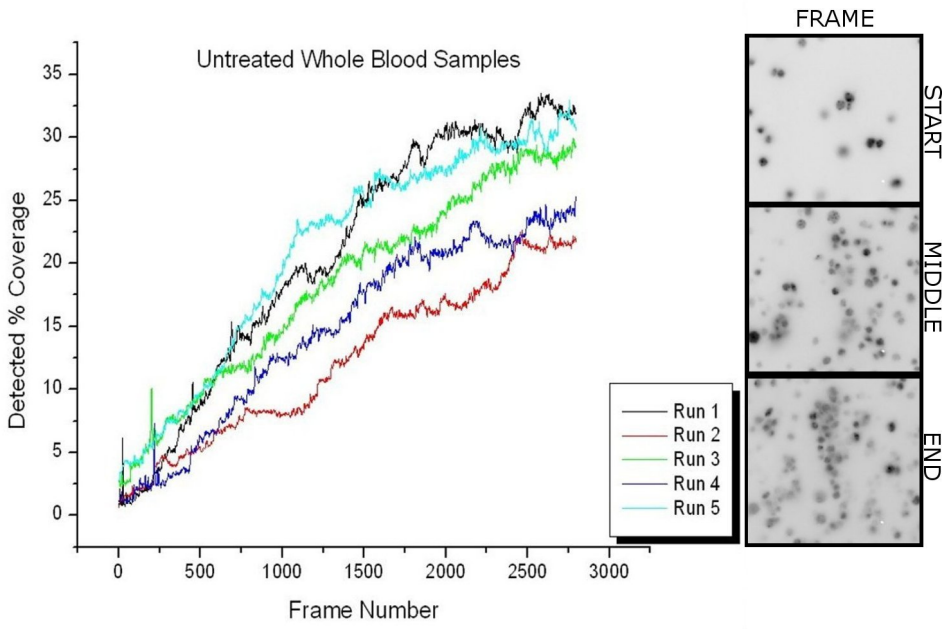

Figure 4.3: Plot showing detected surface coverage of non ReoPro-treated whole blood under physiological shear conditions in response to VWF

In contrast, the ReoPro-treated whole blood samples as shown in Figure 4.4 show an initial increase in detected surface coverage followed by a

visible decrease in surface coverage detected. This initial increase in surface coverage is mediated primarily by the interaction between the A1 domain VWF on the glass surface of the device and Gp Ib/IX/V on the platelet surface and can be seen to correlate well with the non ReoPro-treated data as expected. The apparent reduction in surface coverage can be attributed to ReoPro inhibiting receptor αIIbβ3 on the platelet surface and affecting the platelets ability to adhere in a stable manner to the C1 domain of VWF. On closer inspection of the images however, for example, the highlighted areas on the 'MIDDLE' and 'END' images in Figure 4.4, it can be seen a photobleaching effect contributes, at least partially, to this apparent reduction in surface coverage.

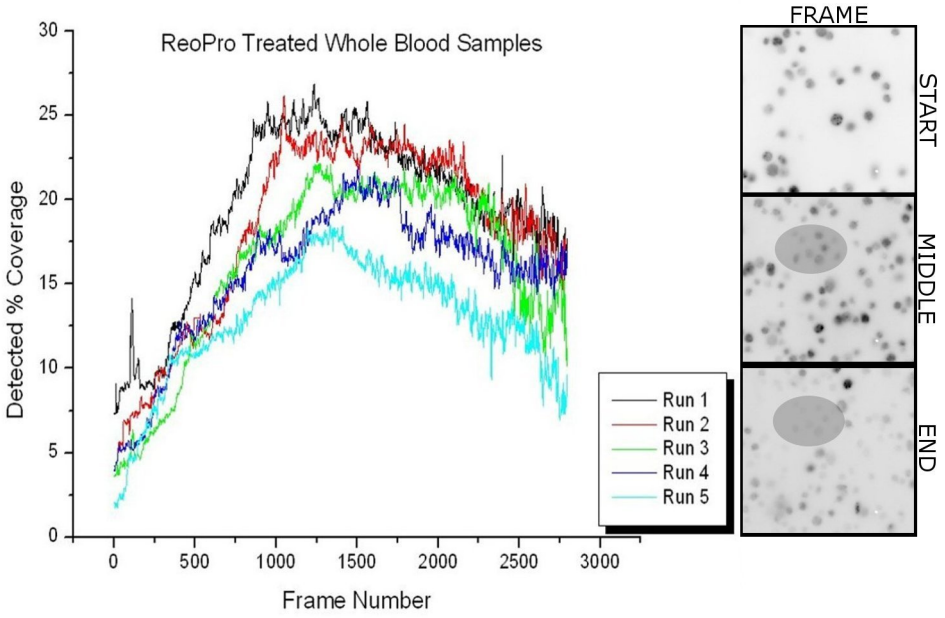

Figure 4.4: Plot showing detected surface coverage of ReoPro-treated whole blood under physiological shear conditions in response to VWF

Photobleaching is a photochemical destruction of a fluorescent molecule caused by incident light. This can cause problems when studying time

lapsed response of a fluorescent molecule, as the fluorescence decreases as a function of the incident light. In practical terms this results in a 'dimming' of the platelets adhered to the surface of the parallel plate flow device making, fluorescently labelled, adhered platelets progressively difficult to detect over time.

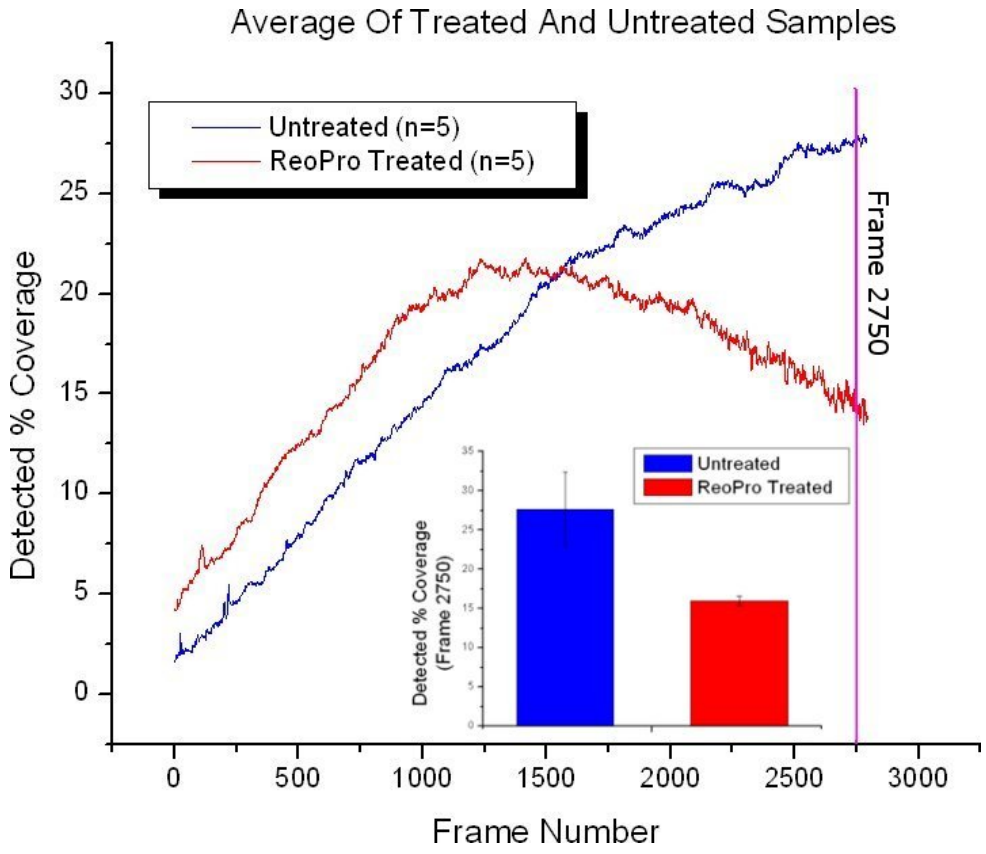

Figure 4.5: Plot of average detected surface coverage. Inset histogram of average detected coverage taken at frame 2750

This detected difference between ReoPro-treated and non ReoPro-treated whole blood can be further visualised if both sets of experimental flow runs are averaged as shown in Figure 4.5. Figure 4.5 shows the average detected surface coverage of ReoPro treated and untreated whole blood over the experimental period of 125 seconds. The inset graph shows a histogram

of average detected surface coverage from frame 2750 taken from the raw data. The histogram data shows an approximately 40% reduction in detected surface coverage on the ReoPro treated sample compared to the untreated sample.

While a photo-bleaching effect can be seen to impact, at least partially, on surface coverage analysis for ReoPro-treated whole blood, the software does demonstrate the ability to detect differences in both ReoPro-treated and untreated whole blood. However this experimental procedural effect should not detract from the overall validation of the functionality of the new device as a potential alternative parallel plate flow device for platelet function studies.

4.4.2 Platelet Aggregation

In the case of platelet aggregation analysis, a selection of 10 images (frame numbers 2745 - 2755) were taken as a representative snapshot of surface coverage at a given time. A snapshot of 10 images would give information for almost 0.5 seconds of data while also allowing noise to be averaged out of the system. The area of every detected particle in each of the 10 images was then recorded and a mean particle size and standard error recorded. The average particle sizes for each flow run can be seen in Figure 4.6

As expected the ReoPro data has a significantly lower mean particle size and smaller standard error than the untreated sample. Since ReoPro inhibits fibrinogen-mediated platelet-platelet binding via receptor αIIbβ3, this in turn inhibits the formation of platelet aggregates on the surface. In contrast, the mean detected particle size for the untreated sample is significantly greater than in the case of the ReoPro-treated sample, indicating larger platelet aggregates. Further, the standard error of these particles is also significantly larger in the case of the untreated samples, indicating a

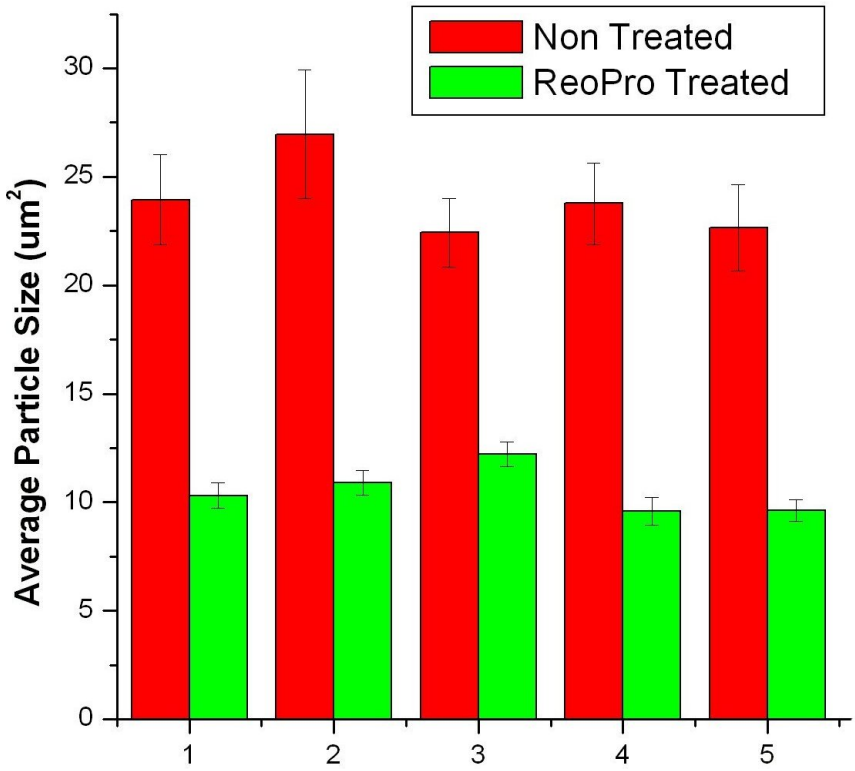

Figure 4.6: Average platelet aggregate distributions on treated and untreated samples

larger spread of platelet aggregate sizes i.e. from single platelets to platelet aggregates.

4.5 Conclusions

The newly designed parallel plate device was shown to function with significant advantages over existing commercial systems. These advantages are:

- The device can be permanently assembled, thereby eliminating the requirement for extraneous hardware for ensuring a consistent seal during a flow run. This sealing also facilitates a more reproducible

and controlled environment for protein deposition as well as reducing the amount of protein required of a single platform assembly.

- The reduction in flow path over the commercial device represents a significant reduction in the flow rate required to generate a given shear force (a reduction of approx 97% in the case of a physiologically relevant shear stress of 6N/m^2). This has significant implications when running multiple tests on a single sample.

The functionality of the device and manufacturing strategy was validated using fluorescently labelled platelets in a whole human blood sample. Five minimally-treated samples were passed through the device and a series of fluorescent images of platelet interactions were recorded. Further, an additional five samples were treated with a commercially available integrin blocker used primarily for reducing platelet-platelet aggregations. These samples were also passed through the newly designed parallel plate devices under the same conditions as the minimally treated samples.

The effect of the integrin blocking agent, ReoPro, was investigated in two ways. A software algorithm was developed to investigate both surface coverage representing the αIIbβ3 VWF surface interaction while a particle size distribution algorithm was developed to investigate fibrinogen-mediated platelet-platelet binding via the αIIbβ3 receptor. In the case of the surface coverage significant differences were seen in the profile of changes in surface coverage over time. While some of these changes may be attributable, in part, to a photobleaching effect, this experimental effect does not detract from the fact that differences in ReoPro and non ReoPro-treated whole blood samples under shear are observed in the newly designed parallel plate flow device. In the case of particle size distribution, the untreated whole blood shows both a larger average particle size and larger standard deviation of particle sizes than the ReoPro-treated whole blood. This indicates a

larger level of localised platelet-platelet aggregations as would be expected under normal conditions in response to VWF.

In short the new device performs with diagnostic potential, requiring a significantly reduced volume flow rate for a given flow run while also being a more user-friendly device. Further, automated software was developed to characterise these differences in a time-efficient, unbiased manner.

Bibliography

[1] A.M. Lincoff, J.E. Tcheng, R.M. Califf, D.J. Kereiakes, T.A. Kelly, G.C. Timmis, N.S. Kleiman, J.E. Booth, C. Balog, C.F. Cabot, et al. Sustained Suppression of Ischemic Complications of Coronary Intervention by Platelet GP IIb/IIIa Blockade With Abciximab One-Year Outcome in the EPILOG Trial. *Circulation*, 99(15):1951–1958, 1999.

[2] S.M. Trivedi, J. Shani, and G. Hollander. Bleeding Complications of Platelet Glycoprotein IIb/IIIa Inhibitor Abciximab (ReoPro). *Journal of Invasive Cardiology*, 14(7):423–425, 2002.

[3] S.D. Berkowitz, R.A. Harrington, M.M. Rund, and J.E. Tcheng. Acute profound thrombocytopenia after C7E3 Fab (abciximab) therapy. *Circulation*, 95(4):809–813, 1997.

Chapter 5

System Modifications

5.1 Introduction

In the previous two chapters the validation of a manufacturing technique for the development of a parallel plate type platelet function device has been reported. Further, in these chapters the development of a design based on commercially available devices, its implementation and testing using custom design software for validation of treated and untreated blood is described. This chapter reports further system enhancements which builds on these developments while also deviating significantly from the traditional parallel plate type device and associated detection systems. Some of the problems inherent in the parallel plate type device for shear-mediated platelet surface studies are discussed while the advantages of a lower cost, dedicated detection system which has the propensity to make these platelet function tests more accessible to clinical laboratories are highlighted. The ultimate goal is to make these entire systems readily accessible to a general practitioners for a rapid low cost platelet function test. The first section of the chapter details the deviations from the traditional parallel plate type device and proposes a unique solution by combining two microsystem techniques

without compromising shear-mediated response. In the remaining section of the chapter the development of a dedicated bench-top readout system incorporating the optical microscopy, fluid delivery, thermal stability and software integration is discussed. This leads to a functional device comparable to existing large scale, laboratory based, financially prohibitive readout devices.

5.2 Chip Design

Among the main advantages of the parallel plate-type flow chamber is the particular nature of the governing equations describing the device, ensuring an almost constant wall shear force along the imaging wall. It is this advantage of the device, however, that up until now has had negative impact on the amount of sample required. Typical devices are on the order of millimetres across while typical detection areas are on the order of microns. This results in a significant fraction of the sample passing through the detection system undetected. Further, while the device as described in Chapters Three and Four did provide a significant improvement over existing commercial devices in terms of required volume flow rate, the common requirement for syringes and tubing for storing and delivering sample in, resulted in the requirement for significant portion of sample dead volume for any given flow run. Considering these disadvantages, a new type of flow chamber was developed in an effort to:

1. Further reduce required sample volume for an entire experiment.

2. Efficiently utilise any sample passing through the device to ensure maximum amount of sample passes over the detection area.

To this end, a platform was developed to combine the advantages of the parallel plate flow chamber exploiting the microscale nature of the flow

regime by utilising a variation of the hydrodynamic flow focussing effect shown in Chapter 1.

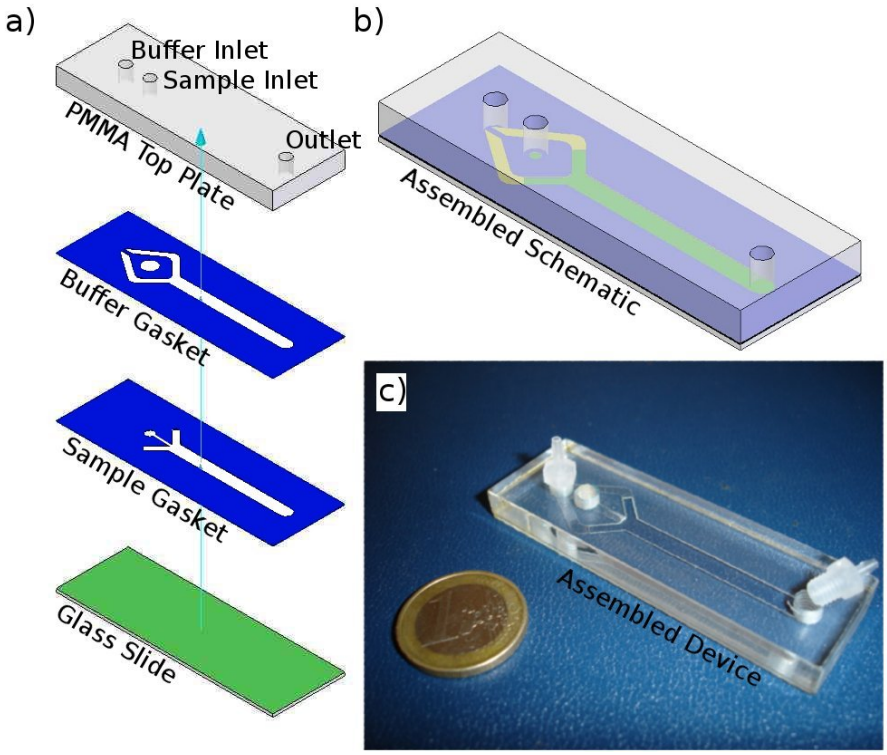

Figure 5.1: Dual inlet platelet flow device

Figure 5.1 shows an illustration of the proposed device. Figure 5.1 (a) shows an exploded view of the device while Figure 5.1 (b) and (c) shows the chip in assembled form as schematic and actual device, respectively. In contrast to the previous (single inlet) device described in Chapters Three and Four, this (dual inlet) device uses multiple layers of adhesive material to form a three dimensional flow chamber. The ability of the PSA to be patterned and stacked sequentially makes this a very attractive option for chip manufacture and opens up another avenue for conceptual design and manufacture of microfluidic devices. The resulting effect of this three dimensional configuration results in the sample flow stream being focussed towards the centre of the device while also being shaped in such a way as to ensure con-

tact with the protein-coated activating wall where shear-mediated platelet surface interactions are being investigated. This hydrodynamic 'shaping' effect is mediated by the introduction of a buffer solution which runs through the device in tandem with the sample as shown in Figure 5.2. Since flow in micro devices is primarily laminar in nature, the introduction of this secondary/buffer flow will have minimal impact on the physiological components of the blood stream. Any mixing will be primarily a diffusive process and at appropriate flow velocities can be deem insignificant to the operation of the device.

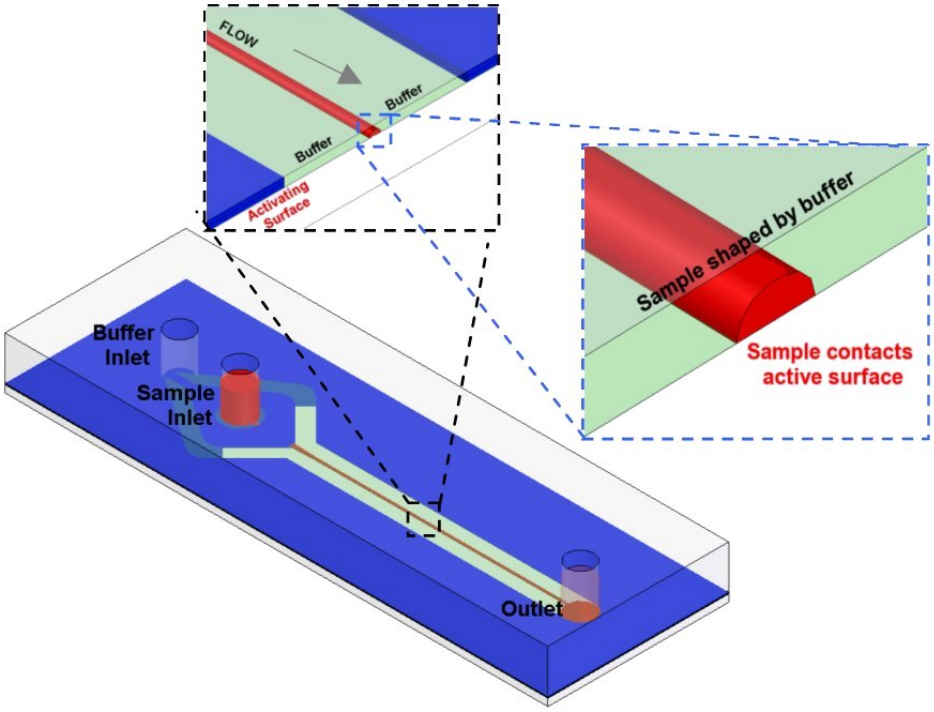

Figure 5.2: Schematic of the hydrodynamic shaping effect in parallel plate flow configuration.

This dual inlet chip is manufactured in a similar manner to the single inlet chip as described earlier.

For the top plates, 6-mm-thick PMMA stock (Ensinger Plastics, UK) is machined to standard microscope slide dimensions, 75 mm long x 25 mm wide, using conventional milling. This piece is then drilled and tapped to accept inlet and outlet connection ports.

The middle layer materials, which define the flow path, are manufactured from the same commercially available double-sided pressure-sensitive adhesive (PSA) laminate. ArCARE 8890®(Adhesives Research, Limerick Ireland) is a 12.5-μm polyester film coated on both sides with a medical-grade acrylic adhesive, resulting in an overall thickness of 50 μm. The flow path layers were cut using a Coherent GEM-100™liquid-cooled CO_2 laser embedded in a Micromaster Turnkey dual-head laser system from Optec SA, Belgium. As with the top plate, the outer dimensions of the PSA laminate layer correspond to microscope slide dimensions.

The base layer of the platform was chosen to be a commercially available glass microscope cover slip. This base material was chosen since high quality glass cover slips are a widely available commodity with tightly controlled dimensional, optical, and surface-finish tolerances, in addition to having predictable and reliable surface chemistry.

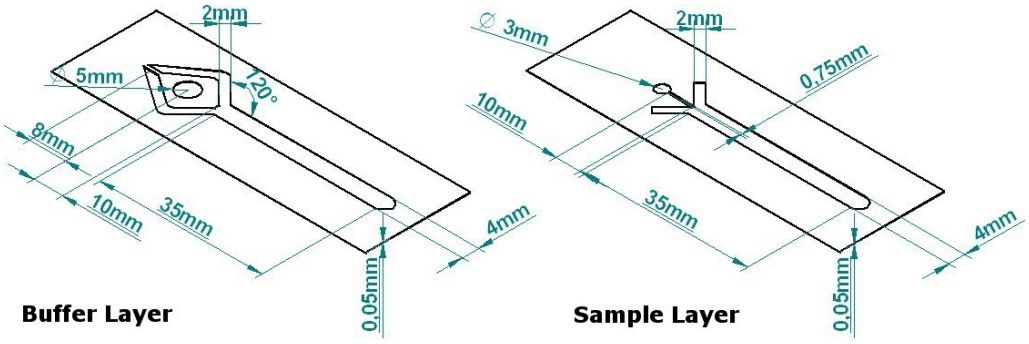

Figure 5.3: Dimensions of pressure sensitive layers. Buffer layer shown left and Sample layer shown right.

In terms of dimensions of both flow defining layers, the main flow channel of the 'Buffer Gasket Layer' as indicated in Figure 5.3, is patterned to be 4 mm wide in order to maintain the same aspect ratio as the previous single inlet device (1:400). Each of the bifurcated channels is 2 mm wide in an effort to minimise the pressure drop when recombining with the overall channel width of 4 mm. The main channel length was designed to be 35 mm in order to provide flexibility in terms of imaging and to ensure imaging could be carried out down stream of any entrance length effects in the main channel of the device. Further to the flow defining channels there is also a 5mm diameter hole in the gasket allowing sample access to the 'Sample Gasket Layer'. The 'Sample Gasket Layer' as indicated in Figure 5.3 contains the same main channel dimensions of 4mm wide x 35 mm long and height defined by the gasket thickness of 50 μm. The entrance area consists of a 750 μm wide x 10 mm long channel for sample delivery to the device. Further, the layer contains a similar bifurcation to the 'Buffer Gasket Layer' allowing for buffer fluid entrance effects to be minimised as much as possible before introduction to the sample entrance area.

Assembly of the device is also carried out in a similar manner to the single inlet device. The glass cover slip is placed in a custom designed alignment jig while sequential layers of patterned PSA are added (as indicated in Figure 5.1) followed by the top plate of the device. The entire fixture is then pressed together through two rollers to form a sealed device. As described previously the platform undergoes a thorough cleaning protocol involving a wash step with absolute ethanol which is then allowed to evaporate prior to chamber assembly and rinsing by perfusion with aqueous buffer (PBS) post assembly.

5.2.1 Chip Operation

In terms of standard device operation, the device operates under a summation of flow rates principle. The application of a negative pressure, typically via a pump, at the outlet generates a volume flow rate (Q_o) through the device. In order to satisfy conservation of momentum this flow rate Q_o must, equal the sum of both the flow rate through the buffer inlet (Q_b) and flow rate through the sample inlet (Q_s). If, however, the volume flow rate through the buffer inlet Q_b was also independently controlled, via an additional pump, this in turn would facilitate indirect control of the sample flow rate Q_s through the device for a given fixed outlet flow rate. In other words

$$Q_s = Q_o - Q_b$$

In principle, for a fixed outlet flow rate Q_o there are three possible outcomes

- $Q_b = Q_o \Rightarrow Q_s = 0$. (Resulting in no net sample flow.)
- $Q_b > Q_o \Rightarrow Q_s$ is -ve. (Resulting in sample flow out from the device.)
- $Q_b < Q_o \Rightarrow Q_s$ is +ve. (Resulting in sample flow through the device.)

For the remainder of this Chapter consideration will only be taken to the case where $Q_b < Q_o$ i.e sample is flowing though the device.

Consider the case where the outlet flow rate of the device Q_o is fixed at 0.6 mL/min (corresponding to a physiological shear rate of 1500 s^{-1}). For a fixed buffer flow Q_b of 0.4 mL/min and in order to maintain the principle of conservation of momentum this results in the flow rate of sample (Q_s) through the device being 0.2 mL/min. Figure 5.4 illustrates the effect of

varying the buffer flow rate Q_b over a range of flow rates for a fixed outlet flow rate of Q_o of 0.6 mL/min.

As can be seen from Figure 5.4 as the buffer flow rate is increased the sample volume (red dye) through the device becomes narrower. However since the overall flow rate through the main channel is constant the shear force imparted on the wall remains constant. It should be noted that there are relative fluid viscosity issues to be taken into consideration and these will be dealt with in the following sections. In this case, however, both dye and water were considered to have the same viscosity (0.001 Pa.s). In an effort to gain a more quantitative impression of events occurring as buffer flow rate is varied with respect to a fixed outlet flow rate, the images in Figure 5.4 were further analysed.

Figure 5.5 show the effect of varying the buffer flow rate between 0.4 and 0.59 mL/min for a fixed outlet flow rate of 0.6 ml/min. The graphs were obtained by taking a 10 pixel wide sample band through the centre of each of the images shown in Figure 5.4. A representative sample band in shown in Figure 5.5 (a). The pixel values in the 'Y' direction as indicated in Figure 5.5 (b) were averaged and plotted against the corresponding pixel position 'X' as indicated in Figure 5.5 (b). Figure 5.5 (c) shows the resulting plots of sample widths over the range of buffer flow rates as described. As expected, as the volume flow rate of buffer increases relative to a fixed outlet volume flow rate, the amount of sample passing through the chip is seen to visibly decrease. Since the sample flow rate through the device is now independent of overall flow rate through the device this means significantly less sample is required for a given experimental flow run. This reduction in overall required sample, also facilitates alternative sample delivery techniques to the device. Since sample flow rate through the device is on the order of μL/min and any dead volume requirements have been circumvented by the introduction of the buffer solution, μL sample volumes can be delivered directly

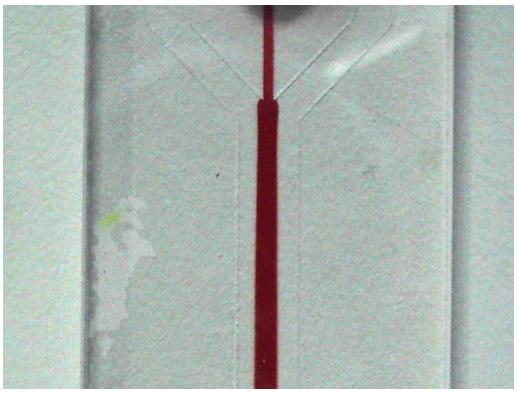

$0.4mL/min$

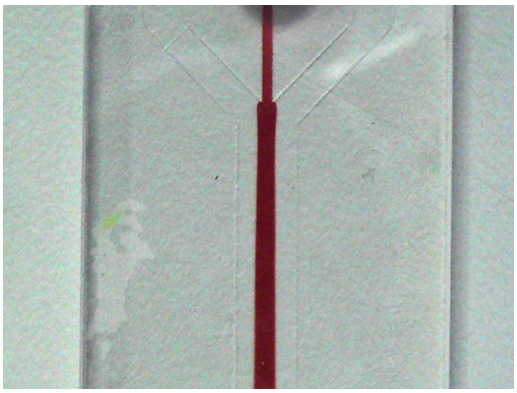

$0.44mL/min$

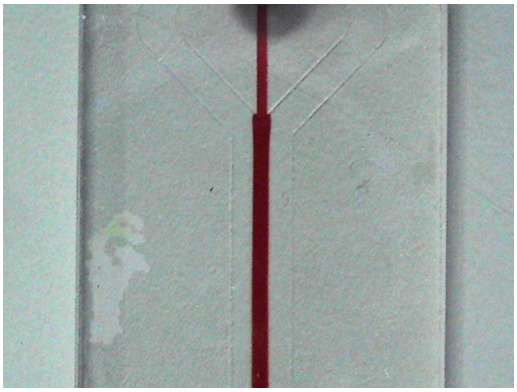

$0.48mL/min$

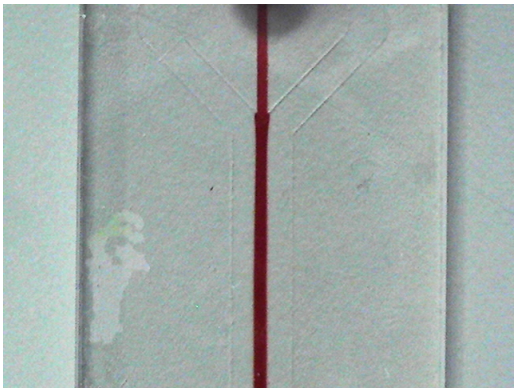

$0.52mL/min$

$0.56mL/min$

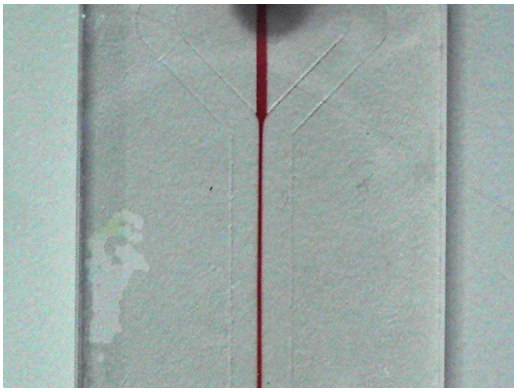

$0.58mL/min$

Figure 5.4: Flow variation due to hydrodynamic shaping

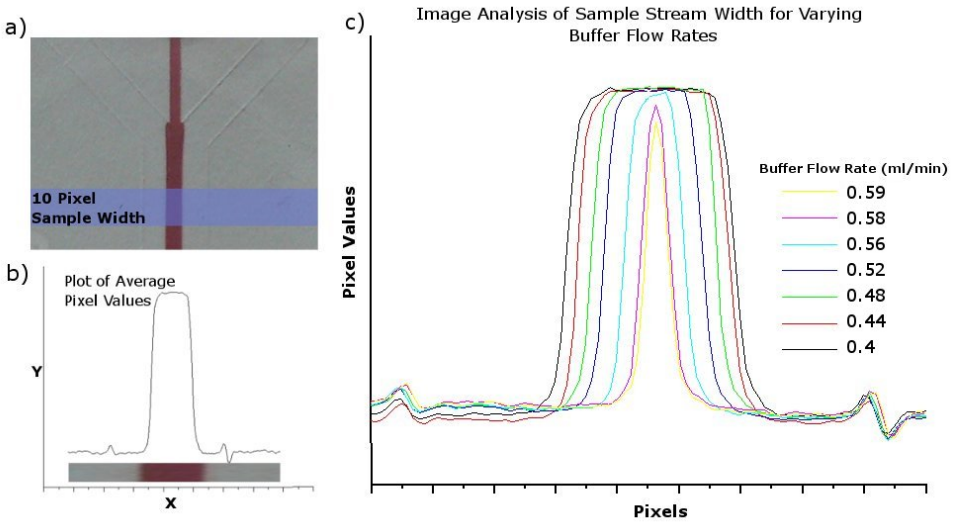

Figure 5.5: Profiles of observed variations in sample width caused by variations in buffer flow rate.

into the sample inlet port of the device, without compromising device function. This method of delivering sample also has the potential to facilitate a 'finger stick' type approach for sample delivery, thereby eliminating the requirement for citrated blood and also making the entire procedure more patient friendly compared to a relatively intrusive blood draw via syringe.

In order to gain a deeper understanding of this shaping effect and to allow more flexibility in its exploitation, a Computational Fluid Dynamic model of the device was developed. In a similar manner, to the single inlet device previously described, the symmetry of the device could be utilised in the preprocessing stage of model development in order to maximise run time while minimising the computational power required for a convergent solution.

Figure 5.6 shows the grid generation stage of the model development which highlights the symmetrical nature of the model. In contrast to the single inlet device, symmetry is only available in a single dimension for the

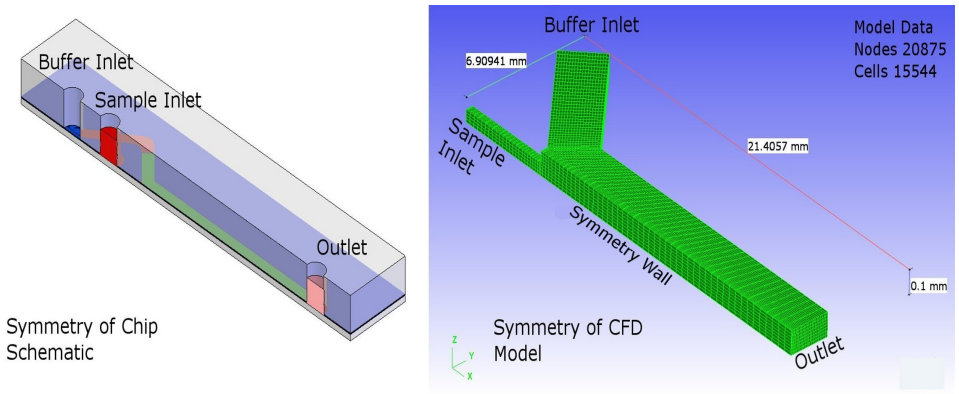

Figure 5.6: Dual-inlet device schematic and CFD model highlighting device symmetry.

dual inlet device, thereby resulting in a model containing 20875 nodes and 15544 cells. In order to improve accuracy of the model in the area surrounding the shaped stream, a technique known as power factor reduction of the mesh size, was implemented. Power factor reduction essentially, increases cell density in the areas of interest of the model (in this case, along the centre stream) at the expense of a reduction of cell density in areas of less interest on the model. The net effect of power factor reduction is an improvement in resolution of modelled data output in the areas of interest, at no extra computational cost. This is offset by a reduction in data quality in areas of less interest in the model. For simulation purposes both the platform outlet and buffer inlet of the device were modelled as inlets and the sample inlet of the device was modelled as an outlet.* A symmetrical wall boundary condition was placed on the wall as indicated in Figure 5.6.

For the simulation phase, buffer was modelled as a continuum fluid with a density (ρ_{bu}) of $997kg/m^3$ and a dynamic viscosity (μ) of $0.004Pa.s$ while

*From a modeling perspective any active inlet or outlet i.e. any port connected to a pump is typically modelled as an inlet. Similarily any non active port (in this case the sample inlet port) is typically modelled as an outlet.

blood was also modelled as a continuum with a density (ρ_{bl}) of $997kg/m^3$ and initially with a matched viscosity of $0.004Pa.s$

The symmetrical boundary conditions, as described, were imposed on the geometry and the mass flow rate through the model outlet was determined to be 2.5 x $10^{-6}kg/s$. This value was found using equations developed in Chapter 2 and taking into account the symmetrical boundary conditions and based on a wall shear stress of $6N/m^2$, representative of a typical vascular shear stress. The buffer flow rate was inputted over a range of 7 values from 2.45 x $10^{-6}kg/s$. to 1.66 x $10^{-6}kg/s$. in increments corresponding to the flow rate increments as described in Figure 5.5. The default solver for CFD ACE+ utilises the finite volume method as described in Chapter 2 and running the model under these conditions resulted in a model convergence after an average of 57 iterations per analysis with a total run time for all 7 variations in buffer inlet flow rate of 482 seconds.

Once the results for each buffer flow rate had been calculated this was compared to the experimentally derived image analysis data from the actual device in an effort to validate and further utilise the model to gain more information specific to its application as a platelet function device. In order to perform the validation, the interface between buffer and sample as calculated by the model was compared to the experimentally derived interface between the buffer and sample as shown in Figure 5.5.

Figure 5.7 shows the correlation between the buffer sample interface as obtained experimentally (solid lines) and those obtained using the computational model (dashed lines). While there are variations between modelled and experimental data, the model can be seen to correlate extremely well with image data in the area of flow rates of interest as shown in Figure 5.7. In areas of apparent disparity, (e.g area of Figure 5.7 labelled 'Diffusion') the magnitude of error can be attributed to the fact, the model neglected any diffusion effects between sample and buffer solution while this diffusion

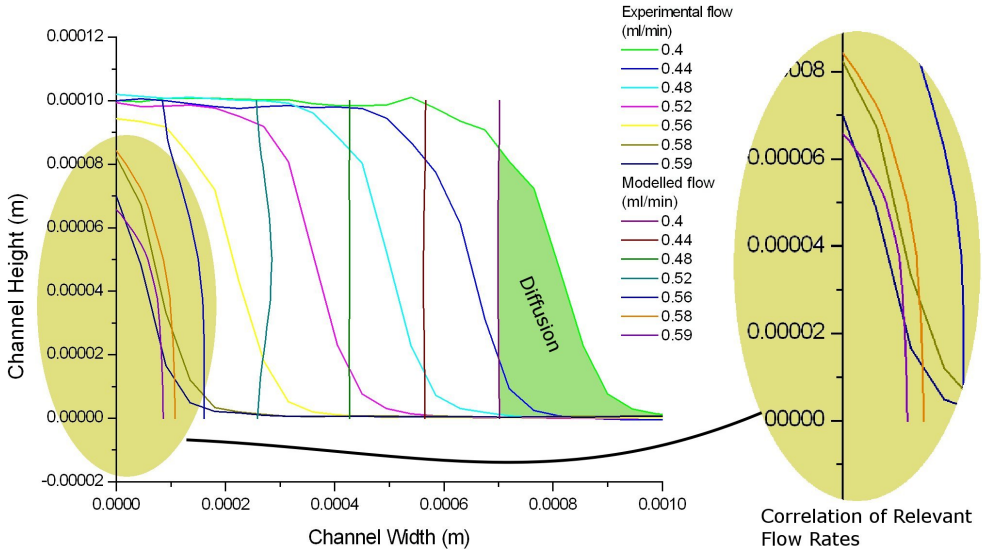

Figure 5.7: Plot of comparisons between modelled and experimentally derived buffer-sample interfaces for a fixed outlet flow rate and over a range of buffer flow rates.

gradient is clearly visible in the image data. Furthermore, considering the cell-to-cell distance of the model increased laterally away from the centre of the model due to power factor reduction of the mesh, disparities between model and image data in these areas of reduced interest were expected. In general, however, the computational model compared favourably to the experimental results in terms of rate of reduction of sample stream with increasing buffer flow rate and, as such, was deemed a valid model for further investigations into the effect of hydrodynamic shaping.

Of significant importance to the reproducible functionality of the device is the determination of entrance length effects of the device and also the effect of a mismatch in the viscosities of both buffer and sample.

Entrance Effects

Since, for a constant wall shear stress in the main channel, the outlet flow rate must remain fixed, varying the buffer inlet flow rate can have dramatic effects on the shear stress generated in the sample channel. If the volume flow rate through the buffer channel is reduced, in order to conserve the overall mass flow rate through the device, the sample channel flow rate must increase by the same volume flow rate. Due to the relative channel cross sectional areas, however (buffer channel cross-sectional area ≈ 11 times sample channel cross sectional area), this increase in sample channel volume flow rate dramatically increases the sample velocity through the sample channel inlet.

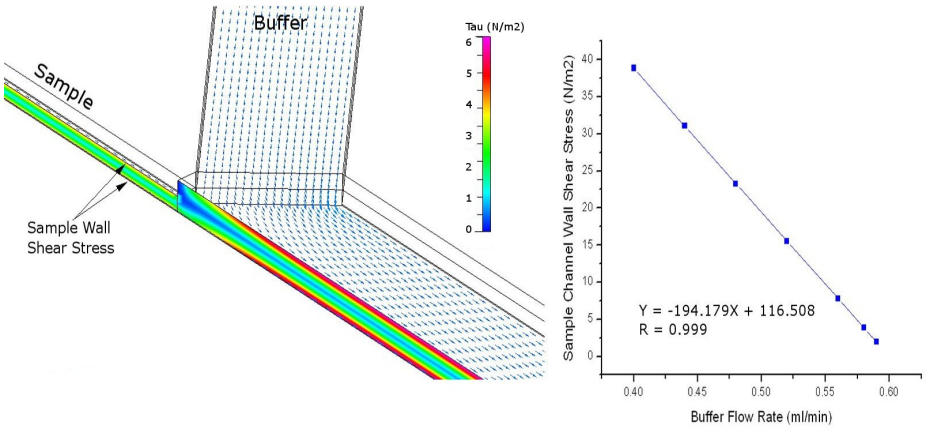

Figure 5.8: Computational model showing shear stress distribution through the dual-inlet chip for an outlet flow rate of 0.6 mL/min and a buffer flow rate of 0.59 mL/min. The graph on the right shows a plot of max shear stress in the sample channel over a range of buffer flow rates for a fixed outlet flow rate fixed of 0.6mL/min.

This increased sample flow velocity directly impacts viscous shear force generated at the wall of the sample inlet channel. To this end, the maximum wall shear stress through the sample channel for each buffer flow rate was

plotted against buffer flow rate and the resulting graph is shown in Figure 5.8. Figure 5.8 shows the shear stress distribution along the centre plane of the dual inlet device (in this case for a buffer flow rate of 0.59 mL/min) The graph to the right shows a plot of maximum (wall) shear stress (as indicated in Figure 5.8) along the sample channel for each given buffer volume flow rate. As can be seen from the graph, reducing the buffer flow rate for a fixed outlet flow rate (in this case 0.6 mL/min) significantly increases the wall shear stress generated along the sample channel. Under normal operation, the shear stress in the main channel is fixed at $6N/m^2$ In order to ensure that this is the maximum shear stress applied to the sample, based on the obtained linear relationship, the buffer flow rate should be greater than 0.5688 mL/min. Any flow rate less than 0.5688 mL/min would result in a shear stress greater than $6N/m^2$ in the sample channel, thereby causing potential platelet activation prior to platelets entering the test area of the device.

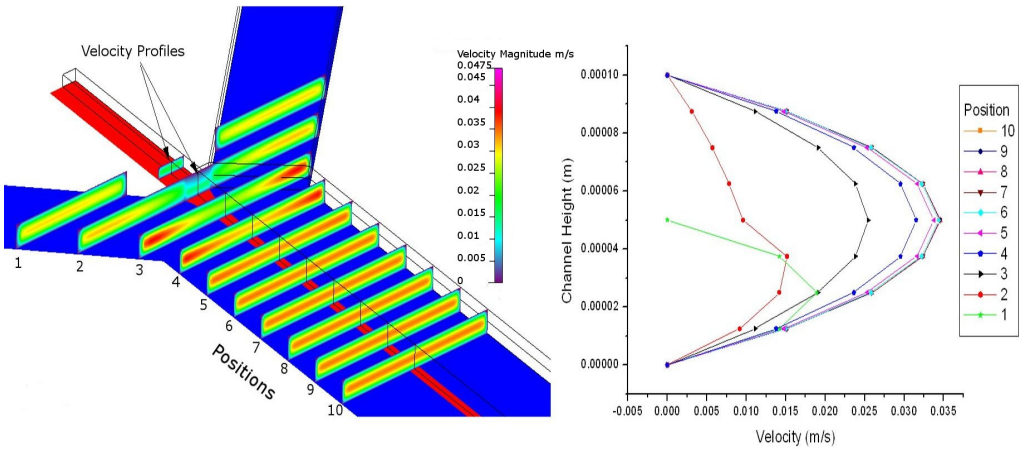

Figure 5.9: Visualisation of velocity profile development through the chip. The graph on the right illustrates the velocity profiles in the direction of the flow along the center of the chip as indicated. Each profile, 1-10, as shown on the graph corresponds to location 1-10 as shown on the model.

The model was then re-simulated using this buffer volume flow rate of 0.5688 ml/min and investigations into flow development were carried out. As in the case of the single inlet platform, as the flow stream enters the device there is an entrance length over which the flow profile goes from a transitional state to a characteristic fully developed parabolic flow profile. Figure 5.9 charts the progress of the velocity profile as it moves from the sample entrance area to further down the main channel of the device. The graph on the right of Figure 5.9 shows the velocity profile taken at each position as indicated on the CFD model. As the flow progresses down stream the profile becomes more developed until it can be assumed to be fully developed at position 5 as indicated in Figure 5.9 corresponding to just over 3 mm downstream of the sample entrance position.

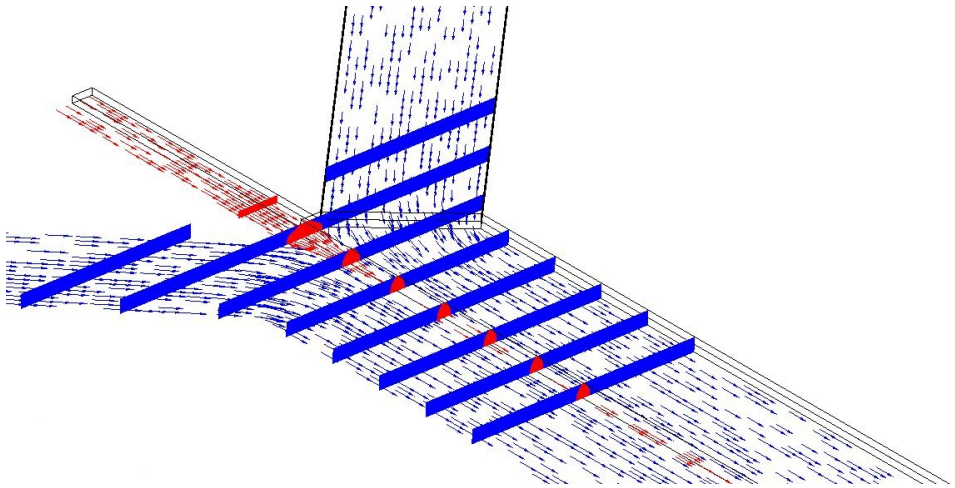

Figure 5.10: Computational model of buffer progression through the device for a maximum practical buffer flow rate of 0.5688 mL/min

Further, the development of the sample stream through the device at the minimum practical flow rate of 0.5688 mL/min was investigated. Figure 5.10 shows the progression of the sample stream as it enters the main channel and traverses through the main channel of the device.

Viscosity Mismatch

All the model data above were based on the assumption of equivalent buffer and sample viscosities ($\mu = 0.004 Pa.s$) resulting in a wall shear stress of 6 N/m^2. In practice however there may be slight discrepancies between the buffer and sample viscosities over a range of sample heights within the main channel. Chapter 2 dealt with the development of equations describing two fluid flow of varying viscosities at various heights between two parallel plates. Utilising these equations the effect of a mismatch of viscosities between buffer and sample, as a function of channel height were tabulated.

Buffer Viscosity (Pa.s)	Sample Viscosity (Pa.s)	Wall Shear Force (N/m^2) at Various Sample Heights				
		10μm	25μm	50μm	75μm	100μm
0.004	0.003	6.3	6.5	6	5.2	4.4
0.004	0.0035	6.1	6.3	6	5.6	5.2
0.004	0.004	6	6	6	6	6
0.004	0.0045	5.9	5.8	6	6.3	6.7
0.004	0.005	5.9	5.7	6	6.6	7.5

Table 5.1: Table showing the effect on wall shear force of varying sample viscosity and sample height in channel.

Table 5.1 shows the effect on sample height on wall shear stress over a range of viscosity values from 0.003 to 0.005 Pa.s for a fixed buffer viscosity of 0.004 Pa.s. In the case where both, sample viscosity and buffer viscosity, are 0.004 Pa.s, no net effect on wall shear stress is observed, since relative viscosities remain constant.

However, in cases of mismatches between sample and buffer viscosities, the effects relative height, on wall shear stress are observed. For example, in the case of a sample viscosity of 0.003 Pa.s, at an in channel height of 10

μm, the calculated wall shear stress is 6.3 N/m^2 as opposed to the desired shear stress of 6 N/m^2. As the relative height increases to 100μm, this wall shear stress is seen to decrease to a value of 4.4 N/m^2. It is worth noting that these figures were calculated on the basis of infinitely wide parallel plates as described in Chapter 2.

In practice, the fact that the buffer surrounds the sample stream from both sides, rather than creating the idealised modelled scenario, would serve to reduce the mismatch between desired and actual wall shear stress. Since the buffer, of known viscosity, surrounds the sample stream from both sides and on top, the buffer stresm would have a greater influence on the wall shear stress through the device than calculated in the idealised parallel plate flow case.

Also of relevance is the fact, the most significant deviations between desired and calculated wall shear stress, occur at a height of 100μm, or in effect, when there is no buffer flow through the system. This has implications when using the standard single inlet-single outlet flow chamber as any deviation between mean and actual blood viscosity may result in experimental error [†]. While this effect is not eliminated using the dual-inlet device the introduction of a known viscosity buffer serves to reduce this experimental error.

5.3 Detection System

In parallel with the development of the new platelet function fluidic device a dedicated readout system was also developed. Current systems are, expensive, bulky, require significant technical expertise to operate and do not

[†]While it is possible to measure each individual whole blood sample, this is impractical in terms of both time and cost for any given flow run. Many laboratories calculate required volume flow rates based on a whole blood viscosity values taken from literature

lend themselves well to the potential point of care setting, that the newly designed platform has the capacity to operate within. To this end, a new, bench-top, user-friendly readout system was designed and developed. This detection system comprises three main sub assemblies, each having the capacity to operate independently or as part of the overall system. Each of the sub-assemblies are detailed in the following section.

5.3.1 Readout System Sub-assemblies

Optical

The optical system for fluorescent platelet detection was configured in an epi-fluorescent format as shown in Figure 5.11 with a blue laser diode (Phototmetrics, excitation wavelength 473nm) used as an excitation source. This beam was expanded, collimated and subsequently reflected from a dichroic mirror through a 20x objective. The spot size generated through the objective can be tuned using the expansion optics. However for the purposes of the platelet readout device, the spot size is approx. 500 μm thereby generating an even illumination over the detector field of view. On excitation with blue light, any resulting fluorescence passes through the objective and the dichroic mirror, becomes reflected from a standard mirror, passes through an optical band pass filter, and falls on the charged coupled detector (CCD) device (Prosilica EC1350 series firewire device). This CCD sensor lies 160mm from the base of the objective, corresponding to the manufacturers tube length guidelines where by magnification of 20x is ensured. The excitation source, associated optical filters and mirrors are all readily interchanged, thereby increasing the flexibility of the microscope for investigations into use of different fluorescent stains. In the case of our experiments, however, the excitation source and filter set were chosen to match the previously used $DiOC_6(3)$ in terms of optimisation of fluorescent

signal capture. See inset graph Figure 5.11 for spectral data.

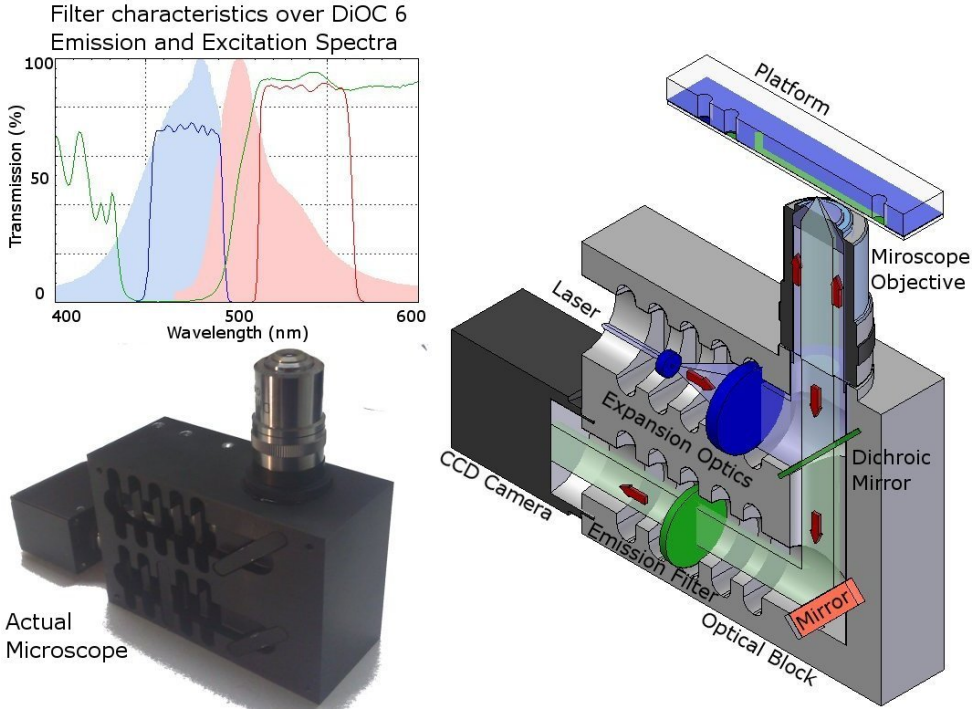

Figure 5.11: Schematic showing design principle of epiflourescent microscope with actual device inset

In terms of resolving platelet surface interactions, since the magnification of the objective is 20x and the each pixel of the CCD detector is 4.65 μm, this results in sub micron resolution of image capture.

$$\frac{4.65\mu m}{20} = 0.2325\mu m$$

In the case of a 2 μm platelet, (assuming circular platelets) this results in

$$\text{Convert } \mu\text{m to pixels}\left(\frac{1}{0.2325}\right) \Rightarrow 1\ \mu\text{m platelet radius} \approx 4.3 pixels$$

$$\text{Area covered} = \pi r^2 \approx 58 pixels^2$$

Similarly, in the case of a 4 μm platelet the corresponding image size is $\approx$ 232 pixels^2 and, this was deemed not to pose any problem in terms of imaging.

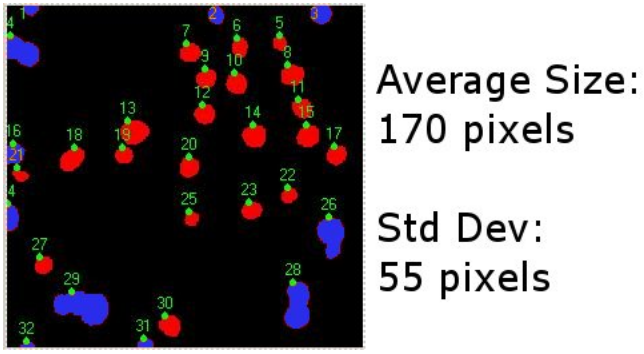

Figure 5.12: Distribution of detected particle sizes

In order to test cameras capability a sample program was written to analyse an image and calculate detected particle area. For the purposes of camera testing particles touching the edge of the image and also platelet-platelet aggregates (shown in blue in Figure 5.12) were omitted from the analysis. As shown in Figure 5.12 the average particle area is 170 pixels^2 falling within the theroetical camera range of 58 - 232 pixels^2. These images are captured via the CCD and transmitted via firewire connection to a laptop computer for further analysis.

The translation stages for the microscope consist of three manually operated linear stages commercially available from Thor Labs US. These stages were assembled and facilitated linear movement of the microscope stages in X,Y and Z directions as indicated in Figure 5.13.

To enable focussing of excitation light onto the chip, a specially designed platform holder was manufactured and assembled as part of the Z direction stage. This holder was designed to promote efficient and reproducible interchange of the newly designed platelet function platforms. Further, both the optical housing and the stage material were chosen to be machine-shop grade

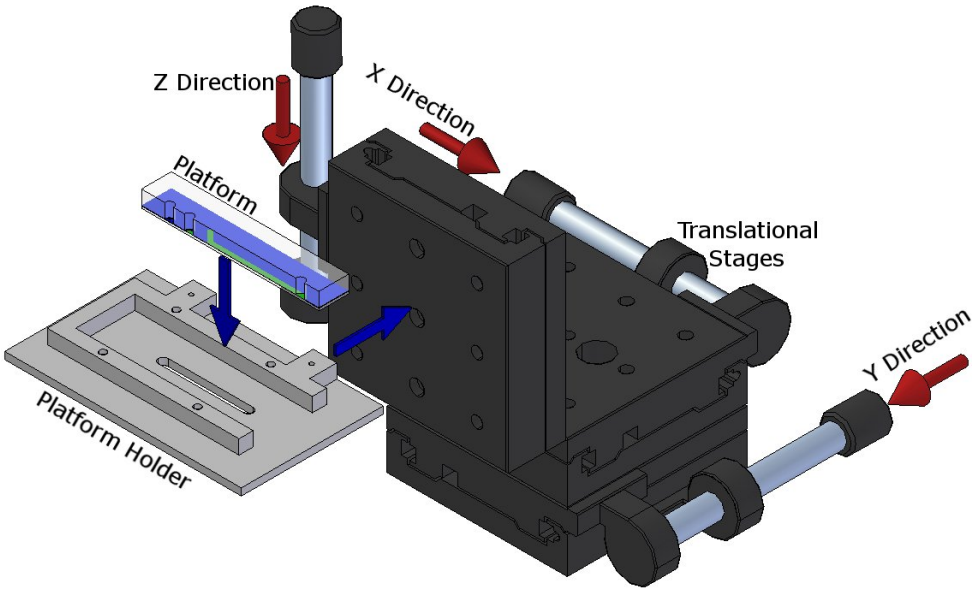

Figure 5.13: Schematic showing stages assembly with designed platform holder

aluminium that was machined using conventional machining techniques and subsequently anodised black to eliminate stray reflections. Aluminium, as a material choice, is robust for its intended application and also exhibits extremely good thermal conductivity (237 $W.m^1.K^1$) making it an ideal choice of material for use in promoting thermal control and stability of the platelet function platform itself.

Thermal

In terms of thermal control for the platform, the aluminium platform holder was actively heated using two polyimide resistive heaters (HK5165R52.3L12 from Minco,UK). These heaters were sealed to the underside of the platform holder as shown in Figure 5.14 . The heaters operate up to 3A and are capable of delivering 15 Watts of power at a 28V supply. Under these maximum operating conditions, the upper surface of the chip holder theoretically in-

creases in temperature by almost 8 ℃ per minute, thereby resulting in an increase to 37 ℃, of the holder, in less than three minutes. In practice however, using a 12 V supply, and taking into account the microscale surface roughness of the chip holder, combined with the thermal conductivity of; the glass, the pressure sensitive adhesive layers and polymer, this results in the actual chamber taking significantly longer to reach the required 37 ℃ equilibrium.

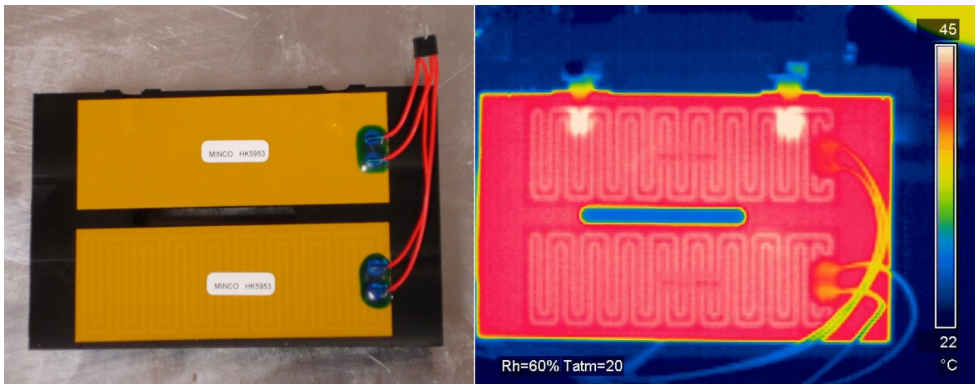

Figure 5.14: Image showing image of polymide heaters (left) and image taken from IR camera under active heating (right). The active elements can be seen to heat to 45 ℃while the overall platform remains at 38.5 ℃

In order to control heating of the platform holder, a temperature stabilisation technique was introduced. This technique allowed the temperature to be stabilised at a user-defined set point via a software controlled feedback loop. The temperature of the aluminium block was independently measured using miniature 10kΩ NTC thermistor coated with a black stycast epoxy (10K4A1AM, from Betatherm, Ireland). These temperature data were sent to a LabVIEW program on board a PC via an electronics control card housed within the microscope stages as shown in Figure 5.17. The measured temperature value was compared to a user-defined temperature and the discrepancy between the desired and actual dictated the length of

time the heaters remained in the 'on' or 'active' state. As the measured temperature approached the user-defined set point the activation time of the heaters was dramatically reduced. Although in many thermal stability systems there is both active heating and cooling it was felt the introduction of an active cooling mechanism, typically a fan, would introduce unnecessary complications to what was designed to be a relatively simple detection system and, as such, ambient cooling was deemed acceptable. This was further justified because under normal operation the chip holder would not require rapid thermal cycling i.e. active temperature increase to a single set point was the main requirement for reproducible device operation.

Although directly controlling the 'in channel' temperature of each platelet function platform independently would be desirable, this would involve introducing a thermistor into the channel of each device. This, it was deemed, would have a negative impact on chamber operation as measuring the temperature directly at the point of interest would ultimately disturb the flow profile at the point resulting in local disturbances in calculated shear force. Further, the introduction of commercially available thermistor epoxy into the channel could in itself promote changes in platelet function independent of deposited protein coating. As a result, an indirect approach to temperature control was taken. A small hole was drilled in the chip holder where a thermistor was embedded, as shown in Figure 5.15. Measuring and controlling the temperature of the chip holder facilitated indirect control of the temperature of the chip itself. While the ability to directly control the 'in channel' temperature is unambiguous, using the indirect approach to control chip temperature introduces additional operational considerations.

Although the thermally conductive chip holder may be at a user defined set point, it would also be necessary to investigate the effects of thermal lag (delay in thermal response) and thermal loss from chip holder to the chip itself. To this end, a chip was manufactured as described with the exception

of a small (dia 1.6mm) hole drilled through the polymer top plate. This hole was drilled in the centre of the main channel at a distance 25mm from the sample entrance zone as shown in Figure 5.15. The entire chip was filled with a thermally stable oil in order to minimise convective heating effects in the channel. Additional 10k thermistors (Betatherm, Ireland) were embedded in both the drilled hole as described and also the sample reservoir which had also been filled with the control oil.

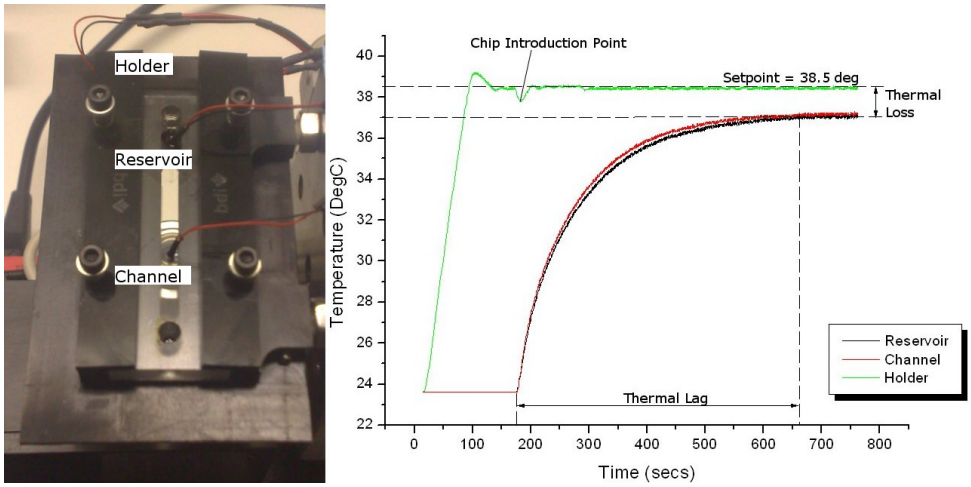

Figure 5.15: Measured temperature over time from various area of chip and chip holder as indicated

Prior to experiments, the chip with embedded thermistors was allowed to sit at room temperature for at least two hours to ensure temperature stabilisation across the chip. In order to investigate the effect of thermal lag and loss, the heating control was activated and the heater was allowed to reach its defined steady state. On reaching steady state, the chip with embedded thermistors, measuring both channel and reservoir temperature, was introduced to the holder and the temperature monitored.

To investigate thermal loss, the required set-point was adjusted from 37^{o}C to 42 ^{o}C in increments of 0.5^{o}C and thermal lag was measured by observing the time delay from chip introduction to the device until chip

steady state temperature was reached. It was observed experimentally that thermal loss for the system was 1.5^{o}C while thermal lag was measured to be approx 500 seconds. This resulted in a required set point of 38.5^oC as shown in Figure 5.15. Figure 5.15 shows the measured temperature response from the actively heated chip holder and also the resulting temperature increase in both the reservoir and channel. It can be seen that while the thermal response of both sample and channel are relatively uniform there is a significant lag time before the chips reach a steady state of 37 ^{o}C which should be taken into account for in order to ensure experimental reproducibility when dealing with biological samples.

Fluid Delivery

For actuating fluid movement through the device a commercially available syringe pump was sourced from Cetoni (Cetoni.de) See Figure 5.16.

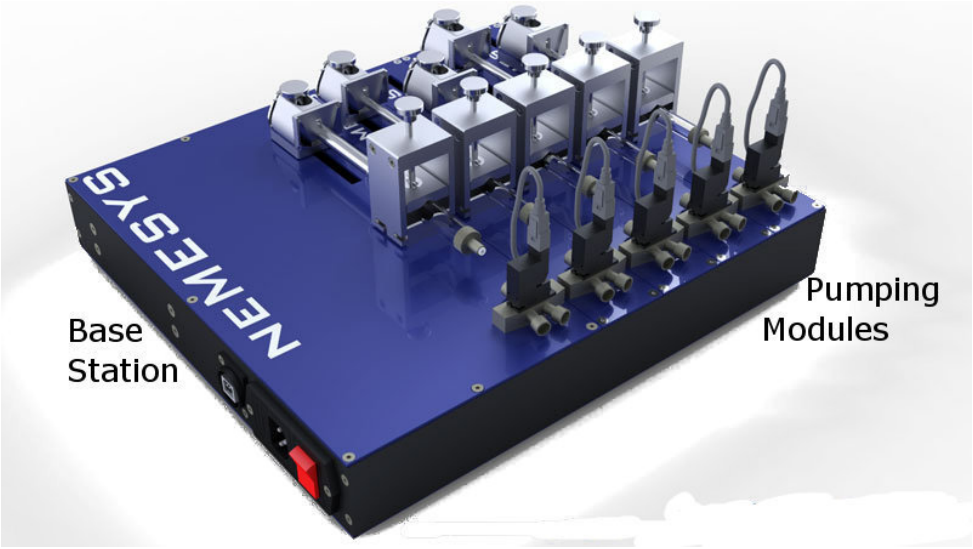

Figure 5.16: NEMESYS pumping system from Cetoni.de. Image shows pump base station and five pumping modules

The NEMESYS pumping system is a high precision syringe pump capa-

ble of delivering flow rates from 0.494 μL/s up to 2.494 mL/s. The pump consists of a base station containing the hardware control, USB connection for software control and a single syringe pump with universal syringe holder. Among the more attractive features of the pump however is the ability to extend functionality by the addition of individual independently controlled pumping modules. Coupled with its relatively small footprint (310 mm x 207 mm x 80 mm) and the ability to develop custom software for pump control, the NEMESYS was an ideal choice for independently controllable delivery of two fluid streams over a range of flow rates. Further, however, it was the technical specifications of the power supply, of the NEMESYS system that made it the fluid delivery method of choice for the platelet function detection system. The ability to exploit additional unused terminals on the output terminal of the NEMESYS power supply allowed the pump power supply be further utilised to power, the laser diode excitation source and also the heater, thereby making the developed system extremely compact and portable.

Integration

In terms of development of a single detection and readout system, the subassemblies as described required integration on a mechanical, electronic and software level. In terms of mechanical integration, both the microscope optical block and stages were fixed relative to each other by a 21 mm thick black nylon plate. Further, the outer dimensions of the black nylon support plate was machined to match the outer dimensions of the NEMESYS pumping system and fixture holes were drilled to match the hole template of the NEMESYS system. On an electronic level, as previously mentioned the power supply used for the pump motors was a step down (240V AC to 24 V DC) transformer with a 5A capacity, thereby making it a capable power

supply for all sub-assemblies. Coupled with the suitable specifications was the fact there were a number of unused outputs from the transformer. These outputs were utilised for each sub system. In the case of the laser system, a 24V to 6 V 1A regulator was used to output the required voltage and a 0.33 μF and 0.1 μF Capacitor placed in parallel across the regulator input and output respectively in order to minimise the effect of noise on the system. Similarly in the case of the heater power supply, the 24 volt supply from the NEMESYS system was used and a 24 volt to 12 volt 2A regulator was integrated into the NEMESYS pump. The addition of both regulators introduced the requirement for a heat sink to be included as part of the overall system. The heat sink (ABL Components) was rated at 1.2 ^{o}C/W. This relatively high thermal resistance was required when dealing with the 24V to 12V regulators which draw up to 1.5 Amps of current over approximately 250 milliseconds (thereby resulting in approximately 4.5 Watts of power to be dissipated). Incorporated as part of the laser and heating systems, were independent on/off switches allowing functionality of each of the subsystems independently or as part of the overall system. Further included in the electronics integration was the development of additional heating control circuitry to facilitate software controlled switching of the heating power supply. The measured thermistor readings for the thermal control were fed through a dedicated LabVIEW compatible electronics card enclosed in the microscope stages as indicated in Figure 5.17.

Also enclosed within the housing was a relatively simple 'H' bridge circuit linking the output from the LabVIEW card to the output from the pump power supply. This circuit essentially acts as a switch for the high voltage (12V) line. If the software deems the heater should be turned on it sends a 5 volt signal to the 'H' Bridge which activates the 12 V supply across the heaters. When the software deems the heaters should be off, the signal goes to 0V and the switch becomes inactive. Using this method for

heater activation it was possible to use standard PC power supplies of 5V and 300mA to control a higher voltage 12V 2A supply.

In terms of software integration, the entire system was fully integrated into a single software program capable of heater control, pump activation, camera configuration, image capture and software analysis. As part of the prerequisite for many of the components sourced (in particular the CCD camera and pumping system) the ability to be independently controlled via software, typically LabVIEW, was of significant importance. The ability to control each sub-assembly via software would improve ease of use of the overall system while also facilitating the ability to more easily record experimental parameters such as pump flow rates or camera settings to ensure experimental consistency over a number of experiments.

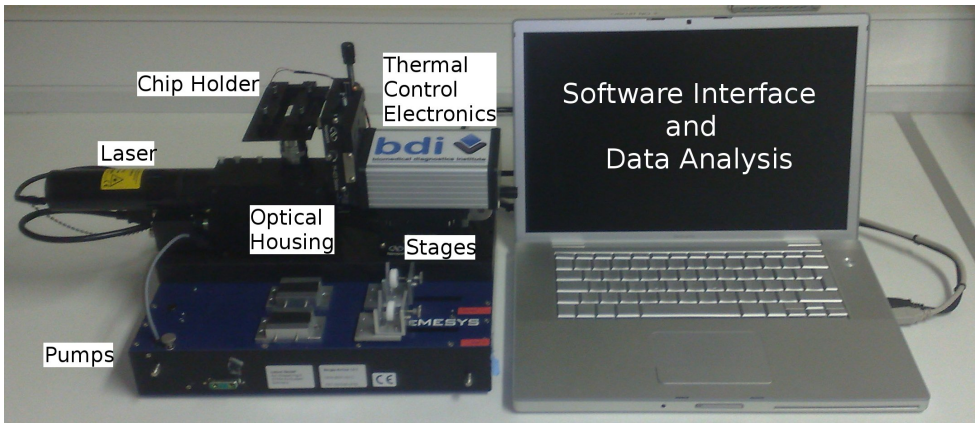

Figure 5.17: Image of developed miniturised platelet function analyis system

The entire assembled system can be seen in Figure 5.17. In its current embodiment, the end-user currently has control over the set point of the heater control while a visual display graphs the temperature of the platform holder. In terms of fluid delivery, the end user can input various syringe parameters for two independently controlled pumps and actuate either or both of these pumps in any given directions at any speed permissible by the pumps hardware. In terms of image capture, the end user defines the saving

location of the images and also the image format and number of images required, while the brightness, gain and shutter speed of the camera are all user-definable depending on the fluorescent intensity of the capture medium. In terms of costings for the overall system, an approximate breakdown is shown in Table 5.2.

Description	**Cost**(Euro)
Pump System	3,500
CCD Camera	1,500
Laser Diode	1,400
Laptop	1000
Filter Set	450
Stages	450
Custom Machining	450
Labview Hardware	100
Microscope Objective	80
Total	8930

Table 5.2: Approximate costings for Platelet Function Readout System

The total cost of the detection system is approximately 8930 euro. In order to gain some perspective on the overall cost of the detection system, a camera for the large scale laboratory system was recently purchased for a cost of 10,000 euro. The ability to deliver an entire readout system at a comparable cost to a single component of existing systems represents significant savings and makes the detection systems more amenable to clinical and GP settings.

5.4 Conclusions

An entirely unique approach has been taken to the traditional parallel plate style of device for shear-mediated platelet function analysis. By combining the existing parallel plate technology with variations on hydrodynamic focussing in a laminar system, the initial goals of a further reduction in required whole blood sample while also maximising sample efficiency were realised. The designed platform was manufactured in a manner suitable to both prototyping and mass production techniques. The functionality of the new device, in terms of fluid 'shaping', was then validated using coloured dyes. This experimental data were then validated against a three dimensional computational fluid model of the device. This model facilitated predictions related to, appropriate buffer flow rates for a defined sample channel shear stress, changes in buffer-sample interface over various flow rates and also entrance length effects for both buffer and sample. Finally, the theory initially developed in Chapter 2, was expanded to show the effect of a mismatch in viscosity of both buffer and sample streams.

In parallel with the extensive characterisation of the new platelet function device, a miniaturised detection system was designed and assembled. The device integrates a number of sub assemblies critical to the reproducible assaying of whole blood samples. In the case of optical detection, a miniaturised epi-fluorescent microscope was designed and built using laser diode excitation and appropriate filters for the detection of suitable dyes for platelet function analysis and image capture via CCD. The microscope stage incorporated active heating elements in order to maintain the platform at a constant 37 ℃. The fluid delivery system was sourced commercially and was capable of independently delivering two fluid streams over a range of volume flow rates suitable for generating appropriate shear stresses in the newly designed platform. In terms of integration, each of these sub assem-

blies was mechanically assembled to form a single portable bench top detection system. Further, these sub assemblies were could be independently or simultaneously controlled via customised software. The software facilitated thermal control, flow control and image capture control of the bench top detection system all from a single user interface on a laptop computer.

In short, a novel platelet function platform was developed capable of testing sub 500 μL samples of whole blood under shear-mediated flow conditions. In parallel, a low-cost, bench-top, detection system was developed specifically with the new platelet function platform in mind. The next stage of development involved validation of the entire system with whole blood samples.

Chapter 6

Results and Analysis II

6.1 Introduction

On completion of the design and fabrication of the dual inlet platelet function diagnostic chip and, in conjunction with the construction of the desktop readout device, the final stage of development was to investigate the potential of the entire systems to return diagnostically relevant information.

To this end the series of experiments as described in Chapter 4 was repeated. As before, an total ten tests was performed. Of these ten, five samples were treated with Abciximab and five remained untreated. The rationale for utilising Abciximab as the drug of choice has been detailed in Chapter 4.

As a reminder, Abciximab, sold under the trade name ReoPro, provided an attractive option as a test case for the entire platelet diagnostic system as it facilitated the ability to carry out multi-parameter testing. Since ReoPro inhibits both stable adhesion of platelets on VWF and also fibrinogen-mediated platelet-platelet binding, this allowed for a dual analysis approach focussing on each interaction independently. As in the case of the single inlet single outlet chip, the output metrics from the dual inlet

platelet function chip in conjunction with the miniaturised readout system were the ability to detect

- changes in surface coverage over time, thereby providing characterisation of the inhibition of αIIbβ3 on stable platelet adhesion to VWF.
- platelet cluster analysis after a predefined length of time, thereby characterising the inhibition of fibrinogen mediated platelet-platelet aggregation.

6.2 Experimental Procedure

Experimental procedure was kept consistent with the procedure described in Chapter 4.

Prior to experimental runs the assembled dual inlet platelet function devices were coated with Von Willebrand Factor at a concentrations of 100μg/mL in Phosphate Buffer Solution (PBS). The flow chamber was incubated for two hours at room temperature and subsequently blocked using a 1% Bovine Serum Albumin (BSA) solution for one hour. The chamber was then washed by perfusion using PBS. The intermediate step of blocking with BSA ensures platelet activation is caused only the VWF bound to the surface and any potentially exposed glass does not contribute to the observed experimental results.

In parallel to chip preparation, whole human blood was drawn, using a 19 gauge needle from the antecubital vein of healthy donors who were not known to have taken any medication within the previous 10 days. The first 5mL of blood collected was routinely discarded to prevent any possible activation of platelets, and blood was drawn into a clean polypropylene syringe containing trisodium citrate as anticoagulant (final concentration of 0.32%, 1:9 ratio of citrate to blood). In the case of ReoPro-treated whole

blood, ReoPro (20 μg/mL in whole blood; Eli Lilly & Co., Indianapolis, USA) was added to the whole blood sample 20 min prior to experimental analysis. For fluorescence imaging of platelets, both whole blood samples were labelled with 3,3'-dihexyloxacarbocyanine iodide ($DiOC_6(3)$) (1 μM; Invitrogen USA), a fluorescent dye commonly used for platelet function studies. The labelling was carried out by addition and gentle mixing by inversion followed by incubation for 10 min prior to experimental analysis at 37 ℃.

Once the dual inlet platelet device and whole blood have been prepared as described, the device is placed inside the heated chip holder as previously shown in Figure 5.15 and the outlet port is plumbed to the pump via a syringe of Phosphate Buffer Solution (PBS) using 1/16' inner diameter Silastic^{TM} tubing via 1/16' threaded polypropylene connectors attached to the device buffer inlet and outlet ports.

In a similar manner the buffer inlet port of the device is plumbed to the pump via a syringe containing the chosen buffer solution. In order to minimise diffusion effects and viscosity mismatch between whole blood samples and buffer solution, Histopaque was chosen as a buffer. Histopaque is a biocompatible reagent with a measured viscosity of 0.004 Pa.s.

As in the case of the experimental procedure used for the single inlet single outlet device, whole blood samples were assayed at a wall shear force (stress) of 6 N/m^2, which, assuming constant blood viscosity of 0.004 Pa.s (4 cP), occurs at a volumetric flow rate through the device of 0.6 mL/min. To this end, the outlet port of the dual inlet device was plumbed to a syringe and a negative pressure applied to generate 0.6 mL/min volume flowrate through the main channel of the device thus ensuring the desired shear stress was generated along the main detection area. The buffer inlet volume flow rate on the other hand was plumbed to an additional syringe pump and a positive buffer volume flowrate of 0.575 mL/min was applied.

This buffer volume flow rate resulted in a whole blood sample consumption of 25 μL/min and was also above the minimum sample flow rate of 0.5688 mL/min as determined by the fluid model detailed in Chapter 5.

For each experiment, 600 images (350 pixels x 350 pixels) were recorded at a capture rate of approximately 4.9 frames/s, corresponding to an overall run time of just over 120 seconds; in that time, a total blood volume of just over 50 μL was consumed. In comparison to the existing commercial system, wherein 5 mL would have been consumed under the same shear force conditions, and also the single inlet single outlet device wherein $\approx$150 μL would have been consumed under the same shear force conditions, this represents a significant reduction in the sample volume required. Although the reduction in sample volume required from single inlet-single outlet device to dual inlet device is just over 67% its also worth remembering that in the case of the dual inlet device this required sample can be delivered to the device without the need for extraneous reservoirs and tubing containing additional sample. In the case of our experiments, $\approx$ 200 μL of whole blood was pipetted into the sample reservoir of the chip and this sample volume represented the entire sample volume required to carry out our experiments.

In order to minimise photobleaching effects seen with the commercial system, the excitation light source was deliberately switched off at regular periods of the flow run for periods of 5-30 seconds. This allowed a visible trend in surface coverage of platelets over time to develop while also serving to minimise the light incident on the platelets thus reducing the effect of photobleaching.

As before, ten experiments were carried out. Of these ten, five samples were treated with ReoPro and five remained minimally treated as described ($DiOC_6(3)$ and trisodium citrate as anticoagulant). The captured images from each experimental flow run performed, as described, were then passed to a PC for investigations into the effect of ReoPro on whole blood.

6.3 Analysis

6.3.1 Image Analysis

As with the case of the experimental procedure, the image and data analysis of shear-mediated, platelet-surface interactions for the dual-inlet device also followed the same procedure, where possible, as the image and data analysis for the single inlet-single outlet device. Since the total analysis (image and data analysis) was based on pixel coverage and pixel distribution, the analysis software developed could be utilised almost unchanged*. Indeed the software could be utilised to operate with any given, appropriately named, image sequence in any of the common image formats typically used.

6.3.2 Data Analysis

In terms of data analysis, since the data analysis was based on spread-sheet analysis, as opposed to dependence on pixels numbers, data transfer rates etc., the same procedures were applied to analysing the data from the dual inlet platelet function device from the bench-top readout system as was used for the single inlet-single outlet device from the commercial system. The main practical difference was in plotting the surface coverage data based on a different frame rate than the commercial system and, in the case of plotting size distribution, the selection of frames to take the distribution of platelet aggregate sizes over. Both these changes were frame-rate based and in no way altered the analysis principle for both systems. The reduction

*The principle of analysis remained exactly the same. The main difference concerned the time stamping of each image. Since the frame rate was approximately 4.9 fps as opposed to 24fps, each image was time stamped with a capture time accurate to 4 decimal places. This time of capture data was then incorporated into the percentage change in surface coverage data to give an accurate portrayal of changes in detected percentage coverage over time

in frame rate for the bench-top system was implemented as a result of the decision to change to a larger field of view size for the benchtop system in order to get a more representative field of view over which to characterise platelet surface interactions. The change from 256 x 256 pixels, in the case of the commercial microscope to, 350 x 350 pixels, in the case of the benchtop system resulted in an increase of analysis area of approximately 87%. This relatively minor changes in conjunction with the hardware limitations of the benchtop system (e.g the images were sent from the camera to the laptop via Firewire connection rather than high speed data bus) resulted in the software capturing 600 images over a 120 second period. It was felt this number of images would be sufficient to give a representative analysis of changes in surface coverage over time.

6.4 Results

The graphs in Figure 6.1 show the resulting plots of detected changes in surface coverage over time. Figure 6.1(a) shows the detected surface coverage response for untreated whole blood while Figure 6.1(b) shows the detected surface for reopro treated whole blood. The results correlate well with the existing experimental data showing an overall increase in surface coverage over 120 seconds for the untreated whole blood sample while showing an initial increase followed by decrease for ReoPro-treated whole blood samples.

The graphs have an appreciable noise level compared to the commercial system. The increase in noise can be explained by a number of factors primarily associated with the camera selection and imaging optics. Of all the components included in the bench-top device, the camera and imaging optics represented the main deviation in terms of hardware quality from the commercial laboratory experimental configuration. Translating from a high

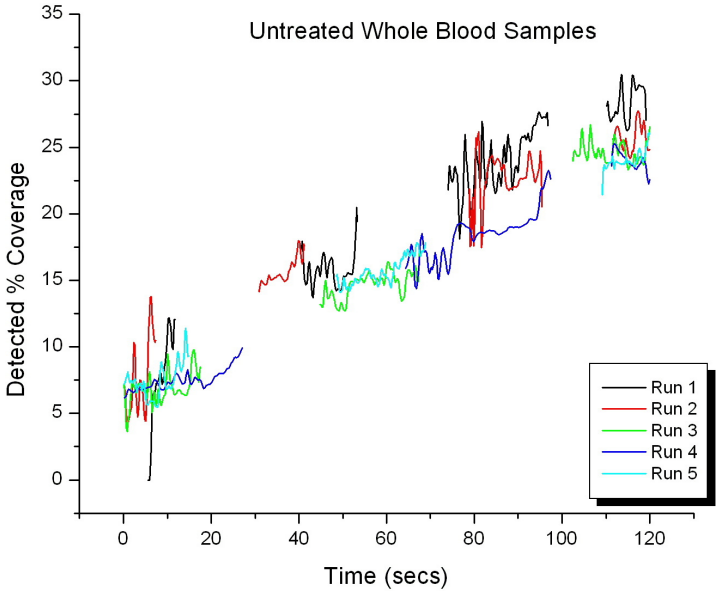

(a)

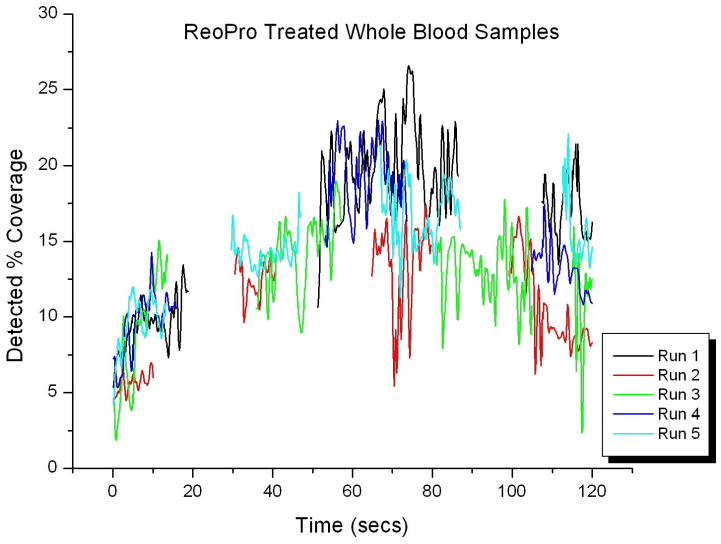

(b)

Figure 6.1: Plots showing changes in surface coverage on VWF through the dual inlet chip of untreated (a) and ReoPro treated (b) whole blood

speed, liquid cooled camera using expensive oil based microscope optics to a low cost objective, imaging onto a non-cooled CCD camera reduces image quality and introduces thermal, electrical and potentially vibrational noise

into the system. However, despite the increase in noise there still remains obvious differences between ReoPro and non ReoPro-treated whole blood samples. Plotting the data from both, commercial and miniaturised systems side by side, as shown in Figure 6.2, we see strong correlations in changes in surface coverage over time for both treated and untreated whole blood.

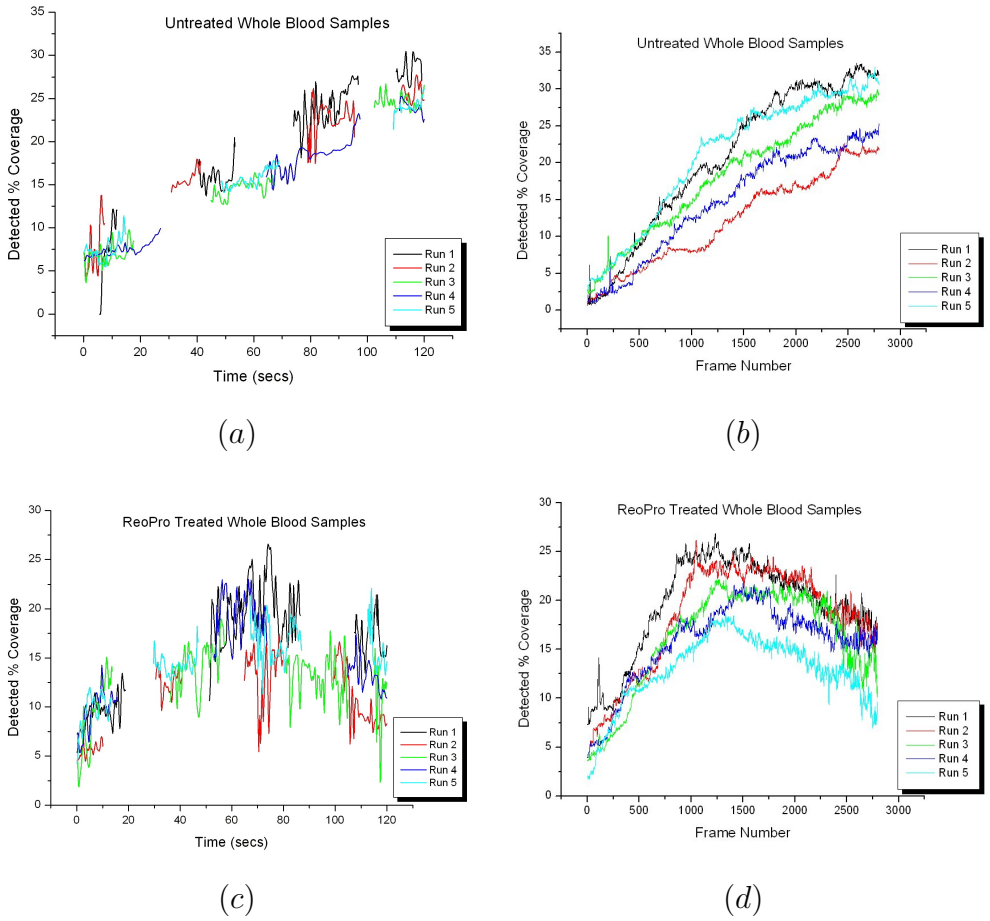

Figure 6.2: Comparison of surface coverage data taken from ReoPro treated and untreated whole blood from the single inlet-single outlet platform ((b) and (d)) taken using the commercial system and also from the dual inlet platform ((a) and (c)) obtained from the bench-top device.

In the case of the untreated blood samples the surface coverage increases in a linear fashion over the experimental flow run while in the case of the

ReoPro-treated samples there is an initial increase in detected surface coverage followed by an apparent decrease after ≈ 60 seconds. This difference between ReoPro and non ReoPro-treated whole blood is consistent across the commercial system, using the single inlet-single outlet device and the miniaturised bench-top system, using the dual inlet device thus validating both the dual inlet device and bench-top system as a viable means to investigate platelet function under shear.

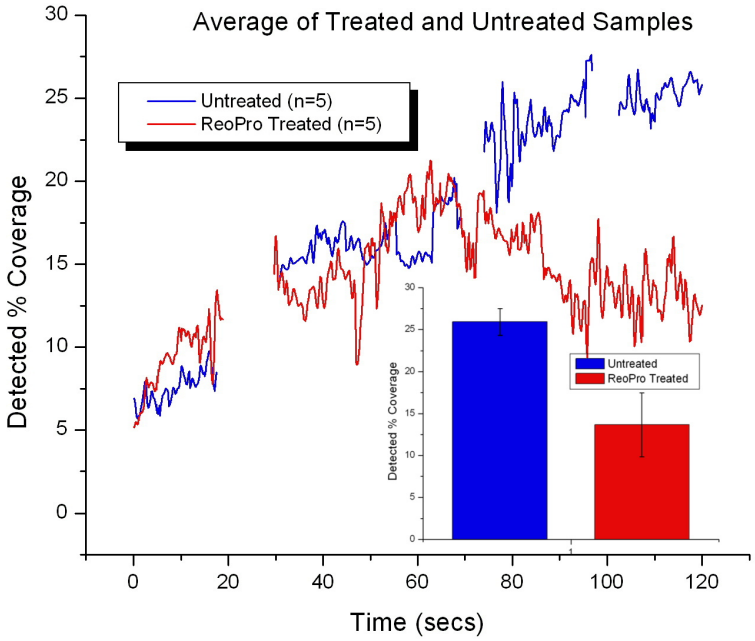

Figure 6.3: Plot of average detected changes in surface coverage through dual inlet chip. Inset histogram of average detected coverage taken at 115 seconds

As before this surface coverage data can be further visualised by plotting the average surface coverage over the each of the five ReoPro treated and untreated experimental flow runs as shown in Figure 6.3. The inset bar graph reveals an average surface coverage for untreated blood of approxi-

mately 26% and an average surface coverage of approximately 14% in the case of ReoPro-treated blood. These figures correlate well with the figures from the single inlet-single outlet device on the commercial chip (approximately 27% coverage in the case of untreated blood and approximately 16% in the case of ReoPro treated blood).

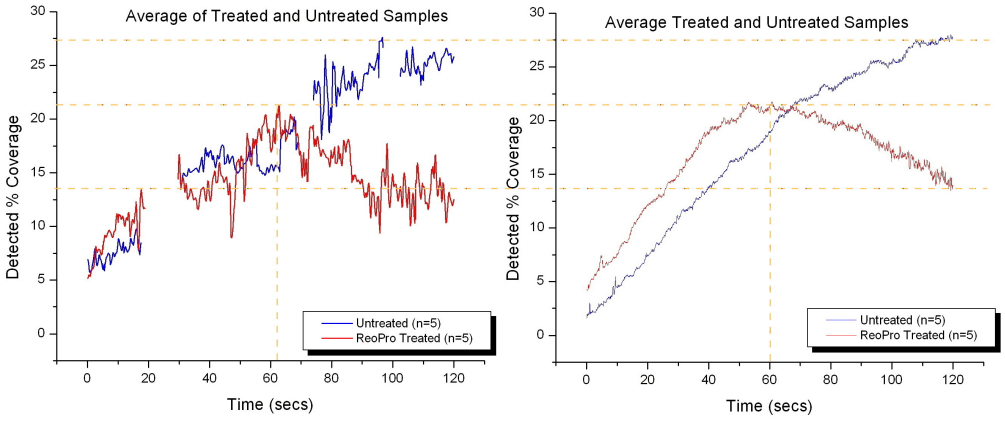

Figure 6.4: Plot of average detected changes in surface coverage of platelets on VWF for both the dual inlet diagnostic on the benchtop readout system (shown left) and single inlet diagnostic on commercial microscopy system (shown right). Note the X axis in the case of the commercial system has been re plotted in seconds, for comparision.

This average surface coverage data can be further visualised in comparison to the commercial system if both graphs are shown side by side as shown in Figure 6.4. Although, as in the case of the individual plots, the data from the bench-top device has an appreciably higher noise level than the commercial system, the similarities between both systems are evident. In both cases, one observes, in the case of non ReoPro treated blood, an almost linear increase for the first 120 seconds reaching a surface coverage of approximately 27.5 %. In the case of the ReoPro-treated blood however, there is a similar linear increase for approx. 60 seconds or up to a detected surface coverage of approximately 22% followed by a decrease in detected

coverage over the remaining 60 seconds to approximately 14%.

In relation to the noise, the development of the bench-top detection system resulted in necessary compromises to be made to facilitate the ability to develop a low cost readout system with a significantly lower overall footprint than the commercial systems in order to encourage the entire platelet function analysis system to be implemented outside specialised facilities.

6.4.1 Platelet Aggregation

In the case of platelet aggregation analysis, a selection of 10 images (frame numbers 575 - 585) were taken as a representative snapshot of surface coverage at a given time. A snapshot of 10 images would give information for just over 2 seconds of data while also allowing some noise to be averaged out of the system. As in the case of the single inlet-single outlet device, the area of every detected particle in each of the 10 images was then recorded and a mean particle size and standard error recorded. The average particle sizes for each flow run can be seen in Figure 6.5

As in the case of the data analysis from the commercial system (See Chapter 4) the ReoPro treated sample data from the dual inlet chip on the bench-top device has a significantly lower mean particle size and smaller standard error than the untreated sample. As previously described, since ReoPro inhibits fibrinogen-mediated platelet-platelet binding via receptor αIIbβ3 this in turn inhibits the formation of platelet aggregates on the surface. In contrast the mean detected particle size for the untreated sample is significantly greater than in the case of the ReoPro-treated sample indicating larger platelet aggregate.

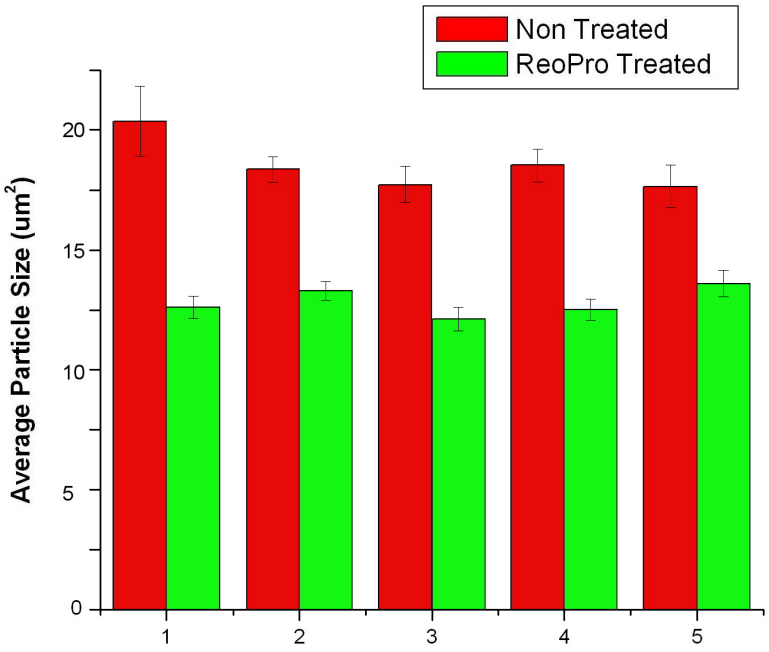

Figure 6.5: Average platelet aggregate distributions on treated and untreated samples using the dual inlet device on the bench-top system

6.5 Conclusions

The functionality of the entirely new platelet function analysis system was demonstrated and results compared favourably to the commercial readout system.

In terms of chip performance, the dual inlet chip resulted in a 67% reduction in required sample volume from the single inlet single outlet device. It is worth remembering that the single inlet-single outlet device itself represented a greater than >97% reduction in sample volume over existing commercial parallel plate flow devices. While the reduction in volume from the single inlet-single outlet device to dual inlet device is significant, the design of the dual inlet device is such that any additional dead volume

requirements are eliminated. This feature facilitates a significant deviation from standard parallel plate devices in terms of sample loading and can potentially be incorporated with a finger stick type approach to blood sampling as opposed to the relatively intrusive blood draw via syringe.

In terms of readout system performance, while there was an appreciable noise level associated with the bench top device the results compared favourably with the commercial, large scale, readout system. The noise resulted from design compromises made during readout system development as discussed, and design constraints such as cost and overall readout system size were central to any design decisions. The ability to develop a low cost, bench-top device for platelet function analysis was of paramount importance in the readout system development. Nonetheless, the data from the bench-top readout system correlated extremely well with data using high speed image capture on a commercial microscope. In the case of average data analysis as shown in Figure 6.4, both ReoPro-treated blood and non ReoPro-treated blood could readily be discerned by its distinctive profile from either bench-top readout system or commercial system.

In short, an entirely novel approach to parallel plate type devices for shear-mediated platelet function analysis has been validated. This approach requires a total sample volume of <200 μL for a 120 second experimental flow run at a shear rate of 1500 s^{-1}. Further, the device has been tested on a miniaturised, user friendly, low cost, readout system for platelet function analysis and results compare favourably with large scale, commercial systems.

Chapter 7

Conclusions

The exploitation of microscale fluid dynamic effects coupled with a relatively unique approach to BioMEMS fabrication, facilitated the development of a platelet function test platform capable of delivering relevant diagnostic information relating to platelet function under shear flow from a whole blood sample.

The objectives of this work as described in Chapter 1 were realised.

1. *To design a robust platform to characterise platelet-surface interactions in whole blood under vascular shear rates in response to VWF.* A variation on existing commercial parallel plate devices was developed based on fluid flow equations governing flow through a rectangular duct. This device resulted in a >95% reduction in required sample volume flow rate for an arterial shear rate of 1500 s^{-1}. Further the device proved to be significantly more user friendly than existing parallel plate devices based on its disposable nature. It also resulted in the elimination of the need for an external vacuum pump to facilitate sealing of the device. The glass surface of the device was coated with Von Willebrand Factor, a protein prevalent in the initial stages

of platelet activation, and fluorescently labelled whole human blood was passed through the device at a shear rate of 1500 $^{-1}$.

2. *To develop an algorithm to objectively quantify platelet-surface interactions in whole blood under physiologically relevant shear rates.*
   An image processing algorithm was developed based on the detection of areas of high intensity corresponding to areas of platelet interaction. Each of these areas of high intensity were recorded, thereby facilitating a calculation of the overall surface coverage for a given image. This process was repeated for each captured image and a profile of changes in surface coverage was generated. This was further validated by the deliberate addition of an anti-platelet drug and differences in changes of surface coverage were observed. Further, the software also facilitated size distribution of areas of high intensity corresponding to the degree of platelet-platelet aggregation.

3. *To utilise developments in the area of BioMEMS to significantly reduce the sample volume required for an experimental run.*
   A significant deviation from the traditional parallel plate type of devices was developed. Using a variation of the well established hydrodynamic focussing technique, a new platelet function device was developed. This device shapes the fluid and ensures contact with the imaging/protein coated surface. This design represented a further reduction in sample volume requirements, eliminated sample dead volume and allowed the end user to vary the wall shear force independent of sample volume consumption.

4. *To develop an integrated low cost miniaturised detection system, incorporating all fundamental aspects of existing laboratory detection systems.*

To test the new platelet function device a dedicated readout system was developed. This readout system was primarily aimed at making platelet function tests more accessible to the general public. As such, the readout system design requirements meant that the system should be low cost and represent significantly more integration than existing detection systems while also being significantly smaller in overall size. The developed system was a bench-top device incorporating epi-fluorescence microscopy, thermal control of the chip holding stage, two independent fluid delivery modules all connected to a laptop computer with a single software interface. The laptop also incorporated the post experiment custom image analysis software. On testing the new platelet function device on the bench-top system under the same experimental conditions, the results were found to compare very favourably with the commercial system and original platelet function chip.

In all, an inexpensive, shear-mediated, platelet function analysis under flow system has been developed. The sample volumes required represent a significant reduction in comparison to existing parallel plate type devices.A time-based metric of surface coverage has been developed and successfully demonstrated against a commercially available anti platelet therapy.

7.0.1 Future Work

Although the overall system has been shown to compare favourably to commercial devices, futher developments could improve overall functionality of the system. These developments should come under the following headings.

Engineering improvements

A reduction in noise from the system would be of obvious benefit. This could be obtained from a hardware perspective by;

- introducing extraneous optics to improve signal quality.
- reduce the effect of background light where possible
- further optimisation of cameras settings
- a reduction in external vibration effects

In terms of software improvements, more in-depth image processing could potentially improve image quality and the further improvement of a threshold algorithm to specifically identify platelets from a given image would reduce any potential photo-bleaching effects.

End use improvements

From an end use of patient perspective the next step in development should be to the transition from traditional blood draw analysis to finger stick approach to sample delivery. This transition is not without complications. Most traditional parallel plate assays use fluorescently labelled and anti coagulated blood. While the addition of the finger stick approach could eliminate the requirement for the addition of anti-coagulants, this in turn could potentially alter resulting data for 'normal' and abnormal blood samples. However the elimination of the addition of anti-coagulant was outlined as highly desirable in the recent communication by International Society on Thrombosis and Haemostasis [1] and a finger stick sampling approach facilitated by the dual inlet approach to parallel plate flow chambers is a significant step to realising this goal. More technically challenging perhaps is the requirement for the addition of the fluorescent stain to visualise

platelets in whole blood. Potential solutions would be coating the sample reservoir in the fluorescent stain and allowing the dye to re-dissolve through the sample before allowing the sample flow through the chamber. Perhaps a more attractive option would be to use a dissolvable film over the sample reservoir. This film could be doped with appropriate concentrations of the fluorescent stain and would dissolve upon contact with whole blood. The dissolution rate of the film could be tuned to ensure appropriate mixing of both dye and whole blood sample. Further, the film would act to prevent the sample channel from being exposed to the environment prior to addition of a whole blood sample.

Diagnostic development

Although the device was validated using the shear-mediated whole blood response to VWF there is no limitation, in principle, to further investigations using alternative proteins of interest. The nature of the device makes using various types of collagen or fibrinogen over various concentrations a valid and viable option. Naturally, depending on the metric of interest, changes made be required to the analysis technique. Nonetheless the device and readout system would remain suited to imaging and recording platelet-surface interactions in whole blood in response to various protein agonists to study the efficacy of the multitude of anti-platelet therapies.

Bibliography

[1] JJ Zwagina, KS Sakariassen, MR King, TG Diacovo, EF Grabowski, G. Nash, M. Hoylaerts, and JWM Heemskerk. Can blood flow assays help to identify clinically relevant differences in von Willebrand factor functionality in von Willebrand disease types 1-3? 1. *Journal of Thrombosis and Haemostasis*, 5(12):2547–2549, 2007.

Selected Publications

Patents:

- Nigel J. Kent, Bryan Lincoln, Lourdes Basabe Desmonts, Antonio J. Ricco, Dermot Kenny, Gerardene Meade, Brian G. Corcoran. **Microfluidic Device for Assessing Cell Surface Interactions.** United Kingdom Patent Application No. 0802084.4 - Currently filed

Peer reviewed:

- Aoife Morrin, Orawan Ngamnac, Eimer O Malley, Nigel Kent, Simon E. Moulton, Gordon G. Wallace, Malcolm R. Smyth, Anthony J. Killard. **The fabrication and characterization of inkjet-printed polyaniline nanoparticle films.** Electrochimica Acta 53 (2008) 5092 - 5099

- Fu-Qiang Nie, Mirek Macka, Leon Barron, Damian Connolly, Nigel Kent and Brett Paull. **Robust monolithic silica-based on-chip electro-osmotic micro-pump.** Analyst, 2007, 132, 417

- William G. Holthoff, Elizabeth C. Tehan, Rachel M. Bukowski, Nigel Kent, Brian D. MacCraith and Frank V. Bright. **Radio luminescent Light Source for the development of Optical Sensor Arrays.** Anal. Chem.2005, 77,718-72

- R. Blue, N. Kent, L. Polerecky, H. McEvoy, D. Gray, and B.D. MacCraith. **Platform for enhanced detection efficiency in luminescence-based**

sensors. Electronics Letters – 9 June 2005 – Volume 41, Issue 12, p. 682-684

- Eadaoin Tyrrell, Ceri Gibson, Brian D. MacCraith, David Gray, Pat Byrne, Nigel Kent, Conor Burke and Brett Paull. **Development of a microfluidic manifold for copper monitoring utilising chemiluminescence detection.** Lab on a Chip, 2004, 4(4), 384 - 390

Non Peer Reviewed

- A. Ricco, N. Kent, G. Meade, B. Lincoln, L. Basabe Desmonts, B. MacCraith, B. Corcoran and D. Kenny **Whole-Blood Diagnostic Sensing System Based on Populational Platelet Rolling Behavior**215th Electro Chemical Society Meeting. May 09

- A. Ricco, N. Kent, G. Meade, B. Lincoln, L. Basabe Desmonts, B. MacCraith, B. Corcoran and D. Kenny **Microfluidic System for Whole-Blood Diagnostic Analysis of Populational Platelet Rolling Behavior** 41st Annual Oak Ridge Conference. April 09

- N. J. Kent, B. O'Reilly, B D MacCraith, B Corcoran. **Low cost manufacturing technique for hybrid microfluidic platforms.** International Manufacturing Conference - Waterford. August 2007

- M. Tweedie, R. Subramanian, P.Lemoine, N. Kent, I. Craig, E.T. McAdams, J.A. McLaughlin, B. MacCraith. **Fabrication of impedimetric sensors for label-free Point-of-Care immunoassay cardiac marker systems, with passive microfluidic delivery.** Proceedings of IEEE 2006 International Conference of the Engineering in Medicine and Biology Society

- McEvoy, Helen M.; Blue, Robert; Kent, Nigel; Polerecky, Lubos; McDonagh, Colette; MacCraith, Brian D. **Novel polymer platform for en-**

hanced biochip performance. Proceedings of SPIE-The International Society for Optical Engineering (2005)

- Eadaoin Tyrrell, Ceri Gibson, Brian MacCraith, David Gray, Nigel Kent and Brett Paull. **Development of a microfluidic based analytical system for copper monitoring in environmental sample matrices.** Research and Development Topics, 21-JUL-03 - 23-JUL-03, University of Sunderland

- Eadaoin Tyrrell, Ceri Gibson, Brian MacCraith, Nigel Kent and Brett Paull. **Development of a microfluidic based analytical system for copper monitoring in environmental samples** RSC Analytical Research Forum 2004, 19-JUL-04 - 21-JUL-04, University of Central Lancashire, Preston, UK

- Nigel J. Kent, Geradene Meade, Lourdes Basabe-Desmonts, Bryan Lincoln, Antonio J. Ricco, Dermot Kenny,Brian D. MacCraith, Brian G. Corcoran. **Development of a Microfluidic Platform and Detection System for Platelet Function Analysis.**12th International Conference on Miniaturized Systems for Chemistry and Life Sciences (μTAS2008), San Diego, USA, October 12-16, 2008:1048-1050.

- B Lincoln, G Meade, N.J. Kent, L Basabe-Desmonts, D Kenny, A.J. Ricco, and L.P. Lee. **Analysis of Whole Blood Platelet Translocation on a VWF-Coated Microfluidic Flow Chamber.** 12th International Conference on Miniaturized Systems for Chemistry and Life Sciences (μTAS2008), San Diego, USA, October 12-16, 2008:453-455.

- Nigel J. Kent, Geradene Meade, Lourdes Basabe-Desmonts, Bryan Lincoln, Antonio J. Ricco, Dermot Kenny, Brian D. MacCraith, Brian G. Corcoran.**Development of a Microfluidic Platform and Detection System for Platelet Function Analysis** Europtrode IX - Dublin March 30th April 2nd, 2008.

- R Blue, N Kent, H McEvoy, S Hearty, R O'Kennedy. B MacCraith **Development of Optical Biochip Arrays for Cardiac Markers** Cross-Border Programme for Research and Education Contributing to Peace and Reconciliation April 2006.

- M. Tweedie, R. Subramanian, I. Craig, E.T. McAdams, J.A. McLaughlin, B. MacCraith, R. O'Kennedy, N. Kent S. Hearty **Impedimetric Microfluidic Point of Care Sensors with RF data transmission** Cross-Border Programme for Research and Education Contributing to Peace and Reconciliation - Showcase Event June 2005

Bibliography

[1] Cardiovascular disease: prevention and control. *http://www.who.int/dietphysicalactivity/publications/facts/cvd/en/*, page Last accessed 7th April 2008.

[2] G. Davi and C. Patrono. Platelet Activation and Atherothrombosis. *New England Journal of Medicine*, 357(24):2482, 2007.

[3] R. R. Seeley, T. D. Stephens, and P. Tate. *Essentials of Anatomy and Physiology*. McGraw-Hill, 2002.

[4] J.N. George. Platelets. *The Lancet*, 355(9214):1531–1539, 2000.

[5] Alan D. Michelson. *Platelets Second Ed*. Elsevier Academic Press, 2007.

[6] M. H. Kroll, J. D. Hellums, L. V. McIntire, A. I. Schafer, and J. L. Moake. Platelets and shear stress. *Blood*, 88(5):1525–1541, Sep 1 1996.

[7] A. S. Kantak, B. K. Gale, Y. Lvov, and S. A. Jones. Platelet Function Analyzer: Shear Activation of Platelets in Microchannels. *Biomedical Microdevices*, 5(3):207–215, 2003.

[8] R. Ross. Atherosclerosis is an inflammatory disease. *American Heart Journal*, 138(5 part 2):S419, 1999.

[9] O.J.T. McCarty, S.A. Mousa, P.F. Bray, and K. Konstantopoulos. Immobilized platelets support human colon carcinoma cell tethering, rolling, and firm adhesion under dynamic flow conditions. *Blood*, 96(5):1789, 2000.

[10] P. Harrison. Platelet function analysis. *Blood reviews*, 19(2):111–123, Mar 2005.

[11] A.D. Michelson. Platelet Function Testing in Cardiovascular Diseases, 2004.

[12] Brown, David and Larson, Richard. Improvements to parallel plate flow chambers to reduce reagent and cellular requirements. *BMC Immunology*, 2(1):9, 2001.

[13] N.A. Mody, O. Lomakin, T.A. Doggett, T.G. Diacovo, and M.R. King. Mechanics of Transient Platelet Adhesion to von Willebrand Factor under Flow. *Biophysical Journal*, 88(2):1432–1443, 2005.

[14] JJ Zwagina, KS Sakariassen, MR King, TG Diacovo, EF Grabowski, G. Nash, M. Hoylaerts, and JWM Heemskerk. Can blood flow assays help to identify clinically relevant differences in von Willebrand factor functionality in von Willebrand disease types 1-3? 1. *Journal of Thrombosis and Haemostasis*, 5(12):2547–2549, 2007.

[15] T.H. Schulte, R.L. Bardell, and B.H. Weigl. Microfluidic technologies in clinical diagnostics. *Clinica Chimica Acta*, 321(1-2):1–10, 2002.

[16] E. Verpoorte. Microfluidic chips for clinical and forensic analysis. *Electrophoresis*, 23(5), 2002.

[17] DA Beebe. Folch,The Science and Applications of Cell Biology in Microsystems,. *Lab on a Chip*, 5:10–11, 2005.

[18] S. D. Minteer. *Microfluidic techniques*. Humana Press, 2006.

[19] NT Nguyen and ST Wereley. *Fundamentals and Applications of Microfluidics*. Artech House, 2002.

[20] P.J. Hung, P.J. Lee, P. Sabounchi, R. Lin, and L.P. Lee. Continuous perfusion microfluidic cell culture array for high-throughput cell-based assays. *Biotechnology and Bioengineering*, 89(1):1–8, 2005.

[21] S.W. Rhee, A.M. Taylor, C.H. Tu, D.H. Cribbs, C.W. Cotman, and N.L. Jeon. Patterned cell culture inside microfluidic devices. *Lab on a Chip*, 5(1):102–107, 2005.

[22] A. Tourovskaia, X. Figueroa-Masot, and A. Folch. Differentiation-on-a-chip: A microfluidic platform for long-term cell culture studies. *Lab on a Chip*, 5(1):14–19, 2005.

[23] W.C. Chang, L.P. Lee, and D. Liepmann. Biomimetic technique for adhesion-based collection and separation of cells in a microfluidic channel. *Lab on a Chip*, 5(1):64–73, 2005.

[24] A. Revzin, K. Sekine, A. Sin, R.G. Tompkins, and M. Toner. Development of a microfabricated cytometry platform for characterization and sorting of individual leukocytes. *Lab on a Chip*, 5(1):30–37, 2005.

[25] A. Bonnefoy, Q. Liu, C. Legrand, and M. M. Frojmovic. Efficiency of platelet adhesion to fibrinogen depends on both cell activation and flow. *Biophysical journal*, 78(6):2834–2843, Jun 2000.

[26] Y. Ikeda, M. Handa, K. Kawano, T. Kamata, M. Murata, Y. Araki, H. Anbo, Y. Kawai, K. Watanabe, and I. Itagaki. The role of von Willebrand factor and fibrinogen in platelet aggregation under varying shear stress. *The Journal of clinical investigation*, 87(4):1234–1240, Apr 1991.

[27] H. Lu, L. Y. Koo, W. M. Wang, D. A. Lauffenburger, L. G. Griffith, and K. F. Jensen. Microfluidic shear devices for quantitative analysis of cell adhesion. *Analytical Chemistry*, 76(18):5257–5264, Sep 15 2004.

[28] N. A. Mody, O. Lomakin, T. A. Doggett, T. G. Diacovo, and M. R. King. Mechanics of transient platelet adhesion to von Willebrand factor under flow. *Biophysical journal*, 88(2):1432–1443, Feb 2005.

[29] M. Bahrami, MM Yovanovich, and JR Culham. PRESSURE DROP OF FULLY-DEVELOPED, LAMINAR FLOW IN MICROCHANNELS OF

ARBITRARY CROSS-SECTION. *Proceedings of 3rd international conference on microchannels and minichannels, Toronto, Canada*, 2005.

[30] DP Bakker, A. van der Plaats, GJ Verkerke, HJ Busscher, and HC van der Mei. Comparison of Velocity Profiles for Different Flow Chamber Designs Used in Studies of Microbial Adhesion to Surfaces. *Applied and Environmental Microbiology*, 69(10):6280–6287, 2003.

[31] I. Papautsky, B. K. Gale, S. Mohanty, T. A. Ameel, and A. B. Frazier. Effects of rectangular microchannel aspect ratio on laminar friction constant. *Proceedings of SPIE-The International Society for Optical Engineering, Proceedings of the 1999 Microfluidic Devices and Systems II, Santa Clara*, 3877:147–158, 1999.

[32] James B. Knight, Ashvin Vishwanath, James P. Brody, and Robert H. Austin. Hydrodynamic Focusing on a Silicon Chip: Mixing Nanoliters in Microseconds. *Physical Review Letters*, 80(17):3863, 04/27/ 1998.

[33] Gwo-Bin Lee, Chen-I Hung, Bin-Jo Ke, Guan-Ruey Huang, Bao-Herng Hwei, and Hui-Fang Lai. Hydrodynamic Focusing for a Micromachined Flow Cytometer. *Journal of Fluids Engineering*, 123(3):672–679, 2001.

[34] R. Miyake, H. Ohki, I. Yamazaki, and R. Yabe. A development of micro sheath flow chamber. *Micro Electro Mechanical Systems, 1991, MEMS'91, Proceedings.'An Investigation of Micro Structures, Sensors, Actuators, Machines and Robots'.IEEE*, pages 265–270, 1991.

[35] Z. Wu and N. T. Nguyen. Hydrodynamic focusing in microchannels under consideration of diffusive dispersion: theories and experiments. *Sensors and Actuators B*, 107(2):965–974, 2005.

[36] Gwo-Bin Lee, Bao-Herng Hwei, and Guan-Ruey Huang. Micromachined prefocused MN flow switches for continuous multi-sample injection. *Journal of Micromechanics and Microengineering*, 11(6):654–661, 2001.

[37] S. Chung, S. J. Park, J. K. Kim, C. Chung, D. C. Han, and J. K. ER . Chang. Plastic microchip flow cytometer based on 2- and 3-dimensional hydrodynamic flow focusing. *Microsystem Technologies*, 9(8):525–533, 10// 2003.

[38] Anne Y. Fu, Charles Spence, Axel Scherer, Frances H. Arnold, and Stephen R. Quake. A microfabricated fluorescence-activated cell sorter. *Nat Biotech*, 17(11):1109–1111, 11//print 1999. M3: 10.1038/15095; 10.1038/15095.

[39] S.A. Wang, W. Soper. *Bio-MEMS Technologies and Applications*. CRC Press, 2007.

[40] H. Becker and C. Gartner. Polymer microfabrication methods for microfluidic analytical applications. *Electrophoresis*, 21(1):12–26, 2000.

[41] H. Klank, J.P. Kutter, and O. Geschke. CO 2-laser micromachining and back-end processing for rapid production of PMMA-based microfluidic systems. *Lab on a Chip*, 2(4):242–246, 2002.

[42] É. Tyrrell, C. Gibson, B.D. MacCraith, D. Gray, P. Byrne, N. Kent, C. Burke, and B. Paull. Development of a micro-fluidic manifold for copper monitoring utilising chemiluminescence detection. *Lab on a Chip*, 4(4):384–390, 2004.

[43] R. Blue, N. Kent, L. Polerecky, H. McEvoy, D. Gray, and BD MacCraith. Platform for enhanced detection efficiency in luminescence-based sensors. *Electronics Letters*, 41(12):682–684, 2005.

[44] Y. Xia and G.M. Whitesides. Soft lithography. *Angew. Chem. Int. Ed*, 37(5):550–575, 1998.

[45] M.L. Chabinyc, D.T. Chiu, J.C. McDonald, A.D. Stroock, J.F. Christian, A.M. Karger, and G.M. Whitesides. An integrated fluorescence detection

system in poly (dimethylsiloxane) for microfluidic applications. *Analytical Chemistry*, 73:4491–4498, 2001.

[46] J.R. Anderson, D.T. Chiu, R.J. Jackman, O. Cherniavskaya, J.C. McDonald, H. Wu, S.H. Whitesides, and G.M. Whitesides. Fabrication of topologically complex three-dimensional microfluidic systems in PDMS by rapid prototyping. *Analytical Chemistry*, 72:3158–3164, 2000.

[47] M.A. Unger, H.P. Chou, T. Thorsen, A. Scherer, and S.R. Quake. Monolithic Microfabricated Valves and Pumps by Multilayer Soft Lithography. *Science*, 288(5463):113–116, 2000.

[48] N. Chronis, G. Liu, K.H. Jeong, and L. Lee. Tunable liquid-filled microlens array integrated with microfluidic network. *Optics Express*, 11(19):2370–2378, 2003.

[49] W.H. Grover, A.M. Skelley, C.N. Liu, E.T. Lagally, and R.A. Mathies. Monolithic membrane valves and diaphragm pumps for practical large-scale integration into glass microfluidic devices. *Sensors & Actuators: B. Chemical*, 89(3):315–323, 2003.

[50] JM Berg, R. Anderson, M. Anaya, B. Lahlouh, M. Holtz, and T. Dallas. A two-stage discrete peristaltic micropump. *Sensors & Actuators: A. Physical*, 104(1):6–10, 2003.

[51] T.J. Johnson, E.A. Waddell, G.W. Kramer, and L.E. Locascio. Chemical mapping of hot-embossed and UV-laser-ablated microchannels in poly (methyl methacrylate) using carboxylate specific fluorescent probes. *Applied Surface Science*, 181(1-2):149–159, 2001.

[52] H. Becker, W. Dietz, P. Dannberg, and G. Jena. MICROFLUIDIC MANIFOLDS BY POLYMER HOT EMBOSSING FOR μTAS APPLICATIONS. *Micro Total Analysis Systems' 98: Proceedings of the [Mu] TAS'98 Workshop, Held in Banff, Canada, 13-16 October 1998*, 1998.

[53] H. Becker and U. Heim. Hot embossing as a method for the fabrication of polymer high aspect ratio structures. *Sensors & Actuators: A. Physical*, 83(1-3):130–135, 2000.

[54] K. Ueno, F. Kitagawa, H.B. Kim, T. Tokunaga, S. Matsuo, H. Misawa, and N. Kitamura. Fabrication and Characteristic Responses of Integrated Microelectrodes in Polymer Channel Chip. *Chemistry Letters*, 29(8):858–859, 2000.

[55] SA Soper, SM Ford, S. Qi, RL McCarley, K. Kelly, and MC Murphy. Polymeric microelectromechanical systems. *Anal Chem*, 72(19):642A–651A, 2000.

[56] M.A. Roberts, J.S. Rossier, P. Bercier, and H. Girault. UV Laser Machined Polymer Substrates for the Development of Microdiagnostic Systems. *Science*, 261:895–897, 1993.

[57] D. Snakenborg, H. Klank, and J.P. Kutter. Microstructure Fabrication with a CO_2 Laser System. *Journal of Micromechanics and Microengineering*, 14(2):182–189, 2004.

[58] M. Bowden, O. Geschke, J.P. Kutter, and D. Diamond. CO2 laser microfabrication of an integrated microfluidic manifold for application in environmental monitoring. *Lab-on-a-Chip*, 3(4):221–223, 2003.

[59] R.M. McCormick, R.J. Nelson, M.G. Alonso-Amigo, D.J. Benvegnu, and H.H. Hooper. Microchannel electrophoretic separations of DNA in injection-molded plastic substrates. *Anal. Chem*, 69(14):2626–2630, 1997.

[60] G.J. Kellogg, T.E. Arnoldt, B.L. Carvalho, D.C. Dulfy, and N.F. Sheppard Jr. Centrifugal Microfluidics: Applications. *Micro Total Analysis Systems 2000: Proceedings of the [Mu] Tas 2000 Symposium, Held in Enschede, the Netherlands, 14-18 May 2000*, 2000.

[61] N. Thomas, A. Ocklind, I. Blikstad, S. Griffiths, M. Kenrick, H. Derand, G. Ekstrand, C. Ellström, A. Larsson, and P. Andersson. Integrated cell based assays in microfabricated disposable CD devices. *Micro Total Analysis Systems 2000: Proceedings of the TAS 2000 Symposium*, pages 249–252, 2000.

[62] T. Brenner, T. Glatzel, R. Zengerle, and J. Ducrée. Frequency-dependent transversal flow control in centrifugal microfluidics. *Lab on a Chip*, 5(2):146–150, 2005.

[63] B.H. Weigl, J. Kriebel, K.J. Mayes, T. Bui, and P. Yager. Whole Blood Diagnostics in Standard Gravity and Microgravity by Use of Microfluidic Structures (T-Sensors). *Microchimica Acta*, 131(1):75–83, 1999.

[64] B.H. Weigl, R. Bardell, T. Schulte, F. Battrell, and J. Hayenga. Design and Rapid Prototyping of Thin-Film Laminate-Based Microfluidic Devices. *Biomedical Microdevices*, 3(4):267–274, 2001.

[65] B.H. Weigl, R.L. Bardell, and C.R. Cabrera. Lab-on-a-chip for drug development. *Advanced Drug Delivery Reviews*, 55(3):349–377, 2003.

[66] Fluidics Subsystem for GeneSat Experimental Payload. *http://genesat.arc.nasa.gov/fluidics.html*, page Last accessed 7th April 2008.

[67] M.W. Inc. *Merriam-Webster's collegiate dictionary*. Merriam-Webster, 2003.

[68] F.M. White. *Fluid Mechanics*. McGraw-Hill, 2003.

[69] H. Bruus. *Theoretical microfluidics*. Oxford University Press, USA, 2008.

[70] DA Hammer and SM Apte. Simulation of cell rolling and adhesion on surfaces in shear flow: general results and analysis of selectin-mediated neutrophil adhesion. *Biophysical Journal*, 63(1):35–57, 1992.

[71] P. Tandon and SL Diamond. Hydrodynamic effects and receptor interactions of platelets and their aggregates in linear shear flow. *Biophysical Journal*, 73(5):2819–2835, 1997.

[72] A. van den Berg, W. Olthuis, and P. Bergveld. *Micro Total Analysis Systems 2000: Proceedings of the [Mu] Tas 2000 Symposium, Held in Enschede, the Netherlands, 14-18 May 2000*. Kluwer Academic Publishers, 2000.

[73] L. Lin, C.J. Chiu, W. Bache, and M. Heckele. Microfabrication using silicon mold inserts and hot embossing. *Micro Machine and Human Science, 1996., Proceedings of the Seventh International Symposium*, pages 67–71, 1996.

[74] L. Martynova, L.E. Locascio, M. Gaitan, G.W. Kramer, R.G. Christensen, and W.A. MacCrehan. Fabrication of Plastic Microfluid Channels by Imprinting Methods. *Burns*, 144:147.

[75] L. Locasci&, M. Gaitan, J. Hong, and M. Eldefrawi. PLASTIC MICROFLUID DEVICES FOR CLINICAL MEASUREMENTS. *Micro Total Analysis Systems' 98: Proceedings of the [Mu] TAS'98 Workshop, Held in Banff, Canada, 13-16 October 1998*, 1998.

[76] J. Xu, L. Locascio, M. Gaitan, and C.S. Lee. Room-Temperature Imprinting Method for Plastic Microchannel Fabrication. *Science*, 261:895, 1993.

[77] K. UCHIYAMA, W. XU, M. YAMAMOTO, T. SHIMOSAKA, and T. HOBO. Development of Imprinted Polymer Microchannel Capillary Chip for Capillary Electrochromatography. *Analytical Sciences*, 15(9):825–826, 1999.

[78] S. Lazare and R. Srinivasan. Surface properties of poly (ethylene terephthalate) films modified by far-ultraviolet radiation at 193nm (laser) and 185nm (low intensity). *The Journal of Physical Chemistry*, 90(10):2124–2131, 1986.

[79] L. Brown, T. Koerner, J.H. Horton, and R.D. Oleschuk. Fabrication and characterization of poly (methylmethacrylate) microfluidic devices bonded using surface modifications and solvents. *Lab on a Chip*, 6(1):66–73, 2006.

[80] J. Li, D. Chen, and G. Chen. Low-Temperature Thermal Bonding of PMMA Microfluidic Chips. *Analytical Letters*, 38(7):1127–1136, 2005.

[81] A.M. Lincoff, J.E. Tcheng, R.M. Califf, D.J. Kereiakes, T.A. Kelly, G.C. Timmis, N.S. Kleiman, J.E. Booth, C. Balog, C.F. Cabot, et al. Sustained Suppression of Ischemic Complications of Coronary Intervention by Platelet GP IIb/IIIa Blockade With Abciximab One-Year Outcome in the EPILOG Trial. *Circulation*, 99(15):1951–1958, 1999.

[82] S.M. Trivedi, J. Shani, and G. Hollander. Bleeding Complications of Platelet Glycoprotein IIb/IIIa Inhibitor Abciximab (ReoPro). *Journal of Invasive Cardiology*, 14(7):423–425, 2002.

[83] S.D. Berkowitz, R.A. Harrington, M.M. Rund, and J.E. Tcheng. Acute profound thrombocytopenia after C7E3 Fab (abciximab) therapy. *Circulation*, 95(4):809–813, 1997.

Appendices

Appendix A

Platelet Function Analysis Systems

Basis of test	Name of Test	Advantages	Disadvantages
In vivo cessation of blood flow by platelet plug	Bleeding time	In vivo test; physiological	Nonspecific; insensitive; can leave scar
In vitro cessation of high shear blood flow by platelet plug	PFA-100	Simple, rapid; low sample volume; high shear; minimal sample preparation	Dependent on Von Willebrand factor and hematocrit; no instrument adjustment

Basis of test	Name of Test	Advantages	Disadvantages
Shear-induced platelet adhesion	IMPACT (cone and plate (let) analyzer, DiaMed)	Simple, rapid; point-of-care; low sample volume; high shear; whole blood assay	Instrument not yet widely available
Platelet-to-platelet aggregation	Aggregometry (turbidometric)	Historical gold standard	Poor reproducibility; high sample volume; sample preparation; time consuming; expensive
Platelet-to-platelet aggregation	Aggregometry (impedance)	Whole blood assay	High sample volume; sample preparation; time consuming; expensive
Platelet-to-platelet aggregation	VerifyNow (Ultegra RPFA)	Simple, rapid; point-of-care; low sample volume;	No instrument adjustment

Basis of test	Name of Test	Advantages	Disadvantages
Platelet-to-platelet aggregation	Plateletworks (Helena Laboratories)	Minimal sample preparation; whole blood assay	Not well studied
Activation dependent changes in platelet surface Platelet surface	Platelet surface P-selectin, platelet surface activated GP IIb/IIIa, leukocyte-platelet aggregates (flow cytometry)	Low sample volume; whole blood assay	Sample preparation; expensive; requires flow cytometer and experienced operator
Activation dependent signaling	VASP phosphorylation state (flow cytometry)	Directly dependent on clopidogrels target, P2Y12; low sample volume; whole blood assay	Sample preparation; expensive; requires flow cytometer and experienced technician

Basis of test	Name of Test	Advantages	Disadvantages
Activation dependent release from platelets	Platelet-derived microparticles (flow cytometry)	Low sample volume; whole blood assay	Sample preparation; expensive; requires flow cytometer and experienced technician
Activation dependent release from platelets	Serum thromboxane B2	Directly dependent on aspirins target, COX-1	Indirect measure; not platelet specific
Activation dependent release from platelets	Plasma GPV	Platelet specific	Separation of plasma can result in artifactual platelet activation; reflects only thrombin-mediated platelet activation

Basis of test	Name of Test	Advantages	Disadvantages
Activation dependent release from platelets	α-Granule constituents in plasma: platelet factor 4, β-thromboglobulin, soluble P-selectin	Reflect platelet secretion	Separation of plasma can result in artifactual platelet activation; plasma soluble P-selectin also originates from endothelial cells

Table A.1: Platelet function Analysis Systems

Appendix B

Equations of Motion

B.1 Conservation of Mass

Consider the volume in Figure B.1 showing an idealised fixed control volume of fluid. Since the flow through each side is considered approximately one dimensional the conservation of mass states the change in density of the volume over the surface plus mass flow in less the mass flow out sums to zero or:

$$\int_{\Omega} \frac{\partial \rho}{\partial t} d\mathbb{V} + \sum_{i} (\rho_i A_i V_i)_{out} - \sum_{i} (\rho_i A_i V_i)_{in} = 0 \tag{B.1}$$

Since the volume element is so small the integral reduces to the differential term:

$$\int_{\Omega} \frac{\partial \rho}{\partial t} d\mathbb{V} \approx \frac{\partial \rho}{\partial t} dxdydz \tag{B.2}$$

Since the mass flow acts on all six faces of the control and the the fluid is assumed to be a continuum we can list all six flows as shown in TableB.2

Substituting these values into eqn B.1 we get:

$$\frac{\partial \rho}{\partial t} dxdydz + \frac{\partial}{\partial x}(\rho u) dxdydz + \frac{\partial}{\partial y}(\rho v) dxdydz + \frac{\partial}{\partial z}(\rho w) dxdydz = 0 \tag{B.3}$$

The element volume cancels to leave:

Face	Inlet mass flow	Outlet mass flow
x	$\rho u\ dy\ dz$	$\left[\rho u + \frac{\partial}{\partial x}\ (\rho u)\ dx\ \right]\ dy\ dz$
y	$\rho v\ dx\ dz$	$\left[\rho v + \frac{\partial}{\partial y}\ (\rho v)\ dy\ \right]\ dx\ dz$
z	$\rho w\ dx\ dy$	$\left[\rho w + \frac{\partial}{\partial z}\ (\rho w)\ dz\ \right]\ dx\ dy$

Table B.1: Mass flow table

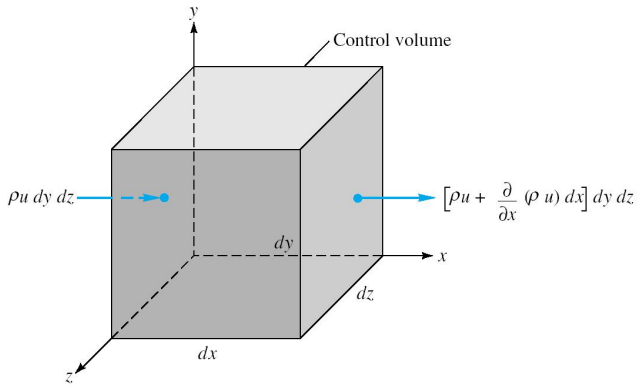

Figure B.1: Control volume showing mass flow in x direction

$$\frac{\partial \rho}{\partial t} + \frac{\partial}{\partial x}(\rho u) + \frac{\partial}{\partial y}(\rho v) + \frac{\partial}{\partial z}(\rho w) = 0 \tag{B.4}$$

Using the nabla function:

$$\nabla = \mathbf{i}\frac{\partial}{\partial x} + \mathbf{j}\frac{\partial}{\partial y} + \mathbf{k}\frac{\partial}{\partial z} \tag{B.5}$$

We can rewrite the continuity equation as:

$$\frac{\partial \rho}{\partial t} + \nabla\cdot(\rho V) = 0 \tag{B.6}$$

Which, for incompressible flow i.e. constant density, further reduces to

$$\nabla\cdot V = 0 \tag{B.7}$$

B.2 Equations of Linear Momentum

In a simliar manner to Appendix B.1 the linear momentum equation for Figure B.1 states:

$$\sum F = \frac{\partial}{\partial t}\left(\int_{\Omega} V\rho d\mathbb{V}\right) + \sum(\dot{m}_i V_i)_{out} - \sum(\dot{m}_i V_i)_{in} \tag{B.8}$$

Again the volume integral reduces to:

$$\frac{\partial}{\partial t}\left(\int_{\Omega} V\rho d\mathbb{V}\right) \approx \frac{\partial}{\partial t}(\rho V)dxdydz \tag{B.9}$$

The table of momentum fluxes is also constructed in a similar vein to give

Face	Inlet momentum flux	Outlet momentum flux
x	$\rho uV\ dy\ dz$	$\left[\rho uV + \frac{\partial}{\partial x}\ (\rho uV)\ dx\ \right] dy\ dz$
y	$\rho vV\ dx\ dz$	$\left[\rho vV + \frac{\partial}{\partial y}\ (\rho vV)\ dy\ \right] dx\ dz$
z	$\rho wV\ dx\ dy$	$\left[\rho wV + \frac{\partial}{\partial z}\ (\rho wV)\ dz\ \right] dx\ dy$

Table B.2: Table of control fluxes

Introducing these terms into eqns B.8 and B.9 we get

$$\sum F = dxdydz\left[\frac{\partial}{\partial t}(\rho V) + \frac{\partial}{\partial x}(\rho uV) + \frac{\partial}{\partial y}(\rho vV) + \frac{\partial}{\partial z}(\rho wV)\right] \tag{B.10}$$

taking the term in the square bracket we can write

$$\frac{\partial}{\partial t}(\rho V)+\frac{\partial}{\partial x}(\rho uV)+\frac{\partial}{\partial y}(\rho vV)+\frac{\partial}{\partial z}(\rho wV) = V\left[\frac{\partial \rho}{\partial t}+\nabla\cdot(\rho V)\right]+\rho\left(\frac{\partial V}{\partial t}+u\frac{\partial V}{\partial x}+v\frac{\partial V}{\partial y}+w\frac{\partial V}{\partial z}\right) \tag{B.11}$$

The term in square brackets can be seen to be the continuity equation and so vanishes. The longer term in the round brackets can be seen to be the acceleration of a particle in the control volume and can be written

$$\frac{\partial V}{\partial t} + u\frac{\partial V}{\partial x} + v\frac{\partial V}{\partial y} + w\frac{\partial V}{\partial z} = \frac{dV}{dt} \tag{B.12}$$

and so eqn B.10 reduces to:

$$\sum F = \rho\frac{\partial V}{\partial t}dxdydz \tag{B.13}$$

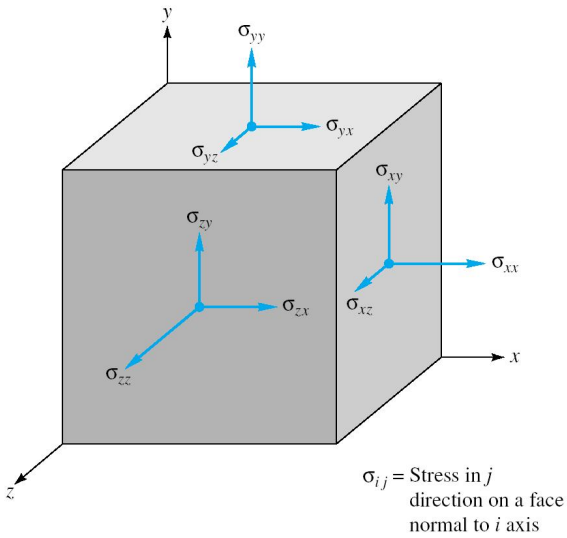

Figure B.2: Notation for stresses

Equation B.13 states the net force on the control volume must be of differential size and proportional to the element volume. These forces are of two types surface forces or body forces. Body forces are due to some external force such as gravity or electrical potential however surface forces are due to stresses on the surfaces of the control volume and are te sum of the hydrpstatic stresses and the viscous stresses τ_{ij}

$$\sigma_{ij} = \begin{bmatrix} -p + \tau_{xx} & \tau_{yx} & \tau_{zx} \\ \tau_{xy} & -p + \tau_{yy} & \tau_{zy} \\ \tau_{xz} & \tau_{yz} & -p + \tau_{zz} \end{bmatrix} \tag{B.14}$$

The notation for which can be seen in Figure B.2 It should be noted that it is not the stresses them sleves but rather thier gradients that cause the net force on

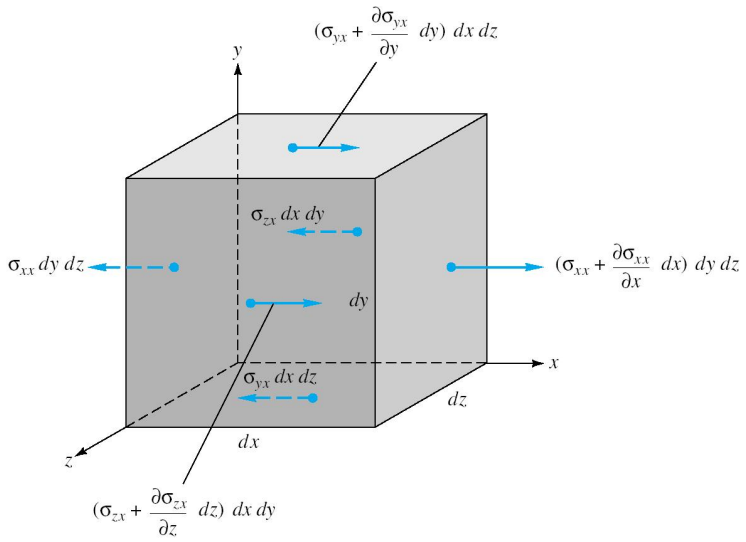

Figure B.3: Control volume showing surface forces in x direction

the control volume. This can be seen from Figure B.3 the leftward force $\sigma_{xx}dydz$ is balanced by the rightward force $\sigma_{xx}dydz$ on the right face leaving only the net rightward force $(\partial\sigma_{xx}/\partial x)dxdydz$. This can be repeated for the other two directions resulting in the net force in the x direction being given as

$$dF_{x,surf} = \left[\frac{\partial}{\partial x}(\sigma_{xx}) + \frac{\partial}{\partial y}(\sigma_{yx}) + \frac{\partial}{\partial z}(\sigma_{zx})\right]dxdydz \tag{B.15}$$

Substituting in values from eqn B.15 we get

$$\frac{dF_x}{d\mathbb{V}} = -\frac{\partial p}{\partial x} + \frac{\partial}{\partial x}(\tau_{xx}) + \frac{\partial}{\partial x}(\tau_{yx}) + \frac{\partial}{\partial x}(\tau_{zx}) \tag{B.16}$$

This can be repeated to give forces in both $y$and z

$$\begin{aligned}\frac{dF_y}{d\mathbb{V}} &= -\frac{\partial p}{\partial y} + \frac{\partial}{\partial y}(\tau_{xy}) + \frac{\partial}{\partial y}(\tau_{yy}) + \frac{\partial}{\partial y}(\tau_{zy}) \\ \frac{dF_z}{d\mathbb{V}} &= -\frac{\partial p}{\partial z} + \frac{\partial}{\partial z}(\tau_{xz}) + \frac{\partial}{\partial z}(\tau_{yz}) + \frac{\partial}{\partial z}(\tau_{zz})\end{aligned} \tag{B.17}$$

Combining these equations we get

$$\left(\frac{dF}{d\mathbb{V}}\right)_{surf} = -\nabla p + \left(\frac{dF}{d\mathbb{V}}\right)_{viscous} \tag{B.18}$$

where

$$\left(\frac{dF}{d\mathbb{V}}\right)_{viscous} = \mathbf{i}\left(\frac{\partial\tau_{xx}}{\partial x}+\frac{\partial\tau_{yx}}{\partial y}+\frac{\partial\tau_{zx}}{\partial z}\right)+\mathbf{j}\left(\frac{\partial\tau_{xy}}{\partial x}+\frac{\partial\tau_{yy}}{\partial y}+\frac{\partial\tau_{zy}}{\partial z}\right)+\mathbf{k}\left(\frac{\partial\tau_{xz}}{\partial x}+\frac{\partial\tau_{yz}}{\partial y}+\frac{\partial\tau_{zz}}{\partial z}\right) \tag{B.19}$$

or

$$\left(\frac{dF}{d\mathbb{V}}\right)_{viscous} = \nabla\cdot\tau_{ij} \tag{B.20}$$

where

$$\tau_{ij} = \begin{bmatrix} \tau_{xx} & \tau_{xy} & \tau_{xz} \\ \tau_{yx} & \tau_{yy} & \tau_{yz} \\ \tau_{zx} & \tau_{zy} & \tau_{zz} \end{bmatrix} \tag{B.21}$$

Combining equations B.20 B.18 B.4 and by taking the gravity as the only body force acting on the volume i.e. $dF_{grav} = \rho g dx dy dz$ we get

$$\rho g - \nabla p + \nabla\cdot\tau_{ij} = \rho\frac{dV}{dt} \tag{B.22}$$

where

$$\frac{\partial V}{\partial t} + u\frac{\partial V}{\partial x} + v\frac{\partial V}{\partial y} + w\frac{\partial V}{\partial z} = \frac{dV}{dt} \tag{B.23}$$

While equation B.22 looks relatively simple but when expanded to illustrate the inherent complexity looks as follows

$$\begin{aligned}
\rho g_x - \frac{\partial p}{\partial x} + \frac{\partial\tau_{xx}}{\partial x} + \frac{\partial\tau_{yx}}{\partial y} + \frac{\partial\tau_{zx}}{\partial z} &= \rho\left(\frac{\partial u}{\partial t} + u\frac{\partial u}{\partial x} + v\frac{\partial u}{\partial y} + w\frac{\partial u}{\partial z}\right) \\
\rho g_y - \frac{\partial p}{\partial y} + \frac{\partial\tau_{xy}}{\partial x} + \frac{\partial\tau_{yy}}{\partial y} + \frac{\partial\tau_{zy}}{\partial z} &= \rho\left(\frac{\partial v}{\partial t} + u\frac{\partial v}{\partial x} + v\frac{\partial v}{\partial y} + w\frac{\partial v}{\partial z}\right) \\
\rho g_z - \frac{\partial p}{\partial z} + \frac{\partial\tau_{xz}}{\partial x} + \frac{\partial\tau_{yz}}{\partial y} + \frac{\partial\tau_{zz}}{\partial z} &= \rho\left(\frac{\partial w}{\partial t} + u\frac{\partial w}{\partial x} + v\frac{\partial w}{\partial y} + w\frac{\partial w}{\partial z}\right)
\end{aligned} \tag{B.24}$$

If we assume incompressible flow we can use the following relationships

$$\tau_{xx} = 2\mu\frac{\partial u}{\partial x} \qquad \tau_{yy} = 2\mu\frac{\partial v}{\partial y} \qquad \tau_{zz} = 2\mu\frac{\partial w}{\partial z} \tag{B.25}$$
$$\tau_{xy} = \tau_{yx} = \mu\left(\frac{\partial u}{\partial y} + \frac{\partial v}{\partial x}\right) \quad \tau_{xz} = \tau_{zx} = \mu\left(\frac{\partial w}{\partial x} + \frac{\partial u}{\partial z}\right) \quad \tau_{yz} = \tau_{zy} = \mu\left(\frac{\partial v}{\partial z} + \frac{\partial w}{\partial y}\right)$$

to give the differential momentum equation for a Newtonian fluid with constant density and viscosity

$$\begin{aligned}
\rho g_x - \frac{\partial p}{\partial x} + \mu\left(\frac{\partial^2 u}{\partial x^2} + \frac{\partial^2 u}{\partial y^2} + \frac{\partial^2 u}{\partial z^2}\right) &= \rho\frac{du}{dt} \\
\rho g_{yx} - \frac{\partial p}{\partial y} + \mu\left(\frac{\partial^2 v}{\partial x^2} + \frac{\partial^2 v}{\partial y^2} + \frac{\partial^2 v}{\partial z^2}\right) &= \rho\frac{dv}{dt} \\
\rho g_z - \frac{\partial p}{\partial z} + \mu\left(\frac{\partial^2 w}{\partial x^2} + \frac{\partial^2 w}{\partial y^2} + \frac{\partial^2 w}{\partial z^2}\right) &= \rho\frac{dw}{dt}
\end{aligned} \tag{B.26}$$

These equations are also known as the Navier-Stokes Equations

Appendix C

LabVIEW Virtual Instruments

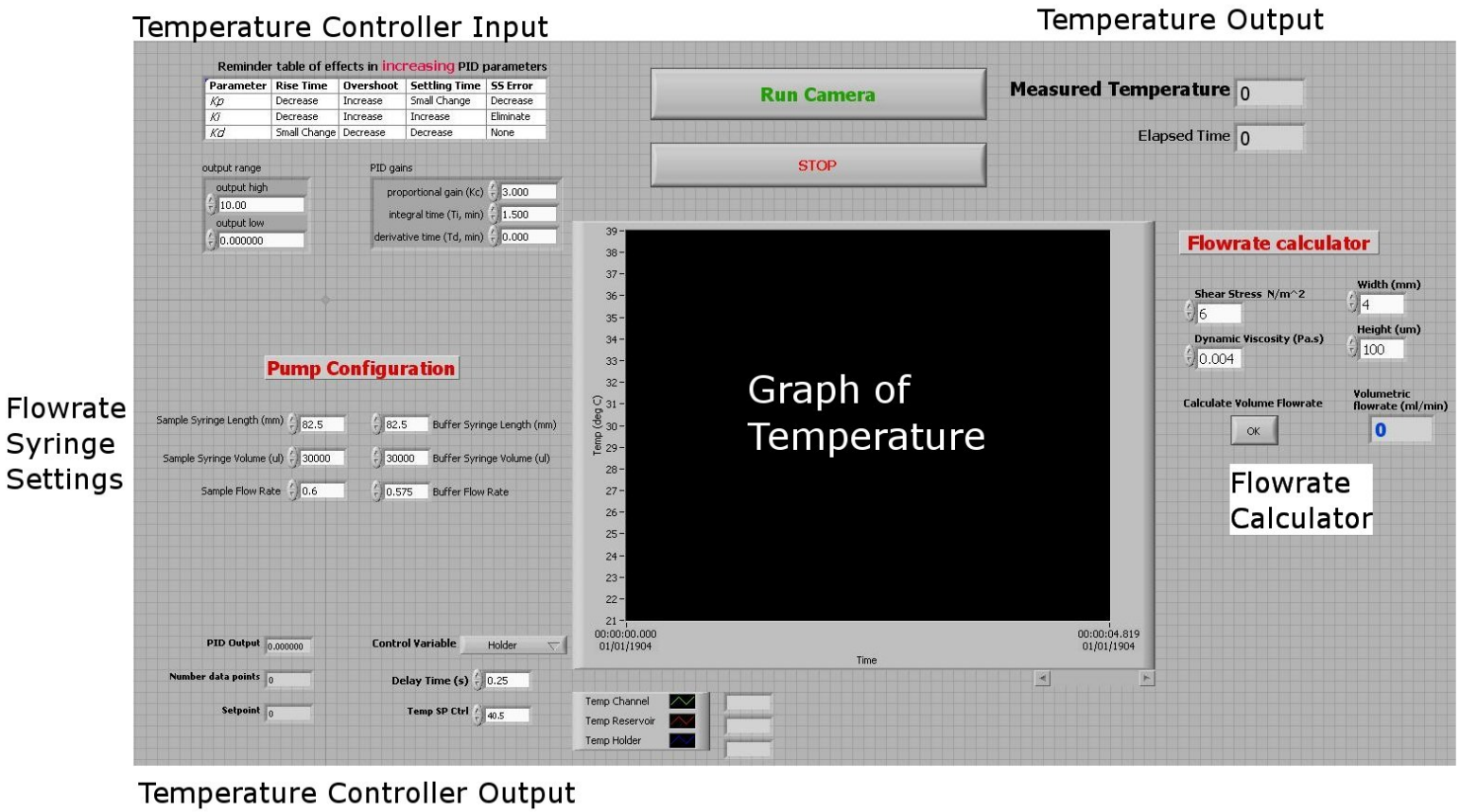

Figure C.1: Screen capture of initial configuration screen. On this screen the software is initialised, the heating of the chip holder stage begins, the appropriate flow rates are calculated and pumps configured accordingly. On completion, the 'Run Camera' control facilitates transition to the screen shown in Figure C.2

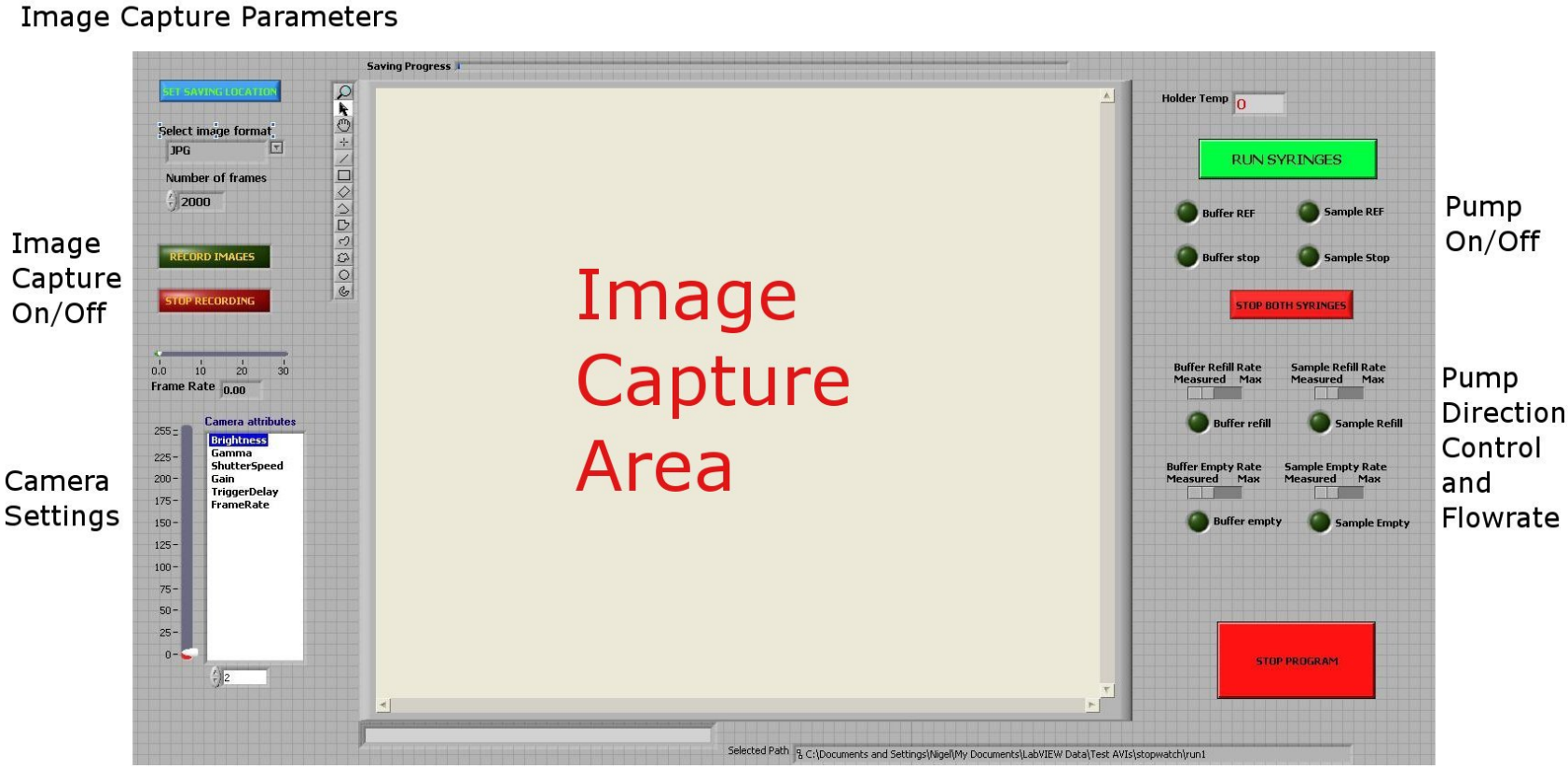

Figure C.2: Screen capture of image capture software control. From here live images are streamed to the laptop screen, camera settings are adjusted, both sample and buffer pumps can be controlled. In terms of image capture, image format, number of images required and saving location are also defined.

List of Figures

List of Tables